Universidad Zaragoza
1542

Proyecto Fin de Carrera

Evolución a largo plazo de redes ópticas aviónicas

Autor

José Manuel Estarán Tolosa

Ponente

Juan Ignacio Garcés Gregorio

Escuela de Ingeniería y Arquitectura

2012

Repositorio de la Universidad de Zaragoza – Zaguan http://zaguan.unizar.es

Proyecto Fin de Carrera

Evolución a largo plazo de redes ópticas aviónicas

Autor

José Manuel Estarán Tolosa

Ponente

Juan Ignacio Garcés Gregorio

Escuela de Ingeniería y Arquitectura
2012

Evolución a largo plazo de redes ópticas aviónicas

Autor:

José Manuel Estarán Tolosa

Ponente:

Juan Ignacio Garcés Gregorio

Este informe es parte de los requisitos para lograr la titulación de Ingeniería Superior en Telecomunicaciones por la Universidad de Zaragoza.

Este informe representa 18 créditos.

Dep. Ingeniería Electrónica y Comunicaciones.

Escuela de Ingeniería y Arquitectura

Edificio Ada Byron del campus Rio Ebro

C/ María de Luna nº 1

50018 Zaragoza

España.

http://diec.unizar.es/index.php/es/diec/presentacion/presentacion

A mi familia.

RESUMEN

Se ha evaluado el rendimiento de una red óptica aviónica bajo las exigentes condiciones del entorno que típicamente se encuentran en los sistemas aerotransportados. Tasas de error (BER), márgenes de potencia y máximas tasas de transmisión conseguibles se han obtenido a -40^{o}C, 25^{o}C y 90^{o}C. Las vibraciones y los impactos han sido estadísticamente analizados a través de desalineaciones radiales, longitudinales y angulares en los conectores del sistema óptico. El test ha sido elaborado para Non-Return-to-Zero (NRZ). Multiplexación óptica por división en frecuencias ortogonales (OOFDM) con modulación en amplitud y cuadratura (4-QAM, 16-QAM y 32-QAM) se ha propuesto como una opción factible y fiable para dar soporte a las futures y crecientes demandas de ancho de banda. Su rendimiento también ha sido evaluado para cada una de las tres temperaturas.

ÍNDICE

LISTA DE SIGLAS Y ACRÓNIMOS

10GbE	10 Gigabit Ethernet
ACO-OFDM	Assymmetrically Clipped Optical Orthogonal Frequency Division Multiplexing
APD	Avalanche PhotoDiode
B2B	Back-to-Back
BER	Bit Error Rate
BW	BandWidth
CAD	Computer-Aided Design
CW	Continuous Wave
DAC	Digital to Analogue Converter
DAPHNE	Developing Aircraft Photonic Networks
DBR	Distributed Bragg Reflector
DC	Direct Current
DCO-OFDM	DC-biased Optical Orthogonal Frequency Division Multiplexing
DMA	Differential Mode Attenuation
DMD	Differential Mode Delay
DMG	Degenerate Mode Group
DMT	Discrete MultiTone modulation
DSL	Digital Subscriber Line
EF	Encircled FLux
EIA	Electronic Industries Alliance
EMB	Effective Modal Bandwidth
EMBc	Effective Modal Bandwidth Computed
EMI	ElectroMagnetic Interference
ER	Extinction Ratio
FOTP	Fiber Optic Test Procedure
FWM	Four-Wave Mixing
GVD	Group Velocity Dispersion
ICI	InterCarrier Interference
IEEE	Institute of Electrical and Electronics Engineers
ISI	InterSymbol Interference
ISO	International Organization for Standardization
LAN	Local Area Networks
LD	LASER Diode
LED	Light Emitting Diode
LI	Light-to-Intensity
LIV	Light-to-Intensity-to-Voltage
LPF	Low Pass Filter
LR	Long Reach
MDA	Mode-Dependent Attenuation
MGD	Mode Group Delay
MMF	MultiMode Fiber
MPD	Mode Power Distribution
NRZ	Non-Return-to-Zero
OFDM	Orthogonal Frequency Division Multiplexing
OFL	OverFilled Launch
OL	Offset Launch

OMA	Optical Modulation Amplitude
OOB	Out-Of-Band
OOFDM	Optical Orthogonal Frequency Division Multiplexing
OOK	On-Off Keying
PAPR	Peak-to-Average Power Ratio
PD	PhotoDiode
PMD	Polarization Mode Dispersion
PMD	Physical Medium Dependent
POF	Plastic Optical Fiber
QAM	Quadrature Amplitude Modulation
QE	Quantum Efficiency
QoS	Quality of Service
RF	Radio Frequency
RML	Restricted Mode Launch
ROFL	Radially OFL
S2P	Serial-to-Parallel
SMF	SingleMode Fiber
SNR	Signal-to-Noise Ratio
SPM	Self-Phase Modulation
SR	Short Reach
SRS	Stressed Receiver Sensitivity
TIA	Telecommunications Industry Association
VCSEL	Vertical-Cavity Surface-Emitting LASER
WDM	Wavelength-Division Multiplexing

1 Introducción

Durante los últimos años, los estándares Ethernet han evolucionado desde 10 y 100 Mbps a 1, 10, 40 e incluso 100Gbps [1]. El rápido crecimiento del uso de internet y servicios en la nube (cloud computing applications) han convertido en convencional el uso de 10 Gigabit Ethernet (10GbE) en muchas redes principales de acceso (backbone networks) y centros de datos [2]. La misma proliferación de conexiones de gran ancho de banda da lugar a la aparición de aplicaciones web adicionales [3] que, a su vez, aceleran la necesidad de instalar capacidades de transmisión adicionales. Esta situación también se está empezando a dar en sistemas aviónicos donde, por ejemplo, la distribución de video de alta calidad a cada pasajero, los precisos y completos sistemas de guiado en pista (taxiing aids) y el reclamo de visibilidad durante el vuelo bajo cualquier condición medioambiental ha precipitado un crecimiento ineficiente de las actuales redes basadas en cobre. Esto ha desembocado en sistemas nodales de comunicación extremadamente complejos, pesados y caros con un amplio abanico de longitudes de cable, anchos de banda y protocolos de control. Se espera que esta tendencia continúe [4].

Este abrumador escenario ha planteado la necesidad de rehacer el concepto que fundamenta el diseño y despliegue de las redes de comunicación en sistemas aerotransportados y la fibra óptica ha sido sensatamente escogida como la tecnología más apropiada para empezar de nuevo. La fibra óptica ofrece un número de ventajas sobre los cables de cobre:

- Al menos 10x más ligera para una sustitución de cable 1 a 1. El beneficio crece cuando se utilizan cables ribbon [5]. ([1])
- A 1GHz, un cable coaxial de bajas pérdidas especial para redes aéreas (S22089) tiene un ratio perdida/distancia de alrededor de 121.4dB/km [6]. Por su parte, se ha demostrado que la fibra de silicio es independiente de la modulación hasta los 10GHz y el peor caso de atenuación ocurre en primera ventana donde en ningún caso exceden 2.5dB/km (una mejora de más de 48x) [7]-[9]
- Parcialmente debido a la menor atenuación, se pueden alcanzar mayores productos distancia-ancho de banda. Gbps·km para fibras multimodo (MMF) y hasta Pbps·km para fibras monomodo (SMF) en contraste con los Mbps·km para cables coaxiales [5]
- Inmunidad ante interferencias electromagnéticas (EMI)
- El cable de fibra óptica es más barato que el coaxial ([2])
- La flexibilidad de la fibra permite un despliegue fácil incluso por los espacios estrechos e irregulares típicos en aviones. Además, las pérdidas por curvatura pueden ser contrarrestadas con fibras anticurvatura (bend-insensitive)
- El cobre tiene un menor limite de tensión de estiramiento (aproximadamente 25lb contra 100-200lb) [10] y [11]

---

[1] Los valores se han calculado para una carga de transmisión comparable sobre la misma distancia.
[2] Aunque el cable en sí es más barato, la electrónica implicada es más cara. Este compromiso debe ser evaluado en cada situación.

El aprovechamiento del conocimiento acumulado durante la implementación de redes ópticas terrestres y sus componentes constituyen un buen punto de partida y referencia. Sin embargo, las duras condiciones ambientales que se encuentran en los aviones (amplios rangos de temperatura, vibraciones, golpes…) junto con la necesidad critica por la seguridad y la fiabilidad, requieren una adaptación detallada del diseño de la red, los componentes y los estándares al entorno aviónico. Se ha alcanzado un notable progreso en relación a conectores, fibras y transceptores [12] y un nuevo estándar para redes locales (LAN) basadas en multiplexación por longitud de onda (WDM) está siendo desarrollado [13].

Otro aspecto importante es la escalabilidad de la red. La tecnología óptica más moderna es compatible con la antigua pero no al contrario [1]. Es crucial diseñar el sistema teniendo en cuenta futuras exigencias de ancho de banda y seguir ofreciendo una buena calidad de servicio en el tiempo actual. Esto se vuelve una consideración ineludible en aviones, donde la sustitución de los componentes que constituyen la red es más difícil y caro que a nivel de tierra. En este aspecto, las simulaciones se usan para explorar como funcionarán las diferentes opciones y arquitecturas en futuras aplicaciones y establecer límites prácticos de acuerdo con múltiples criterios. Por lo tanto, los resultados obtenidos de simulaciones no son simplemente información extra para confirmar estimaciones sino datos clave que deben ser integrados en la fase de toma de decisiones y diseño del proyecto correspondiente. Las simulaciones deben ser precisas y las condiciones de frontera deben ser claramente especificadas para que los datos sean útiles.

Por último, el precio y la modularidad también son factores influyentes. La construcción de una red de bajo coste supone un ahorro en el tiempo presente y un futuro beneficio conforme las piezas de hardware necesiten ser reemplazadas. Una distribución modular garantiza un fácil entendimiento de la red y proporciona la flexibilidad, reconfigurabilidad, escalabilidad y facilidad de mantenimiento que las redes aviónicas necesitan [4].

El trabajo aquí presentado cubre la simulación de una red óptica para su uso en medios de transporte aéreos. La investigación se ha realizado como parte del proyecto DAPHNE (Developing Aircraft Photonic Networks), apoyado por el séptimo programa de marco de trabajo de la Comisión Europea (7th framework programme of the European Comission) ([3]).

1.1 Establecimiento del problema

El principal objetivo fue evaluar el rendimiento de una red óptica específica para la que algunos de los parámetros ya habían sido fijados como resultado de las investigaciones llevadas a cabo durante el desarrollo del proyecto DAPHNE. Por lo tanto, el mayor problema a resolver no fue el diseño de la topología o componentes que satisfacían las necesidades, sino analizar cómo de bien funcionaba dicha red bajo las exigentes condiciones ambientales.

Las restricciones se presentan a continuación:

[3] www.fp7daphne.eu

- Trasceptores a 10Gbps de la familia S-light ([4]). VCSELs integrados a 850nm, chips de fotodiodos PIN de GaAs y electrónica CMOS de bajo consumo. Compatibles con los requisitos ambientales de sistemas aeroespaciales.
- Fibra multimodo tipo OM4 (ver APENCIDE A para las especificaciones y APENDICE B para la descripción física)
- 10 Gigabit Ethernet (10GbE) usando el protocolo de bajo coste 10GBASE-SR.

La conformidad con IEEE 802.3ae (10GBASE-SR) implicaba igualmente una restricción en la tasa de transmisión, longitud de la fibra and diversos rangos de operación.

Los objetivos de la investigación son:

- Para realizar un análisis satisfactorio, la herramienta de simulación debe ser elegida y su precisión evaluada. Esto requiere obtener un material de referencia detallado y escoger únicamente las pruebas verdaderamente relevantes para nuestro caso.
- Tras seleccionar el simulador, el modelado debe ser realizado. Es necesario transformar los parámetros físicos y las especificaciones de estándar en variables matemáticas que el software pueda interpretar. Debido a las aproximaciones numéricas, suposiciones y las variadas referencias utilizadas para el desarrollo de la herramienta, la adaptación exacta al formato usado puede llegar a ser compleja e incluso imposible. Los resultados de la simulación deben ser comparados con aquellos obtenidos experimentalmente para diversos casos de modo que el correcto modelado sea confirmado.
- Finalmente, la red óptica es simulada. La información apropiada debe ser recogida y examinada.

1.2 Metodología

Para conseguir los objetivos previamente mencionados, el trabajo ha sido desarrollado como sigue:

- Dos simuladores comerciales diferentes fueron seleccionados (VPITransmissionmaker™ and OptSim™ with MoseSYS™). Su precisión fue analizada para los dos módulos más críticos en nuestro sistema final, es decir, fibra multimodo y diodo laser (VCSEL) a 850nm.
- La fibra OM4, el VSEL 850nm y el receptor fueron diseñados de acuerdo con sistemas de medición estandarizados y si conformidad con IEEE 802.3ae (10GBASE-SR) fue confirmada.
- El enlace punto-a-punto pretendido fue montado y simulado para modulación NRZ. Se realizaron más de 5000 iteraciones estadísticas para asegurar la mayor precisión en la resolución (~20 horas en total). Además, curvas de tasa de error (BES) vs. potencia óptica recibida, BER vs. distancia, BER vs. voltaje diferencial de entrada al VCSEL y márgenes de potencia fueron estudiados para tres temperaturas diferentes (-40^{o}C, 25^{o}C and 90^{o}C).
- Adicionalmente, se propuso OFDM como una Buena técnica de modulación para copar con la demanda de ancho de banda y proporcionar la fiabilidad requerida. Su incursión relativamente reciente en las comunicaciones ópticas motive su estudio y evaluación. El enlace fue reanalizado

[4] http://www.d-lightsys.com/

para los formatos de modulación 4-QAM y 16-QAM para cada una de las subportadoras para las tres temperaturas mencionadas. Los resultados son presentados y comparados con NRZ.

1.3 Organización del informe

El resto del informe está organizado como sigue. En el capítulo 2 se presentan los resultados obtenidos y las conclusiones en relación a la elección de la herramienta de simulación.

El capítulo 3 recoge una descripción del proceso de diseño y la comparativa con las especificaciones del estándar IEEE 802.3 (10GBASE-SR).

El capítulo 4 presenta los resultados obtenidos de la simulación del enlace.

Finalmente, en el capítulo 5, se extraen las principales conclusiones de la investigación y se proponen futuras líneas de trabajo.

2 Evaluación de software

Esta sección describe el procedimiento seguido para elegir la herramienta de simulación. Entre los varios aspectos que caracterizan un software de simulación, hay dos especialmente importantes y que la mayoría de las veces suponen un compromiso: precisión y eficiencia. Dada la naturaleza de la red óptica bajo evaluación y las concretas especificaciones eléctricas y ópticas, el hecho de que los resultados se ciñeran a la realidad en la mayor medida posible era especialmente importante incluso a expensas de cierto tiempo de adicional de cálculo. En el contexto del diseño de redes de datos las soluciones exactas son a menudo imposibles de obtener (en términos de recursos de computación) y por consiguiente, todas las suites de simulación usan métodos numéricos elegidos a la discreción del desarrollador que efectúan lo que ellos consideran estimaciones aceptables para, manteniendo la desviación por debajo de cierto umbral, proporcionar soluciones aproximadas. La exactitud de los resultados dependerá de tales técnicas, y deben ser analizados para encontrar aquellos que cumplen mejor con nuestros requisitos.

Como se ha comentado, el tiempo de procesado no es tan relevante aquí como la exactitud. Sin embargo, el tiempo de ejecución no debería ser despreciado e incluso menos cuando se pretende hacer una análisis estadístico tan amplio. Algoritmos eficientes y estructuras modulares agilizan y facilitan los cálculos. El usuario debe establecer los parámetros de acuerdo con la simulación concreta que se pretenda hacer para evitar que datos innecesarios sean procesados.

Otro punto a considerar es la capacidad y facilidad de interacción con productos de terceros (concretamente MATLAB®) debido a la deseada intención de tener control total de la modulación y demodulación en el presente estudio. Esto permitiría aplicar ecualizaciones especiales de canal, aplicación de sistemas de modulación complejos, calculo eficiente de BER, gestión inteligente de la potencia y en general ayuda a alcanzar un entendimiento más profundo de toda la comunicación. Esta característica puede no estar disponible o puede requerir conocimientos de programación o familiaridad con ellos.

Tres posibilidades han sido estudiadas: VPItransmissionMaker™, OptSim™ junto con el modulo ModeSYS™ y nuestra propia implementación del link basada en MATLAB®. A pesar de la flexibilidad y el control que esta última ofrece, se consideró inapropiada como resultado del tiempo necesario solo para crear el escenario correspondiente. Las dos primeras galardonadas herramientas soportan cosimulación con terceros y proporcionan una interfaz gráfica intuitiva y fácil de usar. El principal inconveniente en relación con el uso de suites tan compactas es que se nos permite un nivel limitado de personalización y que los parámetros o su formato no siempre encajan con los que el usuario tiene a su disposición, forzando su adaptación. Otra desventaja es que los módulos son “cajas negras”. Esto significa que los procedimientos matemáticos y algoritmos no son editables, hacienda imposible el entendimiento de la obtención de unos resultados inesperados y, consecuentemente, su optimización o corrección.

La importancia de realizar test similares para ambas piezas de software es digna de mención. Es importante enfatizar que no solo es necesario evaluar cómo de bien los resultados de simulación individuales encajan con los reales sino también cual de las herramientas lo hace mejor. Nuestro interés recae sobre la fuente óptica (VCSEL) y el canal (MMF).

El ancho de banda en una fibra multimodo esta principalmente limitado por efectos dispersivos modales. La precisión del software en la emulación del ancho de banda esta inherentemente ligada a su precisión en la precisión o capacidad de simular DMA, MGD y MPD. Las pruebas deben ser realizadas de tal modo que se permita la comparación directa con el material de referencia; lo cual no es siempre fácil.

El análisis de DMA fue posible gracias a la descripción exacta de los perfiles de índice de refracción y las representaciones gráficas de los resultados en [14]. Con respecto a MGD y MPD, la principal fuente comparativa de información fue el modelo de 108 fibras de la Universidad de Cambridge (Versión 1.2, Octubre 2004). Dicho modelo considera un set de defectos de índice predeterminados que son representativos de aquellos que se encuentran en las fibras multimodo actualmente desplegadas. Se eligió porque es un modelo de canal que plantea un compromiso entre un escenario pesimista y uno optimista [15] y porque permitía hacer dos test con el mismo paquete de datos.

En lo concerniente a los VCSELs, hay tres importantes gráficas que resumen sus características de emisión: luz-intensidad-voltaje (LIV), función de transferencia/s_{21} y espectro de emisión [16]. El modelado de un VCSEL es una ciencia en sí mismo ([17], [18] y [19]) y por ello se requería una aproximación inteligente al problema. La idea fue utilizar valores por defecto para la composición específica del laser a modelar y ajustar inicialmente aquellos parámetros cuyo impacto en las propiedades de emisión fuera conocido o deducible (longitud de onda, temperatura, eficiencia de inyección ganancia, resistencia térmica, corriente umbral, Resistencia de entrada, elementos parasites, anchura espectral, método de polarización y spotsize entre otros). A pesar de la simplificación, debido al gran nivel de interrelación entre todas las variables, encontrar la combinación deseada conllevó un proceso iterativo largo y de gran carga de trabajo.

2.1 Resultados

La Tabla 2-1 muestra los resultados obtenidos para cada uno de los programas y tests realizados. Debido a su gran precisión, posibilidades de configuración, facilidad de uso y buenas referencias, el software finalmente elegido para realizar el diseño y simulación de nuestro enlace fue OptSim™ junto con el modulo ModeSYS™. Un desglose más detallado de las fuentes de información y los procesos de evaluación pueden ser encontrados en el anexo B

Tabla 2-1 Resultados de las pruebas efectuadas a las herramientas de simulación.

Módulo	Test	VPItransmissionmaker	OptSim (ModeSYS)
MMF	Atenuación modal diferencial (DMA)	No implementado	95%+ precisión
	Retraso de grupo modal (MGD)	50% cumplen 10 perct.	5% precisión en factores de escala
	Distribución de potencia de modos (MPD)	Desviación 2 avg. / 4 max.	Desviación 0.36 avg. / 1 max.
VCSEL	L-I-V & S21	VCSEL 850nm no implementado	Ok

2.2 Conclusión

Las pruebas realizadas muestran que ModeSYS™ ofrece una modelo de MMF considerablemente más preciso. A diferencia de VPITransmissionmaker™, ModeSYS™ tiene implementado un algoritmo DMA basado en la formula empírica encontrada en [20]. Los resultados de la simulación coinciden con aquellos en [14].

La diferencia de precisión en relación al MPD es abrumadora. El número de errores en la excitación de grupos de modos degenerados (DMG) es 2 para VPItransmissionmaker™ con una desviación máxima de 4 DMGs de alto orden. Por su parte, el número medio de errores con ModeSYS™ es 0.36 con una desviación máxima de 1 DMG de alto orden.

La prueba de MGD fue la más complicada de realizar. Se ha probado que VPItransmissionmaker™ ofrece un rendimiento pobre en el cálculo del retraso relativo de modos cuando se utilizan perfiles de índice de refracción particulares. Aproximadamente el 50% de las fibras analizadas no satisfacen el percentil 10. Con respecto a ModeSYS™, los datos a nuestra disposición junto con el formato particular en el que venían dados en el material de referencia impedía una comparación fiable y rápida. Para comprobar el buen funcionamiento, tres publicaciones que probaban el soporte complete del modelo de 81 fibras de la Universidad de Cambridge por parte de ModeSYS™ fueron consultadas y analizadas. Se muestra un error en los factores de escala de los índices de refracción de menos del 5% para tres tipos de fibra diferentes. Además, se estudiaron dos notas de aplicación llamadas “CambridgeModel_case1” y “CambridgeModel_case2” que investigan el efecto de los defectos en el índice en el ancho de banda de la fibra y posteriormente en el diagrama de ojo para enlaces de datos con tasas concretas de modulación. Dichas notas de aplicación trabajan específicamente con el modelo de canal distribuido por la Universidad de Cambridge y muestran de forma clara la similitud y correspondencia de los resultados.

Las pruebas sobre el modulo de VCSEL confirmaban que ModeSYS™ era la mejor opción. Mientras que es imposible emular un VCSEL a 850 con el modulo por defecto proporcionado en VPItransmissionmaker™, ModeSYS™ ofrece un modelo matemático completo que además tiene en cuenta variaciones espaciales de la distribución de campo, algo necesario para estudiar el acoplo de modos en una fibra multimodo. Las propiedades físicas fueron analizadas (LIV y s_{21}) así como su rendimiento en un enlace de comunicación de datos.

3 Diseño

Tras garantizar la precisión de los algoritmos y las aproximaciones numéricas usadas en ModeSYS™ para los componentes críticos, esos mismos elementos y el resto de bloques fueron diseñados de acuerdo a las especificaciones y requisitos establecidos dentro del marco de trabajo del proyecto DAPHNE.

En primer lugar se presenta el diseño del transceptor (VCSEL y receptor) y de la fibra multimodo. A continuación, se muestra la conformidad con el estándar 10GBASE-SR. Finalmente se explican los principales aspectos considerados en el modem OFDM.

El anexo C muestra un desarrollo completo de los esquemáticos utilizados, las especificaciones y los procedimientos seguidos para el diseño y comprobación de la conformidad con IEEE 802.3ae (10GBASE-SR) de cada uno de los componentes.

3.1 VCSEL

Los transceptores, los cuales integran un VCSEL AlGaAs a 850nm, son producidos por la compañía francesa D-Lightsys™. Son parte del consorcio del proyecto DAPHNE y son los responsables de desarrollar un módulo a 10Gbps que satisfaga los severos requisitos ambientales. El objetivo es cumplir el estándar 10GbE al tiempo que se logra compatibilidad con las exigentes condiciones aeroespaciales. El producto no es comercial y por lo tanto solo se mostrarán los parámetros estrictamente necesarios respetando el acuerdo de confidencialidad.

A diferencia de la verificación del modelo de VCSEL llevada a cabo durante la evaluación del software, en este caso disponíamos de los rangos operativos eléctricos y ópticos en lugar de las curvas LIV y funciones de transferencia. Esas especificaciones proporcionan los valores típicos y los peores casos para un grupo muy concreto de parámetros tales como longitud de onda de emisión, anchura espectral, potencia óptica de salida, voltaje diferencial de entrada, capacidad de entrada, tiempo de subida/caída, amplitud de modulación óptica (OMA) y ratio de extinción (ER) entre los más relevantes. Sin embargo, y a pesar de la completa descripción de funcionamiento proporcionada, los datos eran ligeramente insuficientes para diseñar el diodo laser con precisión suficiente. Por ejemplo, se daba el valor típico para la potencia óptica media de salida pero se desconocía el valor exacto de la corriente de polarización y la temperatura a la que ese valor fue tomado. Este tipo de situación hizo el proceso de diseño considerablemente complicado y algunos valores tuvieron que ser asumidos.

3.1.1 Resultados

Las especificaciones para los bloques principales de acuerdo con las hojas de datos se presentan en Tabla 3-1 ([5]):

[5] Los números en negrita representan estimaciones.

Tabla 3-1 Resumen de las especificaciones de los bloques principales en el transmisor.

Bloque	Parámetro	Min	Típico	Max	Unidad
PRBS	Longitud	-	2^{11}-1	-	-
	Tasa de transmisión	0.5	-	10	Gbps
Generador eléctrico	Tipo de flanco	-	Rampa On/off	-	-
	Voltaje diferencial	100	**600**	950	mV
	Tiempo de subida/bajada ([6])	-	**30**	45	UI ([7])
	Jitter	**0**	**-**	0.6	UI
VCSEL	Longitud de onda	840	850	860	nm
	Máxima anchura espectral	-	-	0.85	nm
	Mínimo OMA	-4.3	-	-	dBm
	Típico ratio de extinción	3	5	-	dB
	Potencia de salida media	-4	-2	-0.7	dBm
	Temperatura	-40	**25**	90	°C
	Variación máxima de la potencia óptica de salida dentro del rango de temperaturas especificado	-	0.5	1	dB
	Corriente de polarización	-	**8**	**9**	mA
	Respuesta de modulación ([8])	-	**11±1**	-	GHz

No se daba ninguna información sobre el tamaño de haz o la distribución espacial de los campos en la apertura, de modo que se asumió absoluta flexibilidad en este aspecto.

Los resultados numéricos para los valores típicos se recogen en la Tabla 3-2

Tabla 3-2 Valores típicos para el modulo VCSEL.

Bloque	Parámetro	Valor	Unidad
VCSEL	Longitud de onda	850	nm
	Anchura espectral ([9])	<0.85	nm
	Resistencia serie	70	Ω
	OMA	-2.7	dBm
	ER	3.6	dB
	Potencia óptica de salida media	-1.5	dBm
	Temperatura	25	°C
	Variación máxima de la potencia óptica de salida dentro del rango de temperaturas especificado ([10])	0.25/0.995	dB
	Corriente de polarización	8	
	Voltaje diferencial de entrada	600	mV

[6] Los tiempos de subida/bajada y el jitter se especifican como características ópticas. Debido a la imposibilidad de realizar su ajuste en el dominio óptico, estos dos parámetros son aplicados en el generador de señal eléctrico.
[7] Unit Interval. Tiempo normalizado al periodo de la tasa de transmisión.
[8] Ancho de banda para Corrientes de polarización dentro del intervalo predefinido [8mA, 9mA].
[9] La anchura espectral no ha sido especificada porque es completamente ajustable con módulos incluidos en el software
[10] Para -40°C y 90°C respectivamente

	Respuesta de modulación	10.2	GHz

Nótese que 10Gbps es al máximo flujo de datos nominal conseguible. Esto significa que no es posible lograr el valor típico de ER (5dB) debido a la elevada corriente de polarización necesaria para situar la respuesta de modulación del laser por encima de los 10GHz. Esto, a su vez, es la razón por la ligeramente elevada potencia media de salida. La curva LI resultante para 25°C, -40°C y 90°C y el s_{21} (25°C and 8mA) son mostrados en Ilustración 3-1.

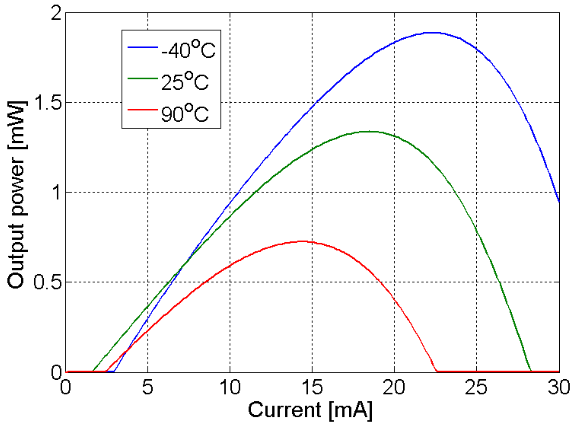

Ilustración 3-1 Curva LI simulada y respuesta de modulación de pequeña señal.

La variación de potencia con la temperatura ha sido calculada para una corriente fija de polarización de 8mA; sin embargo, dichas diferencias pueden variar dependiendo de la intensidad de corriente utilizada. A pesar de que se observa en Ilustración 3-1 que las diferencias se reducen claramente para menores corrientes, también se muestra que la corriente umbral aumenta y el ancho de banda disminuye para 90°C y -40°C. La consecuencia es que aparece un compromiso ente estabilidad térmica ratio de extinción y ancho de banda de modulación.

La variación de la respuesta de modulación para 7mA, 8mA y 9mA a 25°C así como el diagrama de ojo óptico con jitter desactivado se muestra en Ilustración 3-2.

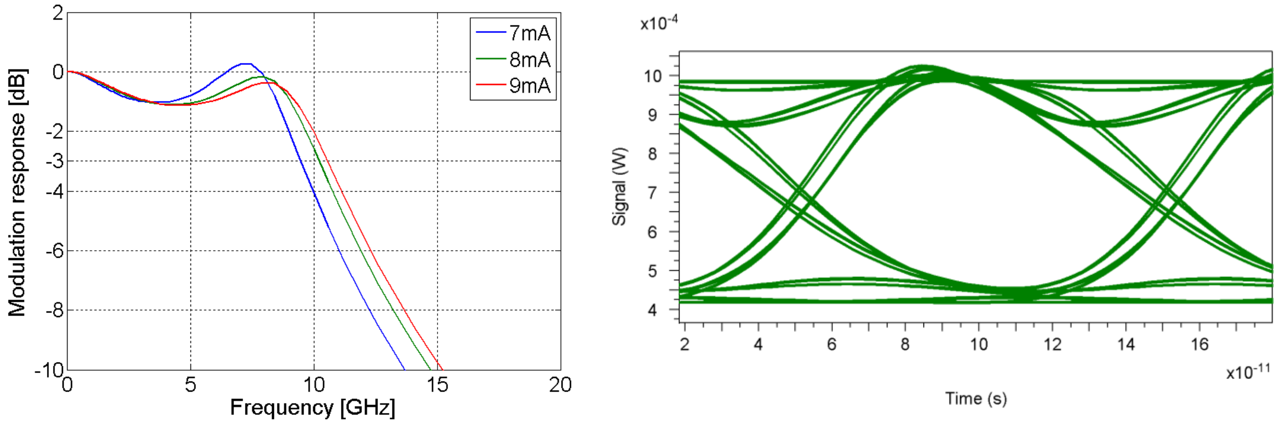

Ilustración 3-2 Respuesta de modulacion de pequeña señal a a 25oC para 7mA, 8mA y 9mA de corriente de bias (izquierda). Diagrama de ojo óptico con jitter desactivado (derecha).

Se observa que se necesita 8mA o más para conseguir más de 10GHz de ancho de banda. Dado que uno de los retos del proyecto DAPHNE es crear un sistema que pueda soportar tasas desde los kbps hasta los Gbps, se debería considerar la posibilidad de implementar un sistema inteligente para adaptar la corriente de bias dependiendo del flujo de datos requerido. Esto también sería beneficioso para reducir el estrés del diodo laser.

3.2 Receptor

El transceptor incluye fotodiodos PIN GaAs y electrónica CMOS de bajo consume para la conversión de corriente. El filtro paso bajo después del amplificador no está integrado y debe ser acoplado externamente. La tarea de diseño comprende la determinación de la responsividad, potencia de ruido, ganancia y la frecuencia de corte y orden del filtro.

Los rangos de operación ópticos y eléctricos fueros proporcionados en la hoja de datos. El VCSEL previamente diseñado fue utilizado para el diseño del propio receptor.

3.2.1 Resultados

Las especificaciones se recogen en la Tabla 3-3 ([11]).

Tabla 3-3 Especificaciones del receptor.

Parámetro	Min	Típico	Max	Unidad
Longitud de onda	760	850	860	nm
Máxima anchura espectral	-	-	1	nm
Máxima potencia óptica media	**-5**	**-3**	0	dBm
Sensibilidad óptica a 10Gbps	-	-15	-12	dB
Voltaje diferencial de salida	200	400	700	dBm

Tabla 3-4 Valores de configuración del receptor.

Parámetro	Típico	Unidad
Eficiencia cuántica	0.98	%
Transimpedancia	1600	Ω
Potencia de ruido	9.5E-23	A^2/Hz
Frecuencia de corte	12.3	GHz
Orden del filtro	Bessel 5	0

La eficiencia cuántica fue fijada de acuerdo a las indicaciones en [21], donde se declara el excelente rendimiento (cerca del 100% de eficiencia) de los fotodetectores PIN de GaAs en el entorno de los 600nm a los 900nm. El valor fue ajustado para coincidir con la respuesta querida

[11] Los números en negrita representan estimaciones.

Para la determinación de la transimpedancia, los valores típicos de funcionamiento fueron cargados en el modulo VCSEL y la potencia de salida regulada con un modulo software específico. Los valores típicos y mínimos de la potencia óptica fueron igualados con potencia de salida media del VCSEL menos 1dB. Tras la comprobación de los resultados para todo el rango de voltajes, la mejor respuesta se observó para 1600Ω.

La potencia de ruido viene representada por el primer coeficiente (y el único contemplado) de la aproximación polinómica de su densidad espectral de potencia. Su cálculo fue realizado para una potencia de entrada de -15dBm con una modulación NRZ a 10Gbps. Aquel valor para el que el BER igualaba 10^{-12} era el resultado buscado.

3.3 MMF

Se requería que la fibra multimodo fuera del tipo OM4 de acuerdo a ISO/IEC 11801. Tal fibra es la fibra multimodo optimizada para laser (LOMMF) con el mayor producto ancho de banda por kilómetro comercialmente disponible. Su diseño necesita la mayor exactitud en el ajuste de variables y métodos de medición muy específicos.

La información sobre los parámetros generales fue obtenida a través de la página web de Draka Communication, donde se pueden encontrar hojas de datos para fibras anticurvatura OM2/OM2+/OM3/OM4, OM1/OM2 y estándar OM2+/OM3/OM4 (MaxCap-OMx). La fibra anticurvatura fue elegida como la más apropiada para nuestro caso. La información en la hoja de datos de Draka fue contrastada con la de Corning para asegurar la conformidad y completar campos. Los datos obtenidos sirvieron como un ajuste grueso al modelo deseado. Los rangos de valores típicos para parámetros como el coeficiente de atenuación, apertura numérica (NA), pendiente en el punto de dispersión cero e índice de refracción de grupo fueron encontrados.

En lo concerniente a la validación del tipo de fibra, se utilizó el método retraso diferencial de modos (DMD). La máxima tasa de datos de 10Gbps y la simplicidad de la técnica, situó a DMD por encima de ancho de banda modal efectivo computado (EMBc); que es mucho más complejo y abierto a interpretación [22].

3.3.1 Resultados

La gran flexibilidad que el software ofrece permite incluso la creación de perfiles de índice que cancelen totalmente la interferencia intersimbólica (ISI), es decir, guías de onda perfectas sin ninguna distorsión. Debido a ello, se eligió un set no ideal que generara valores de DMD dentro del rango de lo marcado en las especificaciones y no 0ps/m. Era importante lograr un perfil realista debido a su posterior utilización en la simulación de un enlace real. Para OM4, los retrasos particulares están todavía bajo discusión pero un primer borrador ha sido lanzado (Tabla 3-5).

Tabla 3-5 Especificaciones DMD para fibra OM4.

Especificación	DMD interno (ps/m)	DMD externo (ps/m)	DMD intermedio (ps/m)
1	≤0.10	≤0.30	≤0.11
2	≤0.11	≤0.17	≤0.11
3	≤0.14	≤0.14	≤0.11

La gráfica DMD externa resultante, la extensión acumulada y el ancho de pulso sin DMA se muestran en la Ilustración 3-3.

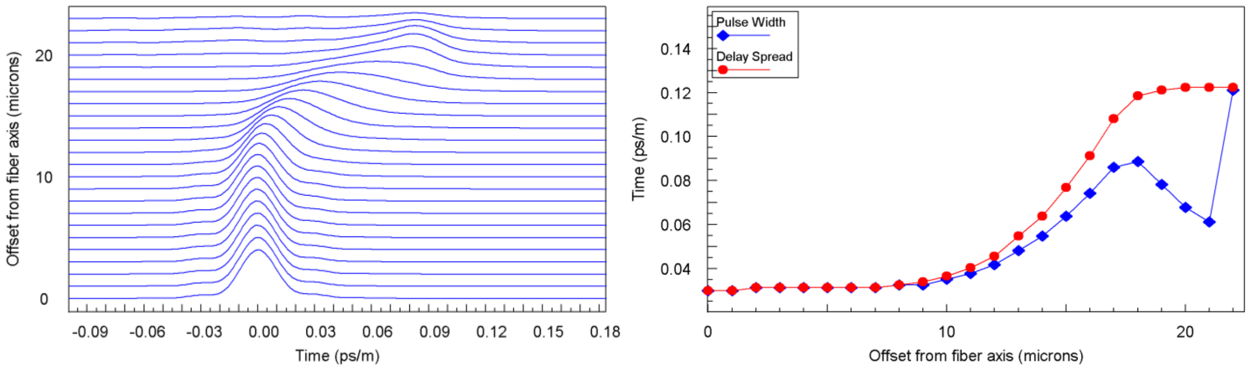

Ilustración 3-3 Gráfico DMD (izquierda), extensión de retraso acumulada (derecha, rojo) y anchura de pulso (derecha, azul) para la fibra OM4 simulada.

Se puede ver en el gráfico DMD que el retraso acorre para desplazamientos en la inyección iguales o mayores de 13µm. Esto significa que el problema esta principalmente causado por los DMGs de alto orden. En este caso, la activación de DMA podría mejorar el ancho de banda de la fibra considerablemente. A pesar de la distorsión, se puede observar que la extensión de retraso acumulado que nunca supera 0.12ps/m por lo tanto cumpliendo con los requisitos establecidos para DMD externo para fibras OM4. Un efecto interesante que se puede nota es el decremento y el repentino incremento del ancho de pulso que tiene lugar a partir de 18µm en adelante y que, a su vez, se puede ver en el gráfico DMD. Conforme el rayo se aproxima la intercara núcleo-cubierta, parte de la luz se radia y no contribuye al ensanchamiento de pulso. SI el efecto es muy severo, el nivel de potencia se reduce drásticamente y de ahí el nivel de referencia (establecido en la cuarta parte del máximo), que al seguir siendo calculado por el software, genera anchuras de pulso extremadamente grandes. La recomendación es descartar aquellos valores y, en general, aquellos para puntos de inyección cercanos a la cubierta.

El mismo análisis se realice para cada una de las secciones de la fibra. Los retrasos resultantes y los parámetros finales de la fibra diseñada se recogen en Tabla 3-6 y Tabla 3-7.

Tabla 3-6 Resultados DMD del modelo OM4.

DMD interno (ps/m)	DMD externo (ps/m)	Max. DMD intermedio (ps/m)
0.117	0.121	0.066

Tabla 3-7 Lista de parámetros del modelo OM4.

Parámetro	Valor	Unidad
Atenuación (850nm)	2.1	dB/km
Longitud de onda de dispersión cero	1315	nm
Pendiente en el punto de dispersión cero	0.102	$ps/nm^2 \cdot km$
Índice de refracción de grupo	1.480	-
Diferencia en el índice de	1	%

refracción		
Índice de refracción del núcleo	1.481	-
Exponente del perfil	2.065	-
Parámetro de dispersión del perfil	0.07	-

De acuerdo a la recomendación IEC 60793-1-49, la fibra diseñada cumple con los requisitos de una fibra multimodo OM4.

3.4 10GBASE-SR

La seguridad se vuelve especialmente importante cuando nos hablamos de sistemas aerotransportados. En este aspecto, construir una red en conformidad con un determinado estándar garantiza un riesgo funcional cero cuando el peor caso de componentes es conectado. Por esta razón, muchos fabricantes de aviones establecen como prerrequisito para sus componentes la certificación de un determinado estándar internacional.

Actualmente, un estándar basado en Ethernet y de seguridad crítica llamado Avionics Full-Duplex Switched Ethernet (AFDX) está siendo satisfactoriamente utilizado por compañías como Airbus y Boeing para transmisiones hasta 100Mbps; sin embargo, no existe ninguna regulación para enlaces a 10Gbps trabajando en el amplio rango de temperaturas y entorno agresivo que se encuentra en aviones; aunque SAE International ha empezado a desarrollar un numero de estándares WDM-LAN [23]. Sin embargo, y dado que la mayor parte de los sistemas ópticos aviónicos desplegados son enlaces MMF punto-a-punto a 850nm [24], parecía razonable pensar en IEEE 802.3ae con 10GBASE-SR como una buena primera aproximación

IEEE 802.3ae proporciona apoyo para extender el protocolo convencional IEEE 802.3 (Ethernet) y las especificaciones MAC para su operación a 10Gbps sobre fibra óptica. Dentro de la descripción del estándar, se proponen varias implementaciones para la capa física pero nuestro interés recae exclusivamente en transmisión LAN serializada a 850nm (10GBASE-SR).

(CONTINÚA EN LA SIGUIENTE PÁGINA)

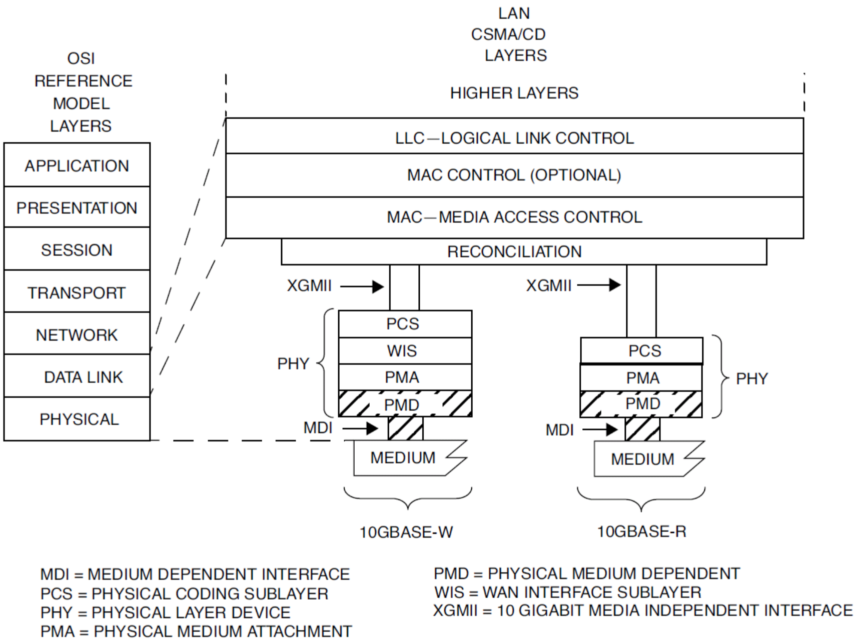

Ilustración 3-4 Relación de 10GBASE-S, -L, y -E PMDs con el modelo de referencia ISO/IEC Open SystemsInterconnection (OSI) y el modelo IEEE 802.3 CSMA/CD LAN [25].

Una de las subcapas de la capa física se llama dependiente del medio físico (PMD) y establece las especificaciones eléctricas y ópticas para el transceptor así como los márgenes de potencia y distancias de operación mínimas. Esos valores son recogidos y presentados en el anexo C.4 con aquellos generados en la simulación para probar la complete conformidad con el estándar. La verificación del resto de subcapas e intercaras se ha considerado fuera del alcance de esta investigación. Los resultados muestran la total conformidad con el mencionado estándar.

3.5 Optical Orthogonal Frequency-Division Multiplexing (OOFDM)

Con la intención de tener completo control sobre la modulación/demodulación y permitir adaptabilidad y futuras modificaciones, la implementación de OFDM fue hecha en MATLAB®.

3.5.1 Modulador

La determinación de los parámetros de diseño de OFDM está directamente influenciada por, la mayor parte de las veces, requisitos encontrados. Por lo tanto, antes de diseñar el modulador es necesario determinar valores específicos o rangos para al menos el ancho de banda disponible, la tasa de transmisión deseada y el ensanchamiento acumulado de pulso.

El ancho de banda disponible en nuestro sistema está principalmente por el VCSEL, que ha sido modelado para ofrecer una respuesta de modulación a 3dB de 11±1GHz. La limitación del receptor está causada por el filtro paso bajo, cuyo máximo ancho de banda ha sido establecido a 12.3GHz de acuerdo a las especificaciones de 10GBASE-SR.

Por su parte, la máxima variación de tasa de transmisión que 10GBASE-SR puede soportar es ±100ppm, lo que fija la velocidad nominal de señal entre 10.3135Gbps y 10.3115Gbps.

Finalmente, el máximo ensanchamiento de pulso acumulado viene determinado por el DMD. De acuerdo a los cálculos en la sección 3.3.1, el peor caso es 0.121ps/m. Para prevenir la ocurrencia de interferencia intersimbólica e interportadoras, se amplió hasta los 0.14ps/m. Por definición, la longitud del prefijo cíclico se elige de modo que iguale o exceda la dispersión máxima del canal I a menudo se expresa como un porcentaje de la duración total del símbolo.

En concordancia con los requisitos de crear una red de bajo coste, se eligió la modulación directa del laser como el método más apropiado. Sin embargo, esto implicaba la adaptación del modulador para crear una señal unipolar. Además, se implemento modulación discreta multitono (DMT) para eliminar el modulador I/Q y reducir el coste todavía más.

3.5.2 Demodulador

La simetría inversa mostrada por el demodulador con respecto al modulador clarifica la elección de los parámetros más generales. Por otro lado, hay algunos aspectos como el método de cálculo del BER o la estimación delo punto de muestreo que son inherentes a esta parte.

Es común incluir la recepción de la señal (captación de la luz, down-conversion cuando sea necesaria y filtrado) en el diseño del demodulador, pero en nuestro caso fue realizado a través de ModeSYS™. Este hecho simplificó la codificación notablemente. Los únicos bloques que debían ser implementados eran la conversión analógico-digital, FFT, ecualización y el cálculo del BER.

3.6 Conclusión

Se ha conseguido una gran similitud con los valores deseados y especificaciones en el diseño de MMF, VCSEL y receptor. Para el transceptor, valores muy concretos para la mayor parte de los parámetros fueron proporcionados en las hojas de datos. Los resultados fueron comparados y la conformidad probada. El grado de libertad en las variables de diseño de la MMF era total con la condición de que los rangos se mantuvieran dentro de límites realistas y que el rendimiento cumpliera con los requisitos del tipo OM4. Los resultados muestran que las especificaciones DMD son cumplidas.

Los componentes diseñados muestran un complete cumplimiento de los requerimientos en IEEE 802.3ae (10GBASE-SR).

Los parámetros OOFDM fueron adaptados consistentemente de acuerdo a los rangos I/O de los componentes del enlace. Los valores que exclusivamente afectaban a OOFDM fueron ajustados en base a los rangos convencionales observados en diversas publicaciones

4 Simulación y resultados

En esta sección se muestran y desarrollan los resultados obtenidos en la simulación final del enlace. Está subdividida en dos partes de acuerdo al formato de modulación. La primera corresponde a NRZ, donde las peores situaciones son presentadas así como un completo análisis estadístico para tres temperaturas diferentes (25^{o}C, -40^{o}C y 90^{o}C) y márgenes de potencia. El estándar 10GBASE-SR se utilizó como referencia a lo largo de todo el proceso para establecer límites prácticos para la simulación y asegurar la conformidad en los casos más exigentes. La segunda parte introduce el modem OOFDM en el enlace.

4.1 Non-Return-to-Zero (NRZ)

El test con NRZ tiene dos objetivos principales: asegurar el buen funcionamiento del sistema para el caso más básico de modulación en amplitud y servir como comparación para el posterior estudio de OOFDM. Además, hacer un análisis amplio y preciso consolida las bases para futuras implementaciones o pruebas y simulaciones adicionales. Por lo tanto, contemplar los peores casos, márgenes de potencia y realizar un intenso estudio estadístico era muy importante.

4.1.1 Esquemático

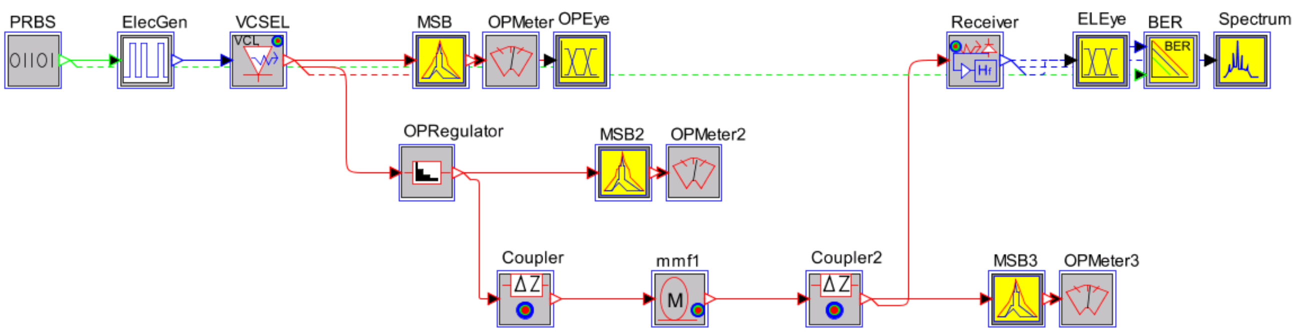

Ilustración 4-1 Esquemático de la simulación NRZ final.

El primer bloque del sistema es un generador de secuencias pseudoaleatorioas que lanza una señal binaria de longitud 2^{11}-1. El convertidor binario-eléctrico viene a continuación. La señal eléctrica se inyecta en el VCSEL a través de un modelo ideal de bias-T para generar la señal óptica. El "OPRegulator" emula el control de la potencia de salida integrado en el transceptor. La señal puede ir al receptor directamente para similar B2B o a un acoplador especial que le da una dimensión especial a la potencia óptica de entrada para, de ese modo, realizar un acoplo de los modos a la fibra OM4. El acoplador especial a la salida de la fibra sirve para tener en cuenta la influencia de la distribución especial de los campos en la recepción de la luz dada una apertura circular concreta en el fotodiodo. Finalmente, la luz se transforma en señal eléctrica, se amplifica y se filtra.

4.1.2 Resultados

La evaluación se ha dividido en dos partes. En la primera se muestra y discute el BER para corrientes de polarización del VCSEL de 7mA, 8mA y 9mA así como el BER en función de la longitud de fibra utilizada. Esto permite el establecimiento de los peores escenarios que se analizan estadísticamente en la segunda parte.

4.1.2.1 25ºc

Los parámetros de transmisión son fijados a los valores típicos recogidos en Tabla 3-1 y Tabla 3-2. La Ilustración 4-2 muestra el BER vs. potencia óptica de entrada y el BER vs. voltaje diferencial de entrada al laser.

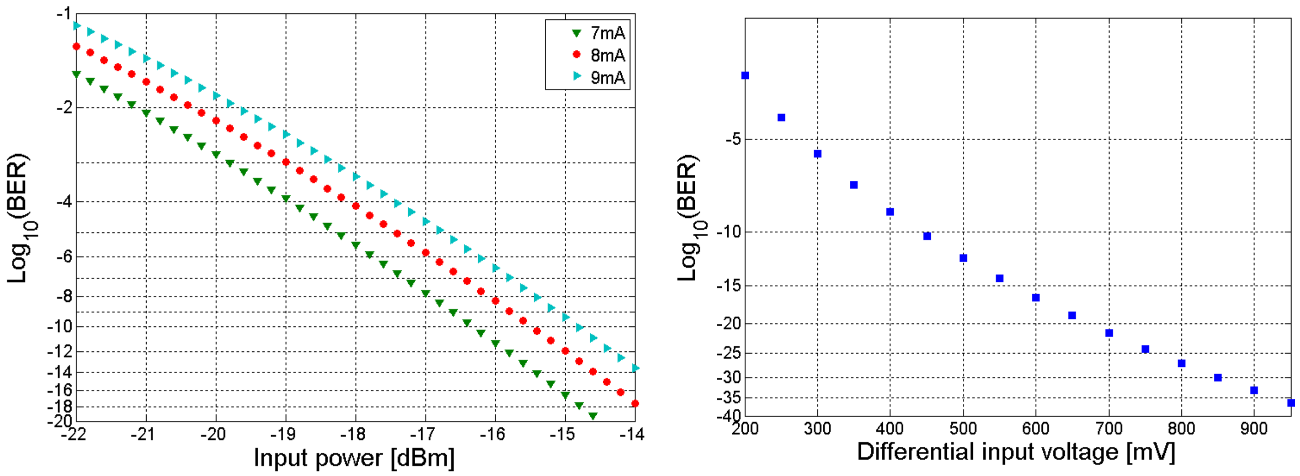

Ilustración 4-2 BER vs. Potencia óptica de entrada (izquierda). BER vs. Voltaje diferencial de entrada al VCSEL. 25°C.

A pesar de haber fijado 8mA como valor típico de corriente de bias, se observa en Ilustración 4-2 como el ratio de error disminuye conforme la intensidad decrece. Esta tendencia se mantiene hasta aproximadamente 6mA pero por razones de seguridad se fijó 7mA como la mínima considerable. Para confirmar que la reducción de la corriente de polarización no producía saturación en el VCSEL para ningún valor de voltaje de entrada, se realizó un test de BER en función de dicho voltaje diferencial para la potencia de sensibilidad. Los resultados muestran que la curva decrece monotónicamente sin aparentes puntos de inflexión. Estos Buenos resultados permiten establecer 7mA como la corriente de polarización optima para 25°C. Con 7mA, la sensibilidad queda fijada alrededor de los -16dBm lo que ofrece un margen de potencia de 9.9dB para 700m de OM4 y 0.3dB de perdidas por conector de acuerdo a dos tipos diferentes conectores aeroespaciales comerciales (MC5 y la familia AVIO/AVIM).

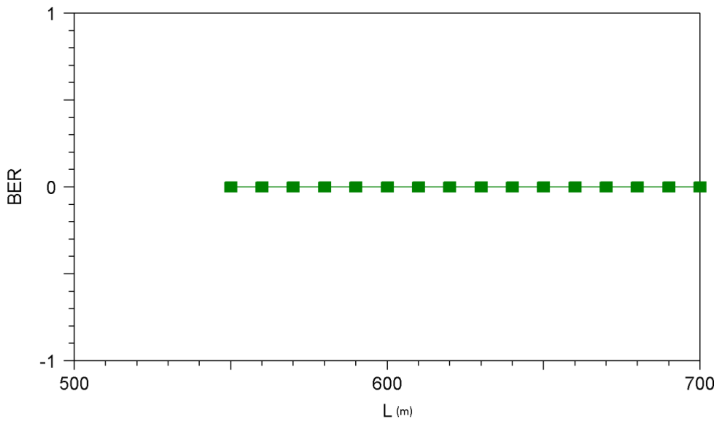

Ilustración 4-3 BER vs. Longitud de fibra MMF. 25°C.

En el siguiente test se comprobó el BER en función de la longitud de la MMF y mínima potencia de salida en el laser (-4dBm). La Ilustración 4-3 muestra los resultados donde se observa que el ratio de error es cero.

Análisis estadístico

En un primer lugar se evaluaron los efectos de la variabilidad de los parámetros más importantes del sistema, no dándoles un valor fijo sino un rango de valores determinado por las hojas de datos o por investigaciones y consultas previas. Posteriormente, con el fin de evaluar la influencia de las vibraciones e impactos en la calidad de la comunicación, el estudio se centró en la desalineación en los conectores al ser los puntos más críticos/débiles de la transmisión. En todos los casos se utilizó distribución gaussiana para la con una desviación típica notablemente exagerada para descartar cualquier caso que pudiera tener lugar en un montaje real.

RANGOS DE OPERACIÓN

La Tabla 4-1 muestra las variables estudiadas organizadas por módulos. Se presenta la media de la distribución gaussiana y la desviación típica utilizada.

Tabla 4-1 Media y desviación típica de la distribución gaussiana de las variables analizadas.

Bloque	Descripción	Media	Desviación estándar	Unidad
VCSEL	Longitud de onda	850	10	nm
	Resistencia serie	70	10	Ω
	Parásitos	1.1	0.1	pF
	Tamaño de haz	12	1	µm
OM4	Radio	25	1	µm
	Atenuación	2.1	0.1	dB/km
	Pendiente en el punto de dispersión cero	0.102	0.001	$ps/nm^2 \cdot km$
	Longitud de onda de	1315	5	nm

	dispersión cero			
	Índice	1.481	0.002	-
	Exponente de perfil	2.065	0.002	-
Receptor	Ganancia	1600	100	Ω
	Ancho de banda del LPF	10	0.5	GHz

El barrido después de 1200 iteraciones se muestra en Ilustración 4-4. Se observa que ninguna muestra supera un ratio de error de 10^{-12}. El menor margen de potencia obtenido es 7.5dB.

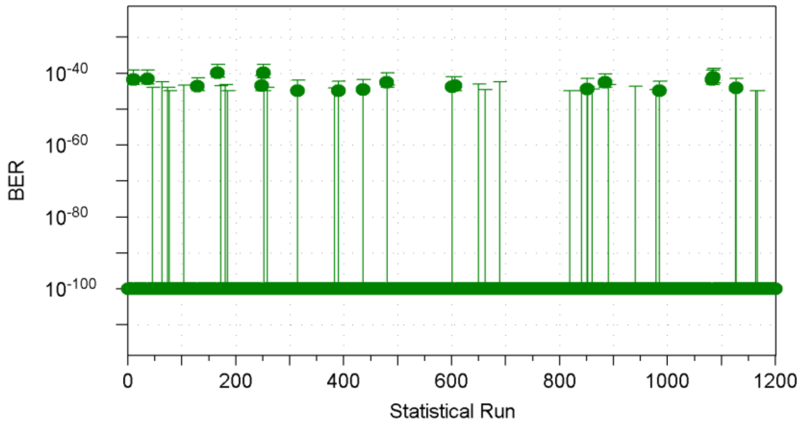

Ilustración 4-4 BER después de 1200 muestras estadísticas. Rangos de operación. 25°C.

CONECTORES

Los valores medios de desalineación y las desviaciones típicas de la distribución gaussiana se muestran en Tabla 4-2. Para el resto de parámetros que no involucraban a los conectores, su valor fue fijado al típico.

Tabla 4-2 Media y desviación típica de la distribución gaussiana de las desalineaciones analizadas.

Descripción	Media	Desviación estándar	Unidad
X-axis offset	0	5	µm
Y-axis offset	0	5	µm
Z-axis offset	0	5	µm
X angular	0	3	grados
Y angular	0	3	grados
Pérdidas de inserción	0.3	0.05	dB

La Ilustración 4-5 muestras los resultados después de 600 iteraciones. A pesar de que el valor medio es bastante parecido al de FIGURE, el valor máximo es sensiblemente mayor ($1.54 \cdot 10^{-8}$). Con el objetivo de averiguar cuál de las desalineaciones tenía mayor influencia, se realizaron tests independientes que demostraron que se necesita una desafortunada combinación de los tres tipos de desalineación para producir BER mayores de 10^{-12}

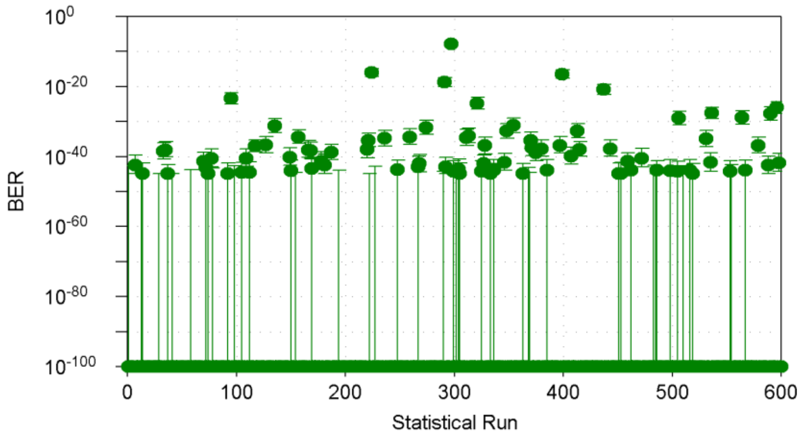

Ilustración 4-5 BER después de 600 muestras estadísticas. Conectores. 25°C.

4.1.2.2 -40ºc

La Ilustración 4-6 muestra el BER vs. potencia óptica de entrada y el BER vs. voltaje diferencial de entrada al laser.

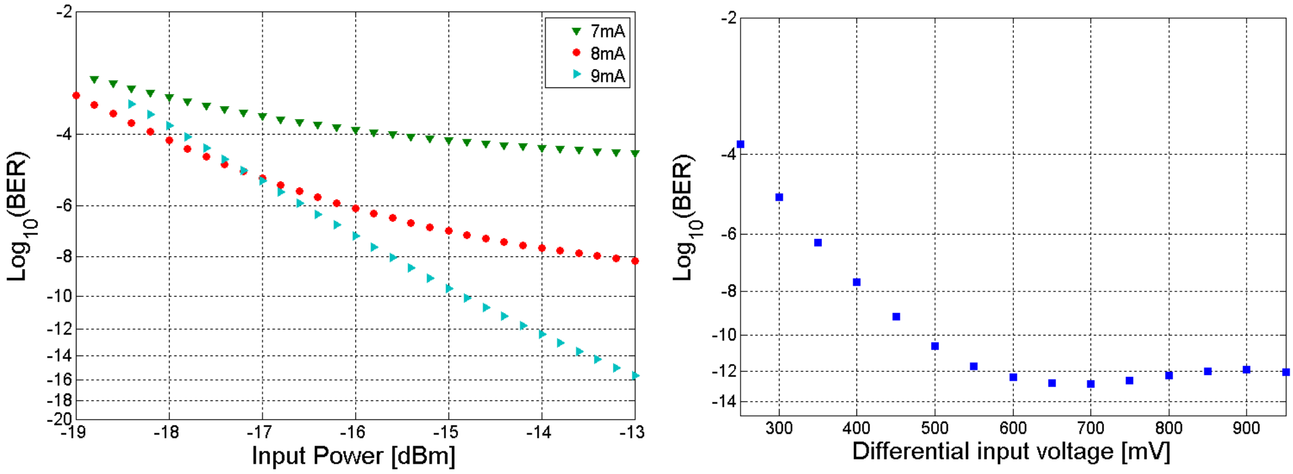

Ilustración 4-6 BER vs. Potencia óptica de entrada (izquierda). BER vs. Voltaje diferencial de entrada al VCSEL. -40°C.

La variación de temperatura a -40°C tiene varios influyentes efectos en el comportamiento del VCSEL: reduce la respuesta de modulación, aumenta la corriente umbral y reduce la resistividad. La dos primeras general la necesidad de elevar la corriente de polarización a 9mA para alcanzar los anchos de banda necesarios para transmitir a 10.3125Gbps y para alejar el punto de trabajo del umbral, de forma que se aumente el factor de amortiguamiento y se reduzcan los overshootings e irregularidades en el diagrama de ojo. El último efecto hace que para un mismo rango de tensión diferencial de entrada, la corriente inyectada sea sensiblemente mayor y, por lo tanto, se llegue a situaciones de saturación con mucha más facilidad. Esto se muestra en el gráfica BER vs. Voltaje diferencial de entrada (a -14dBm y 9mA) en FIGURE, donde se aprecia que a partir de los 650mV la tasa de error se estabiliza e incluso empeora.

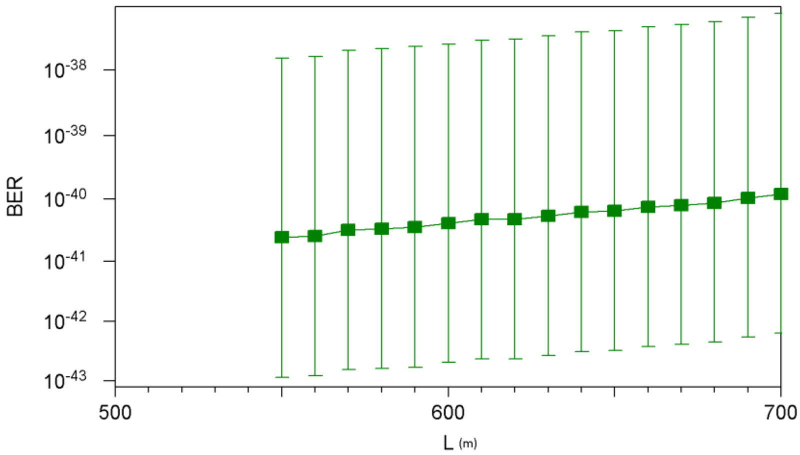

Ilustración 4-7 BER vs. Longitud de fibra MMF. -40ºC.

Siguiendo las mismas pautas que para 25ºC, se realizó el test a mínima potencia de salida del VCSEL para diversos puntos entre la mínima y máxima distancia de MMF permitida por 10GBASE-SR. Los resultados muestran una transmisión libre de error y con un margen de potencia mínimo de 7.9dB.

Análisis estadístico

RANGOS DE OPERACIÓN

El mismo proceso se realizó para -40ºC y los valores de las medias y desviaciones típicas se mantuvieron. La Ilustración 4-8 muestra el barrido estadístico y el correspondiente histograma para -4dBm de potencia de salida del laser, 700m de MMF, 9mA de bias y 600mV de voltaje diferencial de entrada.

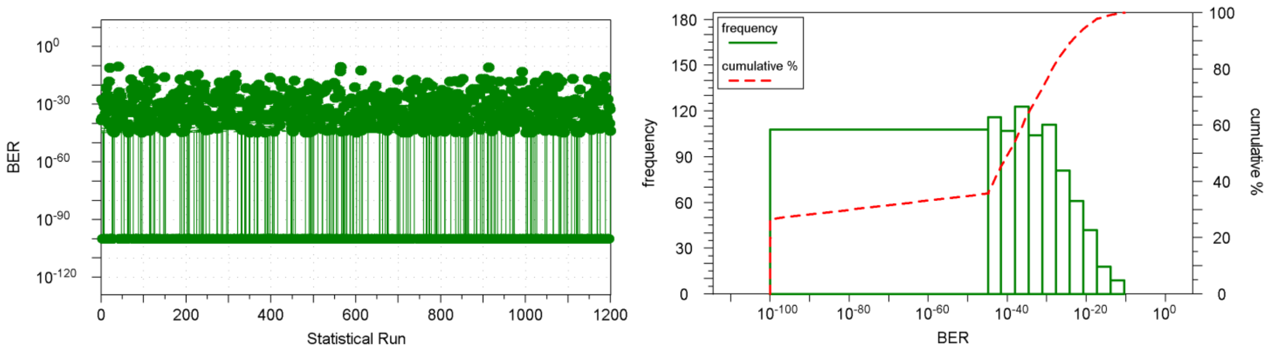

Ilustración 4-8 BER después de 1200 muestras estadísticas. Rangos de operación. -40ºC.

La máxima tasa de error es $4 \cdot 10^{-11}$. El histograma muestra que más del 94% de las muestras están por debajo de 10^{-20} siendo solo cuatro las que superan 10^{-12}.

CONECTORES

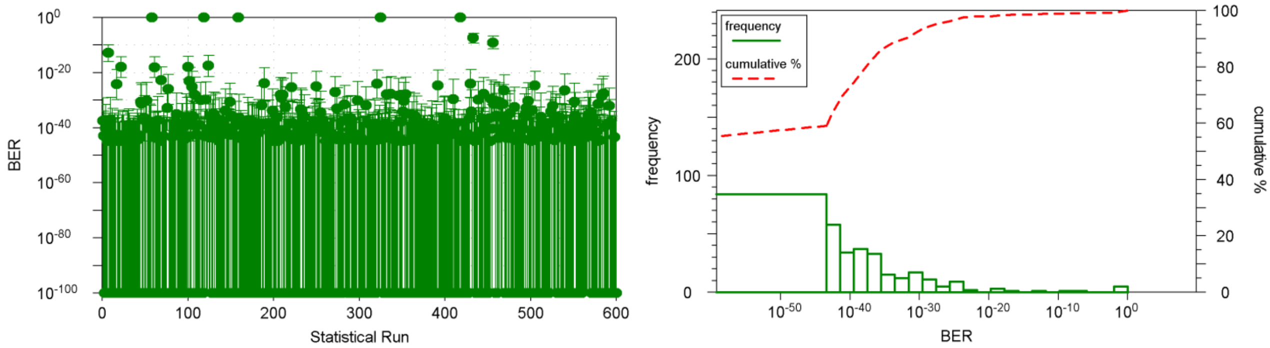

Ilustración 4-9 BER después de 600 muestras estadísticas. Conectores. -40°C.

Sólo el 2% de las muestras son peores de 10^{-20}. El peor caso es $4 \cdot 10^{-8}$.

4.1.2.3 90ºc

La Ilustración 4-10 muestra el BER vs. potencia óptica de entrada y el BER vs. voltaje diferencial de entrada al laser.

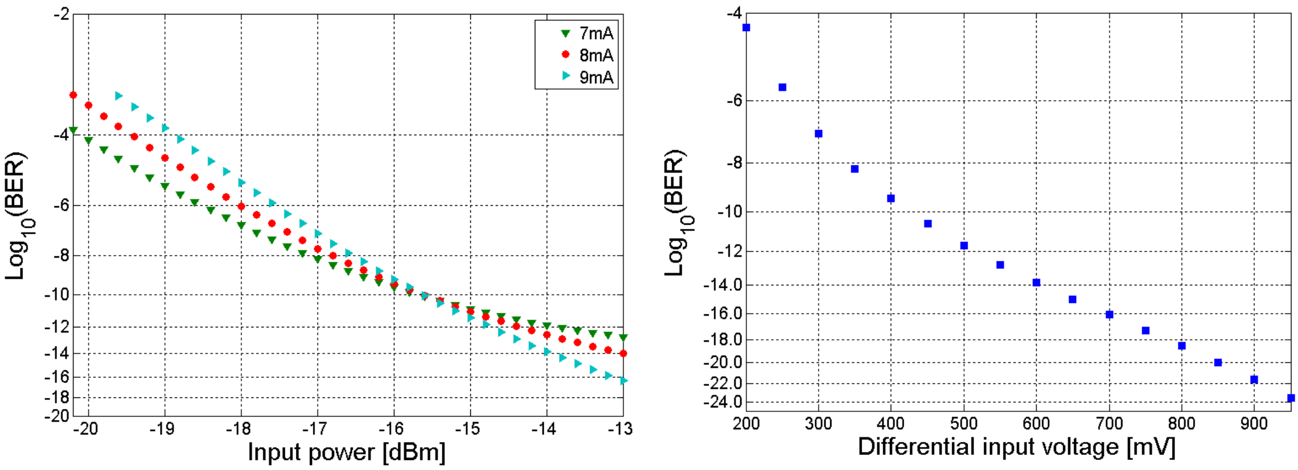

Ilustración 4-10 BER vs. Potencia óptica de entrada (izquierda). BER vs. Voltaje diferencial de entrada al VCSEL. 90°C.

A 90°C se produce una reducción de la máxima potencia óptica de salida, un aumento de la corriente umbral, una reducción del ancho de banda de modulación y un incremento de la Resistencia de entrada. Al igual que en el caso anterior, con el fin de alejar el punto de trabajo de la corriente umbral y elevar el ancho de banda de modulación hasta los valores deseados, se utiliza una corriente de polarización de 9mA. A diferencia del caso anterior y a pesar de la gran compresión de rango dinámico (reflejado en la curva LIV), el hecho de que la resistencia serie haya aumentado hace que todo el rango posible de voltaje diferencial de entrada sea soportado por nuestro modelos de VCSEL sin aparente saturación y que la diferencia entre las curvas BER en función del bias sean menos acusadas para potencias por encima de la sensibilidad. Esto se muestra en la curva BER vs voltaje diferencial de entrada en Ilustración 4-10.

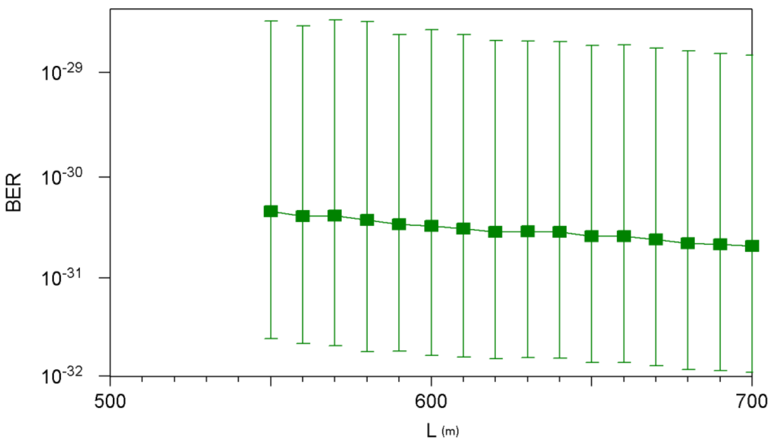

Ilustración 4-11 BER vs. Longitud de fibra MMF. 90°C.

Por último se realizó el cálculo de la variación del BER en función de la longitud de fibra. La Ilustración 4-11 muestra que se consigue una transmisión libre de error con un margen de potencia mínimo de 8.7dB.

Análisis estadístico

RANGO DE OPERACIÓN

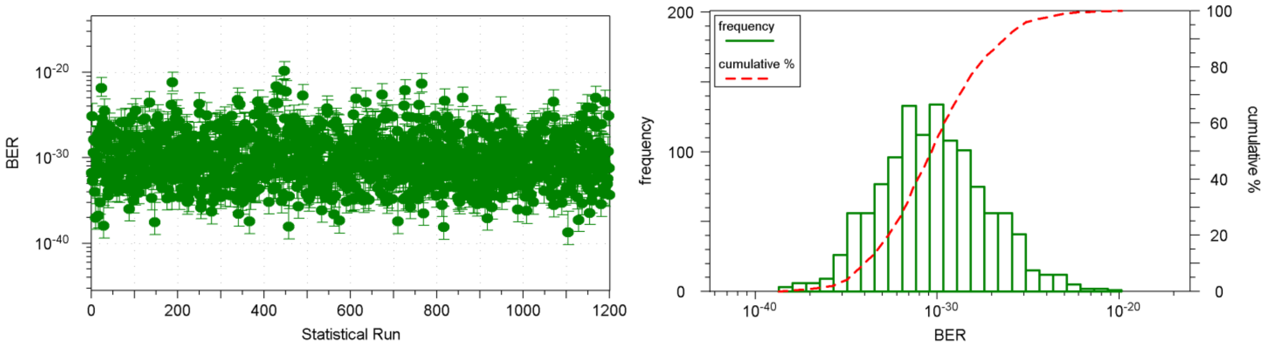

Ilustración 4-12 BER después de 1200 muestras estadísticas. Rangos de operación. 90°C.

El barrido de 1200 muestras indica que en ningún caso se mejoran los 10^{-40}. El histograma refleja que el 90% de las muestras es menor de 2.10^{-30} y que todas ellas son menores de 10^{-20}. El mínimo margen de potencia es 7.8dB.

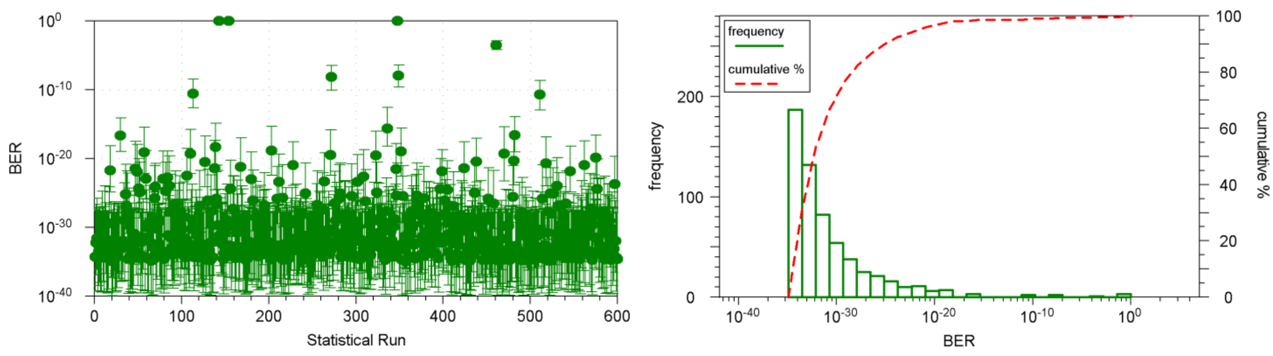

Ilustración 4-13 BER después de 600 muestras estadísticas. Conectores. 90°C.

El mayor BER realista registrado es $2 \cdot 10^{-4}$. El histograma muestra que alrededor del 96% de las muestras tienen un BER menor de 10^{-20} con solo un 1.3% superior a 10^{-12}.

4.1.2.4 Conclusión

Se obtuvieron muy buenos resultados para la simulación con NRZ. Las Corrientes óptimas de bias se calcularon para cada temperatura en base al BER. Para dichas corrientes y 600mV de voltaje diferencial de entrada, la peor tasa de error en función de la distancia de fibra se registro a 90°C y no excedía los 10^{-30}. Para 25°C el máximo BER era 10^{-74} y para -40°C alrededor de 10^{-40}. El mínimo margen de potencia es 7.9dB a -40°C y el máximo 9.9dB a 25°C. Estos resultados prueban que el enlace puede operar con BER por debajo de los 10^{-12} cuando se utilizan valores típicos. Se debe mencionar que se ha sido asumido la implementación de un sistema de polarización adaptativo. Tal algoritmo debe ser cuidadosamente elaborado y no linealmente interpolado en función de la mínima, máxima y temperatura ambiente. Su cálculo se ha considerado fuera del alcance del presente trabajo.

El análisis estadístico mostró que solo cuatro de las 3600 iteraciones superan los 10^{-12} y ninguna es peor de 10^{-10}. Esto significa que incluso para la peor combinación posible de valores el enlace puede seguir funcionando sobre todo el rango de temperaturas con un BER no peor de $4 \cdot 10^{-11}$ (obtenido a -40°C). La evaluación de los conectores mostró que a menos que los tres tipos de desalineación (radial, longitudinal y angular) fueran activados, el BER siempre se mantenía por debajo de 10^{-20}. Además, un BER de 10^{-12} sólo era superado por un 1.1% del número total de muestras (1800). Esto demuestra que a condición de que los parámetros del VCSEL, OM4 y receptor se mantuvieran estables y el link estuviera optimizado para NRZ, el impacto de las desalineaciones es despreciable en nuestro caso. Esto se confirma debido a las notablemente exageradas desviaciones típicas que en cualquiera de los casos serian consideradas inaceptables para un conector óptico orientado a redes aviónicas. Sin embargo, más estudios estadísticos deberían realizarse sobre el impacto de los rangos de operación y desalineaciones como efecto conjunto.

4.2 Optical Orthogonal Frequency-Division Multiplexing (OOFDM)

El test comprende dos partes. En la primera los peores escenarios de transmisión para cada temperatura son evaluados para modulaciones por portadora 4-QAM y 16-QAM. En primer lugar, las Corrientes de polarización usadas para NRZ son usadas con el fin de contemplar una posible combinación NRZ/OOFDM o una futura substitución ([12]). En segundo lugar, se lleva a cabo la optimización específica del sistema para OOFDM. No se contempla límite de tasa de transmisión y se considera el uso de codificación FEC. Los resultados y sus implicaciones son discutidos.

El anexo D presenta el desarrollo de cada uno de los casos, constelaciones y espectros.

4.2.1 Esquemático y parámetros

Para todos los casos, el esquemático utilizado se muestra en Ilustración 4-14.

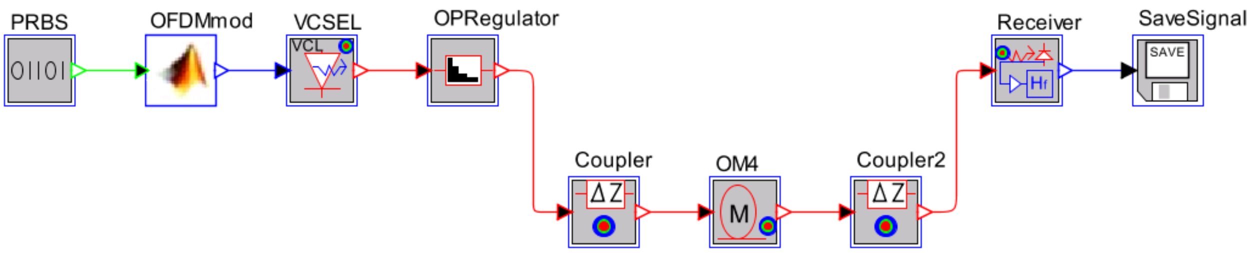

Ilustración 4-14 Esquemático del enlace final para OOFDM.

El módulo PRBS genera una señal pseudoaleatoria de longitud 2^7-1. El “OOFDMmod” inicia MATLAB®, ejecuta el código de modulación y proporciona una señal OOFDM con el formato aceptado por ModeSYS™. La señal de salida es una señal bipolar eléctrica que pasa por un bias-T ideal para hacerla unipolar e inyectársela al VCSEL. La señal óptica generada por el laser se propaga por la OM4 y es recibida igual que en caso NRZ. La señal eléctrica es guardada en un fichero de extensión SGD que se importa a MATLAB® para su demodulación y cálculo de la tasa de error.

Los parámetros más relevantes de la simulación se presentan en Tabla 4-3.

Tabla 4-3 Parámetros eléctricos y ópticos de la simulación.

Descripción	25ºC	-40ºC	90ºC	Unidad
Bias (NRZ)	7	9	9	mA
Voltaje diferencial de entrada		600		mV
Potencia de salida		-4		dBm
Longitud del		700		m

[12] Se asume que el sistema adaptativo de corriente está implementado e integrado en el transceptor, es decir, completamente independiente del modulador.

enlace		
Pérdidas/conector	0.3	dB/$N_{CONNECTORS}$
Ancho de banda del LPF	<10 (Variable)	GHz

Se observó una especial influencia del diseño del filtro paso baso en los resultados. El BER era extremadamente sensible a la frecuencia de corte y unas caídas bruscas de las faldas del filtro mejoraban los resultados ostensiblemente. Se eligió un tipo Butterworth para el filtro eléctrico ya que tiene una caída abrupta pero manteniendo una amplitud constante en la banda de paso. La variación constante de fase que el propio filtro introduce se contrarrestaba con el propio ecualizador implementado en el demodulador OOFDM.

Debido a la limitación impuesta por 10GBASE-SR en lo relativo a la tasa de transmisión, la velocidad de muestreo necesito ser ajustada en función del formato de modulación para obtener unos constantes 10.3125Gbps. Los parámetros específicos OOFDM se presentan en Tabla 4-4.

Tabla 4-4 Parámetros OOFDM.

Descripción	4QAM	16-QAM	Unit
Número de subportadoras	256	256	-
Secuencias de entrenamiento	2	2	-
Prefijo cíclico	1	1	%
Sobremuestreo	2	2	
Modo de modulación en intensidad	DCO-OOFDM	DCO-OOFDM	
Gestión de PAPR	Clipping >90	Clipping >90	%
Tasa de muestreo	20.86	10.43	GS/s

Una de las principales prioridades era mantener la tasa de muestreo lo más baja posible. Aunque en ningún caso excedía los 25GS/s y que DACs a más de 30GS/s ya están comercialmente disponibles [26], [27] y [28], se consideró recomendable operar el sistema holgadamente dentro de los límites especificados por la imperiosa necesidad de garantizar la seguridad y fiabilidad de nuestro sistema. Además el coste se reduce considerablemente.

En relación al PAPR, se observaron Buenos resultados cuando la señal se truncaba por encima del 90% de la amplitud máxima. La eliminación del ruido fuera de banda generado por el truncamiento y el filtrado de reconstrucción se realizaron con un filtro Hamming apropiadamente diseñado.

A.1.1 Resultados y conclusión (configuración NRZ)

Tabla 4-5 Resumen de los resultados OOFDM para el link optimizado para transmisión NRZ.

Temperatura	-40°C		25°C		90°C		Unidad
Modulación (M-QAM)	4	16	4	16	4	16	-
Cuenta de errores	0	0	0	0	0	0	-
BER estimado	$<10^{-20}$	$8\cdot10^{-19}$	$<10^{-20}$	$5\cdot10^{-18}$	$<10^{-20}$	$<10^{-20}$	-
Sensibilidad (OOFDM)	-12	-7.5	-14	-7.5	-14	-9	dBm
Sensibilidad (NRZ)	-14		-16		-14.8		dBm
Mínimo margen de potencia (OOFDM)	5.9	1.5	7.9	1.5	7.9	3	dB
Mínimo margen de potencia (NRZ)	7.9		9.9		8.7		dB

Para un enlace de transmisión de datos a 10.3125Gbps con el modelo de VCSEL, OM4 y receptor diseñados en la sección 4, la modulación 4-QAM ofrece más margen medio de potencia, mayor sensibilidad y menor BER que 16-QAM. En comparación con NRZ, OOFDM ofrece una trasmisión libre de errores para la misma corriente de bias, temperatura y voltaje diferencial de entrada pero con mucho menos ancho de banda (la mitad para 4-QAM y un cuarto para 16-QAM). Por otro lado, NRZ proporciona márgenes de potencia mínimos 1.93dB menores que 4-QAM y 6.83dB mayores que 16-QAM (en media) y sensibilidad mejorada.

Si finalmente se elige IEEE 802.3ae con 10GBASE-SR como el estándar para gobernar la operación de la red, NRZ ofrece transmisión libre de errores sobre todo el rango de temperaturas considerado con un margen de potencia medio de 8.8dB. Además, es más barato y menos complicado de implementar que OOFDM.

Para transmisiones más rápidas de 10.3125Gbps, la alta eficiencia espectral mostrada por OOFDM permitiría conseguir tasas de transmisión considerablemente mayores que NRZ. Dado que la escalabilidad de la red es uno de los aspectos importantes, esta opción debería ser cuidadosamente estudiada. Además, OOFDM es especialmente robusta contra ISI e interferencias selectivas (como por ejemplo, defectos locales en la fibra). Esto se puede ver reforzado por la utilización de modulaciones adaptativas y los ya mencionados códigos FEC.

A.1.2 Resultados y conclusión (optimización)

Una reconfiguración de las Corrientes de bias y de los voltajes diferenciales de entrada se realizó especialmente para OOFDM. La adaptación tuvo tres fases. En la primera, la corriente de polarización fue regulada hasta que el BER se minimizó (configuración en Tabla 4-3). Durante la segunda fase, el voltaje diferencial fue ajustado. Finalmente la tasa de transmisión ([13]) fue incrementada hasta que el BER alcanzó 10^{-12}. La Tabla 4-6 recoge los resultados obtenidos.

Tabla 4-6 Resumen de los resultados OOFDM para el link optimizado para transmisión OOFDM.

Temperatura	-40°C		25°C		90°C		Unidad
Modulación (M-QAM)	4	16	4	16	4	16	-
Corriente de Bias	9	9	7	7	9	9	-
Voltaje diferencial de entrada	900	900	900	900	900	900	-
Máxima tasa de transmisión libre de error (OOFDM)	13.8	23.2	16.8	24.7	12.0	21.2	Gbps
Ancho de banda	6.918	5.806	8.401	6.301	6.054	5.312	GHz
Máxima tasa de transmisión por debajo del límite 7%-FEC (BER<10^{-3})	15.3	26.2	17.8	30.1	12.8	23.2	Gbps
Ancho de banda	7.660	6.548	8.895	7.536	6.424	5.559	GHz
Máxima tasa de transmisión libre de error (NRZ)	12		13.6		12		Gbps
Máxima tasa de transmisión por debajo del límite 7%-FEC (BER<10^{-3}) (NRZ)	16		15.3		14.5		Gbps

Las corrientes óptimas de polarización no han cambiado con respecto a aquellas usadas para NRZ. Esto tiene sentido para -40°C y 90°C donde el uso de las altas corrientes favorece el aumento del ancho de banda de modulación. Para 25°C, los resultados con 9mA son ligeramente mejores que con 7mA pero se decidió mantener 7mA como corriente optima debido al considerable ahorro energético (alrededor de 40% menos) y a la reducción del estrés al que se sometía al laser. Por su parte, se observe que un aumento del voltaje diferencial de entrada mejoraba el BER para todas las configuraciones y por lo tanto se estableció el valor por defecto a casi el máximo (900mV), de tal forma que se considerara un cierto margen de seguridad

Los resultados muestran que 16-QAM es el formato de modulación más apropiado para mayores velocidades de transmisión. La diferencia entre 4-QAM y 16-QAM en lo concerniente a la máxima tasa de transmisión es más del 60% mayor en favor de la segunda. Además, Es necesario un DAC operando a 30GS/s para lograr más de 14.8Gbps con 4QAM y solo 15GS/s para 16-QAM. Un DAC tan rápido incrementaría el coste global substancialmente.

Se puede observar en la Ilustración 3-2 que el ancho de banda (3dB) a 8mA es 8GHz, 9Ghz y 10.2GHz para 90°C, -40°C y 25°C respectivamente (nótese que para 90°C y -40°C se están usando 9mA y

[13] Tasa de transmisión nominal (prefijo cíclico incluido)

consecuentemente el ancho de banda es mayor). Esto significa que el ancho de banda usado para 4-QAM y 16-QAM no está limitado por la respuesta de modulación del VCSEL sino por ISI y potencia de ruido en el receptor. La frecuencia de corte del LPF es ajustada a lo largo de toda la simulación con un máximo de 12.3GHz.

Son dignos de mención los dos casos particulares encontrados durante el análisis. El primero es para NRZ a -40°C, donde la máxima tasa de transmisión por debajo del límite FEC es la más alta de last res temperaturas. El segundo se observa a 90°C, donde el rendimiento de NRZ mejora los resultados obtenidos para 4-QAM.

La conclusión es que OOFDM 16-QAM puede cubrir sobradamente con las futures demandas de ancho de banda con apenas ajustes en el sistema (frecuencia de corte del LPF y voltaje diferencial de entrada al VCSEL). Sin embargo, su rendimiento es pobre cuando se desea trabajar con tasas menores de 15Gbps. En tal caso, NRZ sería la mejor opción dado que ofrece unos resultados muy próximos a un menor coste, menor complejidad y mayores márgenes de potencia.

Debido a los Buenos resultados conseguidos con 16-QAM una última prueba fue realizada. En este caso, se utilizó un formato 32-QAM para la mejor situación posible, es decir, todo el sistema fue optimizado exclusivamente para este caso. La Tabla 4-7 resume los resultados.

Tabla 4-7 Parámetros y resultados para OOFDM/32-QAM.

Descripción	Valor	Unidad
Temperatura	25	°C
Corriente de bias	7	mA
Voltaje diferencial de entrada	900	mV
Máxima tasa de transmisión nominal	33.35	Gbps
Ancho de banda	6.671	GHz
BER	$1.6 \cdot 10^{-3}$	-

La constelación recibida y el espectro del la señal recibida y enviada se muestran en la Ilustración 4-15.

(CONTINÚA EN LA PÁGINA SIGUIENTE)

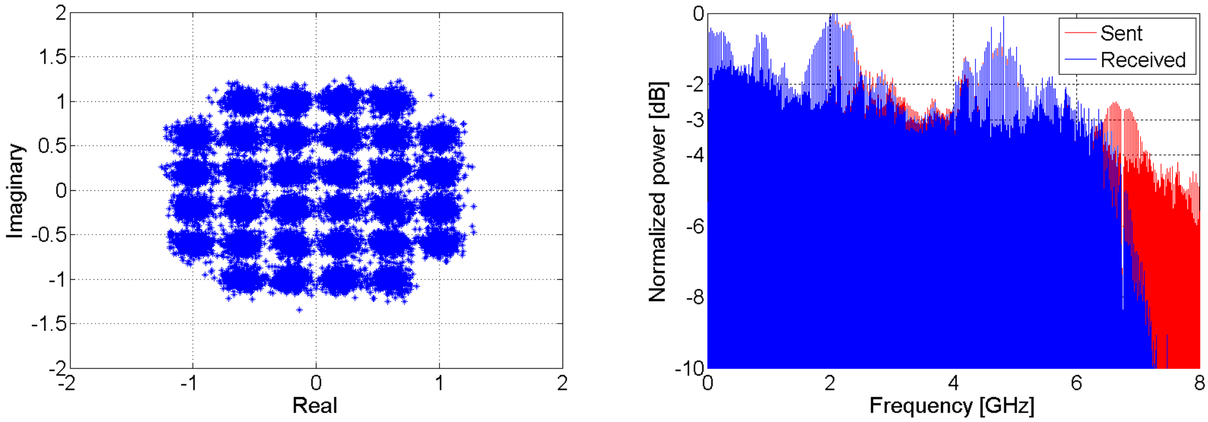

Ilustración 4-15 Constelación 32-QAM recibida (izquierda). Espectro de la señal recibida después del LPF (azul, derecha) y dela señal enviada antes de la propagación (rojo, derecha).

Los resultados muestran que la mejora está claramente limitada por la potencia de ruido en el receptor. Mientras que el ancho de banda utilizado apenas supera los 6.5GHz, únicamente se obtienen un incremento en la tasa de transmisión de 3Gbps en comparación con 16-QAM. Esto confirma lo apropiado de OOFDM/16-QAM para nuestro sistema específico para transmisiones más rápidas de 15Gbps.

5 Conclusión

Una red óptica predefinida para entornos aviónicos ha sido evaluada. La topología de la red así como el transceptor, canal y estándares de regulación fueron proporcionados y acordados como resultado de la investigaciones llevadas a cabo durante el desarrollo del proyecto DAPHNE, apoyado por la Comisión Europea bajo el FP7. Cinco publicaciones se han presentado durante el desarrollo de la investigación. Una de ellas ha sido aceptada para exposición oral en ECOC'12 y otra fue aceptada y presentada como postdeadline en la pasada OFC/NFOEC´12.

Un intense análisis ha sido realizado en lo relativo a la validación de la herramienta de simulación. Dos softwares comercialmente disponibles fueron probados. Para ambos, la precisión de los algoritmos para la emulación de efectos dispersivos modales y la exactitud del modelo de VCSEL a 850nm fueron contrastados resultados experimentales publicados. Se concluyó que ModeSYS™ era la mejor solución para el modelado del sistema pretendido.

Las descripciones técnicas y las especificaciones de los componentes deseados para el enlace óptico fueron interpretadas, reformateadas e importadas a ModeSYS™. El buen funcionamiento de los modelos resultantes fue continuamente validado con las hojas de datos proporcionadas y requisitos de rendimiento hasta que un alto nivel de similitud fue conseguido. Posteriormente, se realizó una verificación de la conformidad con IEEE 802.3ae (10GBASE-SR) para el transmisor, canal y receptor. Se concluyó que el modelado era satisfactorio.

El enlace fue simulado para NRZ y OOFDM a -40°C, 25°C y 90°C, cubriendo así todo el rango de temperature alcanzado en entornos aviónicos. Además, se llevó a cabo un análisis estadístico para el caso NRZ que comprendía dos fases. La primera consideraba la posibilidad de variaciones en los valores de los parámetros más influyentes en el sistema dentro del rango de operación establecido. La segunda parte evaluaba el rendimiento del sistema cuando desalineaciones radiales, longitudinales y angulares altamente exageradas tenían lugar.

Con respecto a NRZ, se obtuvieron excelentes resultados en términos de BER y márgenes de potencia cuando se usaba la configuración típica. El máximo registrado fue 10^{-31} a 90°C lo cual todavía permitía 8.7dB de pérdidas. La evaluación estadística mostró que dentro de los rangos de operación, solo 4 muestras de 3600 (0.11%) eran peor de 10^{-12}, siendo $4 \cdot 10^{-11}$ el máximo y todas ellas a -40°C. En lo concerniente a las desalineaciones en los conectores, se requería una fortuita combinación de los tres tipos de desviación para producir BERs peores que, al menos, 10^{-4}. Se comprobó que si uno de ellos era desactivado, los resultados nunca superaban los 10^{-20}.

Los resultados para OOFDM mostraron que se pueden conseguir tasas de hasta 20Gbps con modulación 16-QAM por subportadora y mantener el BER por debajo de 10^{-12} en un sistema optimizado para OOFDM. Por otro lado se concluyó que para velocidades de transmisión menores de 15Gbps NRZ ofrecía resultados comparables con OOFDM/4-QAM con márgenes de potencia considerablemente mayores y simplicidad para todas las temperaturas. Un último test fue desarrollado para OOFDM/32-QAM para demostrar que la

ISI y la potencia de ruido en el receptor no permiten incrementar la tasa maxima de transmisión en relación a 16-QAM proporcionalmente al coste técnico y económico implicado.

5.1 Trabajo Futuro

Algunas de las posibilidades:

- Ejercicios experimentales deben ser desarrollados para confirmar las conclusiones y resultados aquí presentados así como para proporcionar nuevos datos como feedback para posteriores investigaciones.
- Una mayor variedad de componentes pueden ser modelados e incluidos en la simulación
- Un análisis estadístico combinado de desalineaciones en los conectores y rangos de operación debe ser llevado a cabo.
- Una barrido de temperaturas más detallado proporcionaría un conocimiento completo del comportamiento del enlace en las peores condiciones.
- OOFDM debería ser analizado estadísticamente.
- WDM también podría copar con las necesidades futuras de ancho de banda y proporcionar flexibilidad. El mismo test de rendimiento y comportamiento debería hacerse para dicha tecnología.

6 Fuentes y Bibliografía

[1] "Laser-Optimized Fiber: Built for Price, Bandwidth, and Distance to Make the Most of Your Investment", white paper, ADC Telecommunications, 2010.

[2] R. Rodes et al., "100 Gb/s single VCSEL data transmission link," in *Optical Fiber Communication Conference and Exposition (OFC/NFOEC)*, 2012 and *National Fiber Optic Engineers Conference*, PDP5D.10 March 2012.

[3] C. F. Lam et al., "Fiber Optic Communication Technologies: What's Needed for Datacenter Network Operations," *IEEE Communications Magazine*, vol.48, no.7, pp.32-39, July 2010.

[4] DAPHNE project brochure.

[5] J. Zhang et al., "Developing a Generic Optical Avionic Network," *18th International Conference on Telecommunications (ICT), 2011*, pp.244-249, May 2011.

[6] PIC™ Wire & Cable.

[7] I. Garcés and J. Mateo, "Introducción a las Comunicaciones Ópticas" [Introduction to Optical Communication], class notes for 11958, Department of Electrical Engineering and Communications, Universidad de Zaragoza [University of Zaragoza], Zaragoza, Spain.

[8] Draka technical datasheets.

[9] Corning technical datasheets.

[10] M. Holt, "Sizing Raceway-Part2," *Electrical Construction and Maintenance (EC&M) Magazine*, pp. 66-71, June 2000.

[11] timbercon technical information.

[12] J. Jackel, "Advances in Optical Networking for Aerospace Platform Applications," in *Avionics, Fiber-Optics and Photonics Technology Conference (AVFOP)*, 2011, pp.5-6.

[13] M. Masanovic, "Widely Tunable Optical Transceiver for Avionic WDM Networks," *Avionics, Fiber-Optics and Photonics Technology Conference (AVFOP), 2011*, pp.23-24, Oct 2011.

[14] L. Raddatz et al., "An Experimental and Theoretical Study of the Offset Launch Technique for the Enhancement of the Bandwidth of Multimode Fiber Links," *Journal of Lightwave Technology*, vol. 16,no.3, pp.324-331, March 1998.

[15] S.C. Victor Teichmann et al., "Analysis of Multimode Fiber Impulse Response Simulation Models," *SBMO/IEEE MTT-S InternationalMicrowave & Optoelectronics Conference (IMO*C), 2011, pp.728-732, Oct.-Nov. 2011.

[16] R. Michalzik and K.J. Ebeling, "Operating Principles of VCSELs", in *Vertical-Cavity Surface Emitting Laser Devices*, H. Li and K. Iga, 2003, pp.53−98.

[17] P.V. Mena et al., "A Comprehensive Circuit-Level Model of Vertical-Cavity Surface-Emitting Lasers," *Journal of Lightwave Technology*, vol.17, no.12, pp.2612-2632, Dec. 1999.

[18] P.V. Mena et al., "A Simple Rate-Equation-Based Thermal VCSEL Model," *Journal of Lightwave Technology*, vol.17, no.5, pp.865-872, May 1999.

[19] M.X. Jungo, "VISTAS: a Comprehensive System-Oriented Spatiotemporal VCSEL Model," *IEEE Journal of Selected Topics in Quantum Electronics*, vol.9, no.3, pp.939- 948, May-June 2003.

[20] G. Yabre, "Comprehensive Theory of Dispersion in Graded-Index Optical Fibers ," *Journal of Lightwave Technology,* , vol.18, no.2, pp.166-177, Feb 2000.

[21] Meng-Chyi Wu et al., "High-Speed InGaP/GaAs p-i-n Photodiodes With Wide Spectral Range," *IEEE Electron Device Letters,* vol.28, no.9, pp.797-799, Sept. 2007

[22] T. Irujo, "Measuring OM4/OM3 Fiber Bandwidth", white paper, OFS Optics.

[23] S.F. Habiby and R. Vaidyanathan, "WDM Optical Backbone Networks in Aircraft Applications: Networking Challenges and Standards Progress," *Military Communications Conference, 2009. MILCOM 2009,* pp.1-6, Oct. 2009

[24] N. Chand and B. Eteson, "Optical LAN for avionics platforms," *Avionics, Fiber-Optics and Phototonics Technology Conference, 2009. AVFOP '09.*, pp.42-43, Sept. 2009
[25] *IEEE Standard for Information technology—Telecommunications and information exchange between systems—Local and metropolitan area networks—Specific requirements*, IEEE 802.3ae, 2002.
[26] M. Nagatani et al., "Ultrahigh-Speed Low-Power DACs Using InP HBTs for Beyond-100-Gb/s/ch Optical Transmission Systems," *IEEE Journal of Solid-State Circuits,* vol.46, no.10, pp.2215-2225, Oct. 2011.
[27] J.E. Wilson, "40 GSps, 6-bit RF DAC Design Report", U.S. Army Research Laboratory, Tech. Rep. ARL-TR-5483, March 2011.
[28] "Ultrahigh-Speed DAC for Optical Communications Systems", NTT Photonics Laboratories. Link.
[29] K. Iga, "Surface-Emitting Laser—Its Birth and Generation of New Optoelectronics Field," *IEEE Journal of Selected Topics in Quantum Electronics*, vol.6, no.6, pp.1201-1215, Nov./Dec. 2000.,
[30] R. Szweda, "VCSEL resurgent", *The Advanced Semiconductor Magazine*, vol. 17, no. 8, Nov. 2004
[31] T. Ohtoshi and M.Takahashi, "Band Engineering of the Polarization and Gain Properties in VCSELs", in *Vertical-Cavity Surface-Emitting Laser Devices*, H. Li and K. Iga, 2003, pp.99−100.
[32] J.L.A. Chilla et al., "Polarization Switching in Vertical-Cavity Surface Emitting Lasers Observed at Constant Active Region Temperature", *5th Device Research Conference Digest, 1997*, pp.106-107, Jun 1997.
[33] Y.H. Wu et al., "Frequency-Dependent Thermal Effect on Polarization Switching of VCSELs," *16th OptoeElectronics and Communications Conference (OECC), 2011*, pp.669-670, July 2011.
[34] I. Garcés and J. Mateo, "Láseres de Semiconductor" [Laser Diodes], class notes for 11958, Department of Electrical Engineering and Communications, Universidad de Zaragoza [University of Zaragoza], Zaragoza, Spain.
[35] L.N. Binh and I. Shraga, "An Optical Fiber Dispersion Measurement Technique and System", Department of Electrical & Computer Systems Engineering, Monash University, Victoria, Australia, Tech. Rep. MECSE-14, 2005.
[36] E. Ientilucci, "Fundamentals of Fiber Optics", Nov. 1993. Link.
[37] I. Garcés and J. Mateo, "Atenuación de Señales en Fibras Ópticas" [Signal Attenuation in Optical Fibers], class notes for 11958, Department of Electrical Engineering and Communications, Universidad de Zaragoza [University of Zaragoza], Zaragoza, Spain.
[38] K.S. Schneider, "Fiber Optic Communications for the Premises Environment". Link.
[39] D.R. Goff, "Fiber Optic Cables," in *Fiber Optic Reference Guide: a Practical Guide to Communications Technology"*, 3rd ed., K. Hansen, Ed., Focal Press, 2002, pp.53.
[40] G.P. Agrawal, *Fiber-Optic Communication Systems*, 3rd ed., New Your, NY: John Wiley & Sons, 2002.
[41] H. Aruga et al., "Integrated Receiver for 100GbE," *16th OptoeElectronics and Communications Conference (OECC), 2011*, pp.460-461, July 2011.
[42] M. Eiselt, "Cost-effective 100Gbps Optical Modulation Format for Metro Networks," *ITG Symposium on Photonic Networks, 2008*, pp.1-5, April 2008.
[43] M.A. Mohd and M.M. Ahmed, "Fiber Optics: an Antidote to Electromagnetic Interference (EMI)", in *Southcon Conference Record*, pp.312, March 1994.
[44] I. Garcés and J. Mateo, "Descripción Electromagnética: Fibras Ópticas Monomodo" [Electromagnetic Description: Singlemode Fibers], class notes for 11958, Department of Electrical Engineering and Communications, Universidad de Zaragoza [University of Zaragoza], Zaragoza, Spain.
[45] "Fiber Optic Theory", STRATOS Lightwave™, Haverhill, Suffolk, United Kingdom. Link.
[46] R. Pimpinella and A. Brunsting, "Differential Mode Delay (DMD) for Multimode Fiber Types and its Relationship to Measured Performance," in *Optical Fiber Communication Conference and Exposition (OFC/NFOEC)*, 2005 and *National Fiber Optic Engineers Conference*, NWF2, March 2005.
[47] K.K. Das et al., "An Interferometric Technique for Measuring the Refractive Index Profile of a Graded Index Optical Fiber", in *Aerospace and Electronics Conference*, 1994, *NAECON* and Proc. *the IEEE National*, vol.2, pp.1111-1118, 1994.

[48] H.J.R. Dutton, *Understanding Optical Communications*, IBM Corp. International Technical Support Organization, Research Triangle, NC, 1998.
[49] D. Marcuse. “Loss analysis of single-mode fiber splices,” Bell Syst. Tech. J., vol.56, pp.703-718, 1977.
[50] R. Olshansky, "Mode Coupling Effects in Graded-index Optical Fibers," *Applied Optics*, vol. 14, no. 4, pp. 935-945, 1975.
[51] R.E. Freund et al., "High-Speed Transmission in Multimode Fibers," *Lightwave Technology, Journal of* , vol.28, no.4, pp.569-586, Feb.15, 2010.
[52] I. Garcés and J. Mateo, “Conceptos Básicos de Óptica Guiada” [Basic Concepts of Guided Optics], class notes for 11958, Department of Electrical Engineering and Communications, Universidad de Zaragoza [University of Zaragoza], Zaragoza, Spain.
[53] J. Ingham et al., “Statistical modeling of multimode-fiber links: a supplement to the information provided in the release note of 12 October 2004 in relation to Release 1.2 from the University of Cambridge”, University of Cambridge, Cambridge, United Kingdom, 2004.
[54] I. Garcés and J. Mateo, “Dispersión de Pulsos en Fibras Ópticas Monomodo” [Pulse Dispersion in Singlemode Optical Fibers], class notes for 11958, Department of Electrical Engineering and Communications, Universidad de Zaragoza [University of Zaragoza], Zaragoza, Spain.
[55] I. Garcés and J. Mateo, “Detectores para Sistemas de Comunicaciones Ópticas” [Sensors for Optical Communication Systems], class notes for 11958, Department of Electrical Engineering and Communications, Universidad de Zaragoza [University of Zaragoza], Zaragoza, Spain.
[56] D. Westerman, “Understand and apply the transimpedance amplifier,” National Semiconductor Corp. Link.
[57] D.M. Pozar, “Microwave Engineering”, 3rd ed., New York, NY: John Wiley & Sons, 2004.
[58] R. van Nee and R. Prasad, “OFDM for Wireless Multimedia Communications”, Boston, Massachusetts, MA: Artech House, 2000.
[59] J. Armstrong, "OFDM for Optical Communications," *Journal of Lightwave Technology*, vol.27, no.3, pp.189-204, Feb.1, 2009.
[60] R. Prasad, “OFDM for Wireless Communication Systems”, Boston, Massachusetts, MA: Artech House, 2004.
[61] M. Engels, “Wireless OFDM Systems: How to Make them Work?,” in *The Kluwer International Series in Engineering and Computer Science*, vol.692, 2002, doi: 10.1007/b117438. Link.
[62] E. Giacoumidis et al., "Experimental and Theoretical Investigations of Intensity-Modulation and Direct-Detection Optical Fast-OFDM Over MMF-Links," *IEEE Photonics Technology Letters*, vol.24, no.1, pp.52-54, Jan. 2012.
[63] E. Hugues-Salas et al., "Directly Modulated VCSEL-Based Real-Time 11.25-Gb/s Optical OFDM Transmission Over 2000-m Legacy MMFs," *IEEE Photonics Journal*, vol.4, no.1, pp.143-154, Feb. 2012.
[64] J. Armstrong and B.J.C. Schmidt, "Comparison of Asymmetrically Clipped Optical OFDM and DC-Biased Optical OFDM in AWGN," *IEEE Communications Letters*, vol.12, no.5, pp.343-345, May 2008.
[65] J. Armstrong and A.J. Lowery, "Power efficient optical OFDM," *Electronics Letters*, vol.42, no.6, pp.370-372, March 2006.
[66] S. C. Jeffrey Lee at al., "High-Speed Transmission over Multimode Fiber Using Discrete Multitone Modulation [Invited]," *Journal of Optical Networking*, vol.7, no.2, pp.183-196, Feb. 2008.
[67] H. Mrabet et al., "Impact of Chromatic and Modal Dispersion on Frequency Response of Optical Multimode Fibers," *IEEE Symposium on Computers and Communications, 2009. ISCC 2009.*, pp.188-194, July 2009.
[68] Keang-Po Ho and J.M Kahn, "Statistics of Group Delays in Multimode Fiber With Strong Mode Coupling," *Journal of Lightwave Technology*, vol.29, no.21, pp.3119-3128, Nov. 2011.
[69] J. Morikuni et al., "Simulation of Modal Delays for 10 Gb/s Multimode Fiber Applications," *Lasers and Electro-Optics Society, 2002. LEOS 2002. The 15th Annual Meeting of the IEEE*, vol.2, pp.903-904, Nov. 2002.
[70] J. M. Kahn et al., "Mode Coupling Effects in Multi-Mode Fibers," in *Optical Fiber Communication*

Conference and Exposition (OFC/NFOEC), 2012 and *National Fiber Optic Engineers Conference*, OW3D.3.

[71] M. Webster et al., "A Statistical Analysis of Conditioned Launch for Gigabit Ethernet Links Osing Multimode Fiber," *Journal of Lightwave Technology*, vol.17, no.9, pp.1532-1541, Sep 1999.

[72] "Selection of Multimode Fiber for Premises Applications", Corning Cable Systems LLC., Application Note, AEN 75, Revision 7, July 2008. Link.

[73] "Multimode Optical Fiber Bandwidth Characterization", Application Note, AEN 81, Revision 3. Link.

[74] "Reference Guide for Fiber Optics: Encircled Flux For Multimode Fiber Measurements", The Fiber Optic Association (FOA). Link.

[75] M. Grabherr et al., "Integrated Photodiodes Complement the VCSEL Platform," *Proceedings of the SPIE*, vol.7229, pp.1-9, 2009.

[76] P. Westbergh et al., "Large Aperture 850 nm VCSEL Operating at 28 Gbit/s," *IEEE 21st International Semiconductor Laser Conference, 2008. ISLC 2008.*, pp.7-8, Sept. 2008.

[77] Citations of VPItransmissionmaker™ and VPIcomponentmaker™.

[78] 108-fiber model files.

[79] J. D. Ingham, "More Information on Statistical Modeling of MMF Optical Fiber Links", informative presentation, Department of Engineering, University of Cambridge, Cambridge, United Kingdom, 2004.

[80] [74] G. Shaulov and B.K. Whitlock, "Multimode Fiber Communication System Simulation", *IEEE 802.3aq*, Portland, Oregon, July. 2004.

[81] G. Shaulov and Y. Sun, "DMD Simulations Based on Scaled/Non-Scaled Index Profiles and Comparison with Cambridge Model Results", *IEEE 802.3aq 10GBASE-LRM Interim Meeting*, Ottawa, Canada, Sept. 2004.

[82] "OptSim: Application Notes and Examples", RSoft Design Group, Inc., 2010. Confidential.

[83] P. Westbergh et al., "Large Aperture 850 nm VCSELs Operating at Bit Rates up to 25 Gbit/s," *Electronics Letters*, vol.44, no.15, pp.907-908, July 2008.

[84] P. Westbergh et al., "32 Gbit/s multimode fibre transmission using high-speed, low current density 850 nm VCSEL," *Electronics Letters* , vol.45, no.7, pp.366-368, March 2009.

[85] K. Szczerba, "30 Gbps 4-PAM Transmission over 200m of MMF Using an 850 nm VCSEL," *Optical Communication (ECOC), 2011 37th European Conference and Exhibition*, pp.1-3, Sept. 2011

[86] Algitron mechanical splicer. Technical description.

[87] M. Traverso et al., "Defining 10GBASE-SR over OM4 media". Link.

[88] J. Lee et al., " 24-Gb/s Transmission over 730 m of Multimode Fiber by Direct Modulation of an 850-nm VCSEL Using Discrete Multi-Tone Modulation," in *Optical Fiber Communication Conference and Exposition (OFC/NFOEC)*, 2007 and *National Fiber Optic Engineers Conference*, PDP6, March 2007.

[89] T. Kavatzikidis et al., "Performance Study of Optical OFDM for the ACCORDANCE Ultra High-Speed, Long-Reach Access Network," in *FTTH conference2011*, Feb. 2011. Link.

[90] A.J. Lowery and J. Armstrong, "10Gbit/s Multimode Fiber Link using Power-Efficient Orthogonal-Frequency-Division Multiplexing," *Optic Express*, vol.13, no.25, pp.10003-10009, Nov. 2005.

ANEXOS

A Theoretical background

A.1 Transmitter

A.1.1 VCSEL

Vertical Cavity Surface-Emitting LASERs are semiconductor Laser Diodes (LDs) whose radiated power, unlike conventional edge-emitting LASERs, is perpendicular to the top surface. The first idea and the initial demonstrations appeared in 1977 [29]. Several investigations in 80s showed some of the good properties and proved diverse advantages of this type of source, boasting the interest and encouraging later research that extended their applications and production [29]. Today, VCSELs are used in computer mice, chip-to-chip, laser printers, high-density optical disks, fiber-in-the-car and of course, short-reach single-channel gigabit-per-second datacom links or parallel transceiver modules on optical fiber ribbons amongst others [30]. A typical layout is shown in Figure A-1.

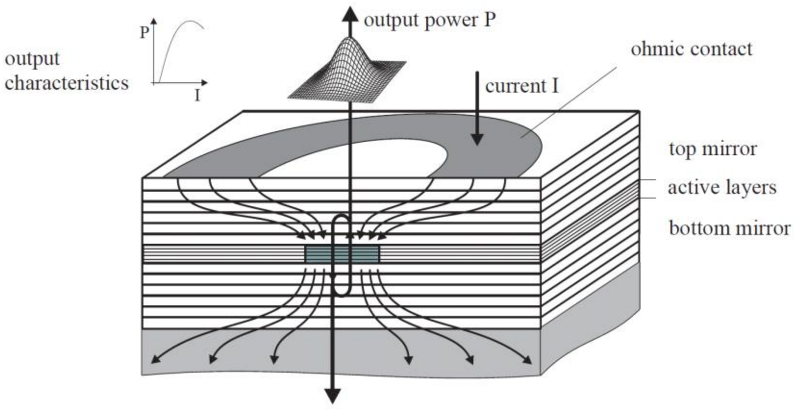

Figure A-1 VCSEL layout [16].

The setting out of the surface-emitting LASERs was motivated by the fully monolithic fabrication of the cavity [29]. This structure itself offers a number of interesting advantages that is increased with the introduction of the vertical cavity. The main advantages of VCSELs are [29]:

- The small cavity volume brings the threshold current down to microamperes.
- Single-mode operation is possible
- Large relaxation frequency allows for high-speed modulation
- Passivated surfaces and embedded active region lengthens their lifetime
- High power conversion efficiency
- Easy coupling to optical fibers due to good mode matching and small nearly circular spot size
- VCSELs can be manufactured by monolithic processes reducing the manufacturing cost
- The test can be done before dicing

- Easy bonding and mounting
- Cheap modules and package cost
- Stacking of micromachining technology can be done without affecting the LASER's resonator. This allows for polarization separation.

On the other hand, the size of the resonance cavity of VCSELs is 1-3 wavelengths of the emitted field. Consequently, it is very unlikely that a photon generates lasing in a single pass of the cavity. In order to increase the number sweeps, it is necessary a very high reflectivity (99.9% for low threshold currents) that cannot be achieved with metallic reflectors. Instead, Distributed Bragg Reflectors (DBR) are used. However, the high reflectance leads to a lower quantum efficiency that, in turn, causes low output power; which is one of the main problems in VCSELs [31].

Apart from the low output power, these LDs suffer from very high thermal dependence. Different temperatures make the semiconductor layers expand/contract and the average refractive index vary so that the physical properties of the resonance cavity are different, creating a noticeable wavelength shift [16]. Internal heating owed to simple laser working has also impact on the performance. It can be observed in the Light-to-Current (LI) curve where, from a certain current on, the output power decays. This is called "rollover" effect [16]. Another characteristic drawback in VCSELs is the polarization switching which happens when the injected current is increased above the threshold. Right before, the laser emits in one linear polarization but as the current is brought beyond the "switching current", the field changes to the orthogonal polarization. This would not be more than steady polarization instability, but it has been observed that the switching current varies with the temperature [32] and [33].

Initially, VCSELs based on GaAs (780nm, 850nm and 980nm) were deeply studied and were the first ones to be commercialized [29]. However, their good properties have motivated the investigation of what is called "long-wavelength" VCSELs based on different material compositions (see Table A-1).

Table A-1 Application and wavelength for different VCSEL compositions.

	GaN	AlGaAs/GaAs	InGaAsP/InP	AlGaAsSb/GaSb
Wavelength [nm]	420 - 520	780 – 980	1300 - 1550	1700 - 5000
Datacom application	Data storage	Short-Reach (SR) Optical interconnects	Long-Reach (LR) optical interconnects	Under investigation

A.1.2 Optical source modulation

The election of the proper modulation scheme for an optical laser is not difficult, but it is not immediate either. It depends on factors like the type of laser, power needed, the overall pursued system complexity and price, system application and modulation speed. Despite the moderate number of influencing parameters there are only two ways to modulate the laser intensity: "directly" or "externally".

This section has been based on [34].

A.1.2.1 Direct modulation

It consists of making the light intensity vary directly with the analogue or digital driving current. Since LDs have a certain threshold current, it is often used a "bias-T" to force the population inversion ([14]) through a continuous DC-source instead of using a biased RF signal. This way, the RF signal can be bipolar simplifying the modulation. Nevertheless, there is a problem inherent to the variation of the current flowing through the laser that has a severe impact on the reachable modulation speeds. It is caused by the strong carrier density variations that produce a frequency oscillation when an abrupt change of intensity takes place. If the period is very long the modulation speed will drop significantly.

Furthermore, it is known that the refractive index of any semiconductor depends on the carrier concentration. If it varies so does the refractive index and hence, the phase of the electromagnetic waves in the cavity through their propagation constant. The consequence is a spectrum spreading that ends up with a pulse spreading. This is called "chirp" effect. A graphical example is shown in Figure A-2.

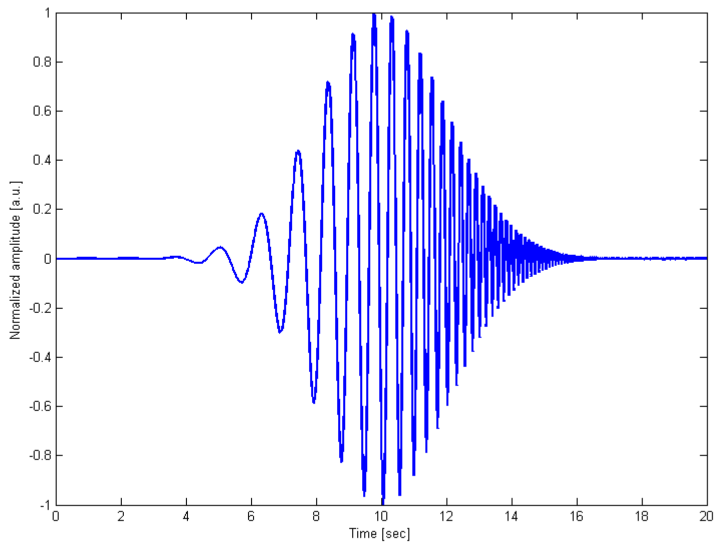

Figure A-2 Up-chirped pulse with Gaussianenvelope.

Figure A-2 should only be regarded as qualitative representation of a random Gaussian exponentially-chirped pulse. Direct modulation is used in communication links where price and complexity need to be minimized.

[14] If this operation is not done, a gain delay happens. By keeping a constant bias current above the threshold, the spontaneous emission period is skipped and the lasing gain variation drastically speeds up.

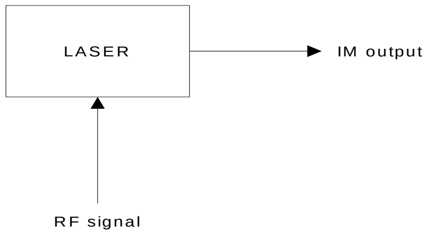

Figure A-3 Direct modulation shcematic.

A.1.2.2 External modulation

External modulation needs an external device to act as a "shutter" and change the optical intensity according to the input information. The laser is set in Continuous Wave (CW) mode hence there is no carrier density variation and consequently none of the problem derived from it. The advantages are the higher modulation speed compared to direct modulation and the possibility of using high-power laser sources. This option is commonly used in high-speed long-haul communication systems.

The most typical apparatus to accomplish external modulation is the Match-Zehnder interferometer [35]. It basically consists of a beam splitter and a pair of electrodes in one of the paths that, based on the RF input, change the refractive index of that stretch producing a phase change. After this, both paths are summed up to create constructive and destructive interferences that result in an intensity modulation. The main problems related to this are the high price and the complex circuitry necessary to manipulate it.

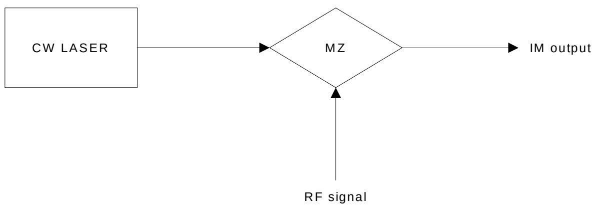

Figure A-4 External modulation schematic.

A.2 Channel

A.2.1 Optics

The first idea of light propagation through glass fiber was introduced in the 50s [36]. However, it was not until two decades later that the fiber-optic transmission was considered feasible and advantageous. This was due to the introduction of efficient light sources called LASERs and the refinement of the existing fibers to low-loss glass fibers [36]. Nevertheless, the price of a fiber-based communication system was too expensive compared to the electric-based systems. Nowadays, investigation and improvements in the fabrication of fibers, transmitters and receivers have decreased the overall price sufficiently to regard a possible incursion of this type of transmission in our daily life. Fiber optics clearly exceeds the performance of coaxial-based systems and sets out a number of overwhelming advantages such as:

- Attenuation
  Losses in a fiber are due to absorption, scattering and radiation. These factors in turn, depend mainly on the fabrication, the material and the wavelength. From last statement it can be inferred that an improvement on the manufacturing process will significantly reduce the losses [37]. Furthermore, the attenuation has been proved to be much lower for fibers and independent of the modulation frequency up to approximately 10GHz [38], [39] and [7]. On the other hand, optical communications require E/Os and O/Es whose efficiency should also be regarded.
- Bandwidth
  The bandwidth of a fiber-based transmission used to be termed "unlimited". The reason is that the usable range in terms of analogue bandwidth is around 45 THz ([15]) with an attenuation that in the worst case (short wavelength window) never exceeds 2.5-3dB/km and in the best case (long wavelength band) reaches 0.2 dB/km [40].
  The real limitation is the electronics used for both transmission and reception which currently rate up to 100Gbps. Some investigations have demonstrated the feasibility and shown the baselines for 100Gbps links [41] and [42]. IEEE released the standard governing Ethernet 40Gbps and 100Gbps operations in June 2010 (IEEE 802.3ba).
- Electromagnetic Interference (EMI) immunity
  Since fibers transmit light instead of current, though there are magnetic fields cutting across the fiber, they will never generate a variation on a non-existing charge flow. This makes fiber a complete EMI-immune transmission medium. Because of the not electric nature of the optic transmission, there are not either ground loops or parasitics that cause dangerous potential unbalance and power coupling between very close lines [43].
- Material
  Optical wires are known to be up to 10 times lighter and much cheaper than state-of-art coaxial cables for a comparable transmission capacity [5].

A.2.1.1 Types and packaging

From the maximum abstraction level, optical fibers are classified according to application (communication, illumination, sensing or thermal insulation), material (PMMA or silica) and size/wavelength relation (multimode, singlemode) [44]. In our case, the attention lies on glass multimode fibers for communication systems.

Physically, fibers consist of several concentric layers with two essential components: core and cladding. The core is the inner cylinder and it is the medium that mostly carries the light signals. The cladding is the surrounding layer which is used to assure total internal reflection. Depending on the application and the severity of the environment, different outer protections are used (submarine cables are not of interest here) [45]:

[15] Calculated by reckoning the widths of the 1st window, 2nd window and C-band in wavelengths and transforming those to frequency using 850nm, 1300nm and 1550nm respectively. Visible range (where the POF work) has been disregarded.

- Indoor
  Surrounding the cladding, a protection layer called "coating" can be found. It is often 250um in diameter and it is also used to strip out any ray travelling over the cladding.
  If further protection is intended, a "buffer" is installed. Its diameter range goes from 500um to 900um.
- Outdoor
  Besides all the protections for indoor, either kevlar and a jacket (1.8mm to 3mm) or plastic tube and jacket (for groups of 2 to 24 fibers).

A.2.1.2 Physical working

The principle behind the guidance of electromagnetic waves over optical fibers is the concept of total internal reflection [44]. It is known that every medium has an associated refractive index. This number is a ratio between the speed of light in vacuum over the speed of light in the medium. The fact that the speed of any electromagnetic wave changes for diverse media, has a consequence on its trajectory when passing through the boundary that separates them (Snell's law).

Usually, electromagnetic optics and Fresnel's laws are used to describe the characteristics of such type of transmission instead of Snell's law given that the latter just offers a geometrical view of the problem whereas the first one provides phase and magnitude information. This geometrical approach to the light confinement is exclusively valid when the diameter of the core is much larger than that the wavelength (multimode condition).

A.2.1.3 Refractive index

Defined above as a ratio between the speed of light in the vacuum and the speed of light in the material, the refractive indices and its relation core-cladding have a strong influence on the propagation characteristics including the distribution of the optical power [46] and it has been shown that the bandwidth of any fiber entirely depends on how these factors are designed [47]. Its variation over the radius draws a shape which can be 2D-plotted. It is named "index profile".

Two aspects must be clarified before developing on the types of profiles: diameter and doping. The first one is often used to distinguish between SingleMode (SMF) and MultiMode Fibers (MMF). These "single" and "multi" prefixes refer to the amount of rays that travel through the corresponding fiber at the same time. Even though this is not strictly correct due to the fact that the actual amount also depends on the wavelength and the medium, it is a fair approximation for the usual frequency bands, glass composition and sizes. Today's standard MMFs have a core diameter of either 62.5µm or 50µm with an overall cladding diameter in either case of 125µm. For its part, SMFs range within 8µm and 10µm for the core (though special purpose SMFs may reach 4µm [48]) with a cladding of 125µm in diameter. Concerning the doping, it is what establishes the refractive index variation with respect to the radius between cladding and core. Taking fused silica ($Si0_2$) as starting point, its index can be either raised by doping with germanium dioxide (GeO_2) or lowered with fluoride [48]. However, because dopants always increase the attenuation per kilometer (differently for each substance), it is not immediate to find the optimum amounts that make the fiber meet certain requirements.

Regardless of the diameters, two main types of profiles exist. The second arose as a solution for the distortion introduced by the disparate propagation of modes within the same core:

- Step index
  It has a step-like shape. It has constant index in the core without any variation with respect to the radial position. It follows the next equation:

  $$n(r) = \begin{cases} n_{core} & r \leq a \\ n_{cladding} & r > a \end{cases} \quad \text{(A.1)}$$

  with a being the core radius. Needless to say that the refractive index on the cladding must be the lowest to guarantee total reflection. Every fiber (MMF and SMF) can be found in this fashion.

- Graded/Grade index
  Most MMFs are designed this way. It shows generally a power-law equation [40]:

  $$n^2(r) = \begin{cases} {n_{core}}^2 \left[1 - 2\Delta \left(\frac{r}{a}\right)^{\alpha}\right] & r \leq a \\ n_{cladding} & r > a \end{cases} \quad \text{(A.2)}$$

  with α [integer] being the profile exponent, and Δ [percentage] the profile height that describes the relative index difference of the core and cladding. According to this, we can express $n_{cladding}$ as:

  $$n_{cladding} = {n_{core}}^2[1 - 2\Delta] \quad \text{(A.3)}$$

  Note that the step index is a particular case of the power-law equation for α equal to infinity.

In Figure A-5, four ideal profiles for a 50µm multimode fiber are shown. The blue, red and green traces correspond to α equal to 2, 2.3 and 1.7 respectively. Usual values for the alpha coefficient fall well within this interval. A pseudo-optimum profile exponent exists ([16]), and it depends on the refractive indices, the wavelength and the material properties. In black, we observe the step index case. The refractive indices for this example have been randomly but sensibly chosen according to commercial fibers from different manufacturers (anexo F).

[16] The optimum profile would cancel completely the intermodal interference. This cannot be done completely because it is not possible to counter the dispersion caused by "meridional" and "skew" rays with a power-law profile.

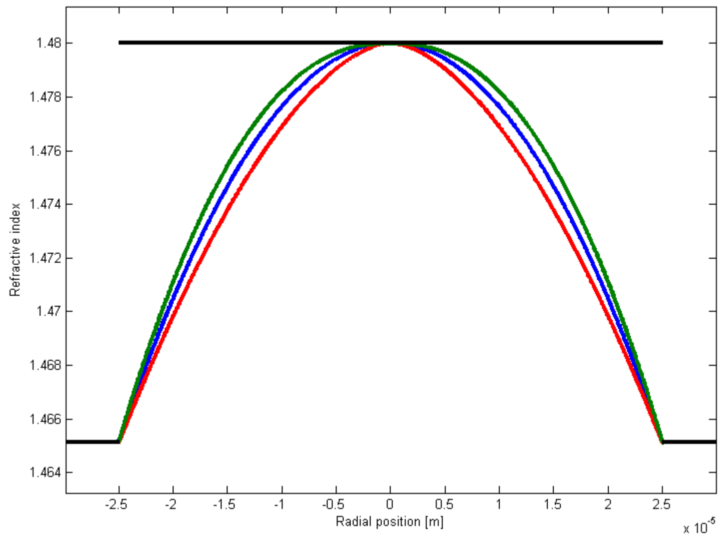

Figure A-5 Grade-index profiles of 2 (blue), 2.3 (green) and 1.7 (red) profile exponents. Step-index profile (black).

A.2.1.4 Propagation

In compliance with geometrical optics, rays propagate by bouncing on the core-cladding interface with different incident angles. Only those for which its phase shift is multiple of 2π will interfere constructively after two reflections and consequently will be guided. This would perfectly explain the propagation over plane waveguides and multimode fibers. But, as the core size becomes comparable to the wavelength (singlemode fibers), a wave-propagation theory is necessary [40]. Besides, despite the inherent complexity of such analysis, it can be extended to multimode fibers as well.

In the same way that electromagnetic fields propagate through air or vacuum because they comply with the "wave equation", those electromagnetic fields coupled into the fiber which are intended to propagate power ([17]) variations (information) must also fulfill it in our particular medium. All the solutions to the wave equation that satisfy certain boundary conditions and whose special distribution does not change with propagation are known as "modes" (up to now called "rays") [40] and these can be guided, leaky or irradiative; being the guided ones the responsible for the real transmission.

Given the cylindrical shape of the medium, the wave equation is written in the corresponding coordinates as:

$$\frac{\partial^2 E_z}{\partial r^2} + \frac{1}{r}\frac{\partial E_z}{\partial r} + \frac{1}{r^2}\frac{\partial^2 E_z}{\partial \phi^2} + \frac{\partial^2 E_z}{\partial z^2} + n(r)^2 k_0^2 E_z = 0 \quad \text{(A.4)}$$

Notice that the z-component of the electric field has been used. This is because Maxwell's equations allow us to obtain the rest of the components from only one, hence it is not necessary to solve it for all of them. Usually, the z-component is reckoned [44].

[17] See Poynting Vector.

One important thing about using the correct coordinate system is that the solutions are separable simplifying the calculations drastically. Therefore, applying separation of variables, E_z can be expressed [40]:

$$E_z(r,\phi,z,t) = KF(r)G(\phi)Z(z) \quad \text{(A.5)}$$

Substituting in (A.4) and evaluating the equation:

$$G(\phi) = e^{j\rho\phi} \quad \text{(A.6)}$$
$$Z(z) = e^{-j\beta z} \quad \text{(A.7)}$$
$$\frac{\partial^2 F}{\partial r^2} + \frac{1}{r}\frac{\partial F}{\partial r} + \left(n(r)^2 k_0^2 - \beta^2 - \frac{\rho^2}{r^2}\right) E_z = 0 \quad \text{(A.8)}$$

with β being the propagation constant of the modes and ρ restricted to integer values since the field must be 2π-periodic in ϕ. It can be seen that Equation (A.8) is directly dependent on the index profile. In the case of step index, the problem is easily separable into two with constant refractive index: core and cladding. The equation is thereby rewritable as two separate Bessel's differential equations. After applying boundary conditions, we discard the non-concurrent solutions and take the Bessel function of the first kind of order m (J_m) for the core and the Bessel function of the modified Bessel function of the second king of order m (M_m) for the cladding. The last step to find out the modes is to evaluate both solutions at the core edge and force the continuity of the fields. This yields the "characteristic equation" whose evaluation generates the propagation constant associated to every mode. For grade index fibers no analytical solution exists and the equation needs to be numerically solved. There are some well-known methods of approximation such us "finite differences" that can be used in this context.

Modes are uniquely described by its propagation constant:

$$\beta = n_{effective}\ \mathrm{k}_0 \quad \text{(A.9)}$$

the effective index or $n_{effective}$ is the refractive index that a given mode sees along its overall propagation. It is inherently associated with the phase velocity and it is affected by the modes trajectory, medium and wavelength for multimode propagation and exclusively medium and wavelength for singlemode.

Guided modes are those for which $n_{cladding}\ k_0 < \beta < n_{core}\, k_0$ and can be classified according to their field components:

- Transverse-Electric ($TE_{m,n}$): the electric field component in the direction of propagation equals zero.
- Transverse-Magnetic ($TM_{m,n}$): the magnetic field component in the direction of propagation equals zero.
- Hybrid ($EH_{m,n}$, $HE_{m,n}$): electric and magnetic field components in the direction of propagations differ from zero. The first letter indicates the dominant field.

Under the assumption of weakly-guided modes ([18]), the field components in the direction of propagation are negligible compared to the transversal ones, giving rise to a new sensible nomenclature for the modes: Linearly Polarized modes ($LP_{m,n}$). Each of them is characterized by the radial (m) [0 up to infinity] and azimuthal (n) [1 up to infinity] orders whose combinations provide every mode with different spatial distribution.

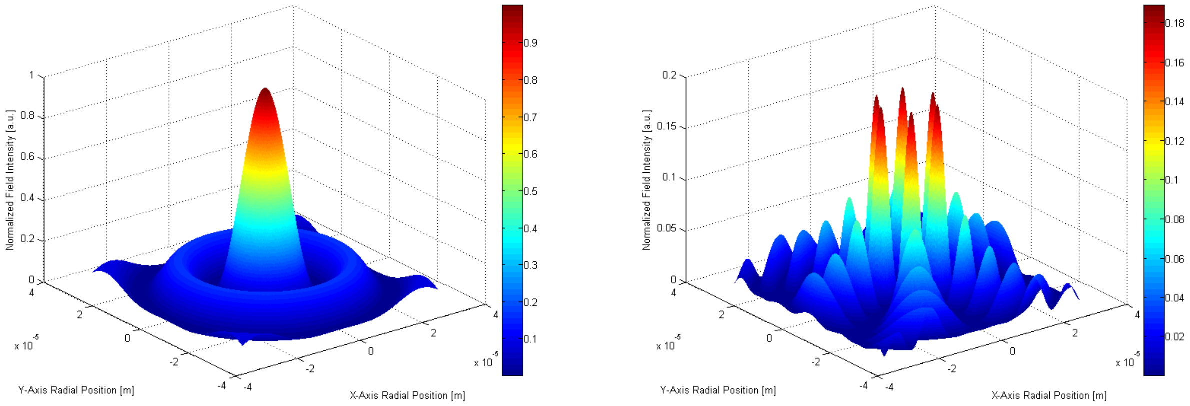

Figure A-6 Normalized field intensity of the mode LP_{01} (left) and LP_{34} (right) for a 50µm fiber.

The mode LP_{01} corresponds to the HE_{11} which is the mode that always propagate (multimode and monomode). Its shape (for step index fibers) is very similar to a Gaussian function and if such approximation is used, the deviance is negligible for single mode fibers. The LP_{34} in Figure A-6 is shown as an example of the symmetry generated by the mode orders.

In the refractive index description it is mentioned that although the usual operating windows, indices and sizes allow saying that a 50µm fiber is multimode and a 5µm one is singlemode, this is not strictly correct. The number of modes that propagate depends on the material, the wavelength and its size with respect to such wavelength. Concerning this, there are two parameters that play an important role in determining the total guided modes named “normalized refractive index” and “normalized frequency”. The first one expresses in a range from 0 to 1 any effective refractive index. Those with a value of 0 are those whose value equals the one of the cladding (therefore not guided) and 1 those that equal the core index. The second can be thought of as a figure of merit of the fiber. Its value gives information mainly about the number of propagating modes ([19]) and how much energy is confined within the core (Marcusse’s approximation to the mode radius for singlemode fibers with 1.2< V<2.4 [49]). Concerning MMFs, several approximations exist to estimate the number of propagating modes for certain V [50]:

- Step index: $M = \frac{V^2}{2}$, with $V > 10$
- Graded/Grade index: $M = \left(\frac{\alpha}{\alpha+2}\right)\frac{V^2}{2}$

[18] Mathematically expressed as $\frac{{n_{core}}^2 - {n_{cladding}}^2}{2{n_{core}}^2} \cong \frac{n_{core} - n_{cladding}}{n_{core}}$, with n_{core} and $n_{cladding}$ being the refractive indices of the core and cladding respectively.

[19] Any fiber whose normalized frequency is less than 2.405 is singlemode

A.2.1.5 Launch conditions

In the context of optic communication for MMF-based transmissions, launch conditions correspond to how the optical source illuminates the fiber facet. The way it is done restrict the number of modes that are actually excited and it is crucial to fully understand the performance of the fiber. The measurement of fiber losses and bandwidth is inseparably related to light launching which in turn, depends on the type of optical source. The most conventional sources are light-emitting diodes Light-Emitting Diodes (LEDs) and laser diodes LDs (VCSELs and Fabry-Perot). This section develops on the types of launch scenarios:

- OverFilled Launch (OFL)
  The core is fully and uniformly illuminated. This is produced by most Light Emitting Diodes (LEDs), whose radiation pattern is wide and Lambertian ([20]). Under these conditions, all the modes that the fiber can support (see section A.2.1.4) are excited.
- Radially OverFilled Launch (ROFL)
  Similarly to OFL, the whole core is illuminated. The difference is that the source is a LD or a SMF ending sufficiently separated from the MMF's facet. Given this situation, only the modes with cylindrical symmetry (radial modes) are effectively excited hence its name.
- Restricted Mode Launch (RML)
  A small part of the core is illuminated. It arose due to the emergence of VCSELs in 90s, whose spot size was significantly smaller than the cores of the commercial MMFs. This kind is also known as underfilled launch and it allows for selective mode excitation.

Quantitatively, the power transmitted from an incoming field to every mode is known as Modal Power Distribution (MPD) and it accounts for the percentage of the input field power that is transmitted to every mode supported in a given fiber. Mathematically, it is the normalized overlap integral of both incident field and mode field [14]:

$$\eta_{m,n} = \frac{\left|\int\int E_i E_{m,n}^* dA\right|^2}{\int\int |E_i|^2\, dA \cdot \int\int \left|E_{m,n}\right|^2 dA} \quad \text{(A.10)}$$

with E_i the incident electric field and $E_{m,n}$ the modal distribution of the mode $LP_{m,n}$.

A.2.1.6 Distortions

Distortions are those undesired mechanisms that keep our link far from ideal. In general, the ideality measurement of a MMF-based communication link such as ours is given by the system's information transmission capacity or bandwidth ([21]), which ranges from 0 (no transmission capacity) to infinity. All the distortions have a negative impact on the bandwidth (directly or indirectly) and thereby on the system's throughput that sometimes can be countered, some other reduced and in the rest just assumed. It is also worthy of mention that some of the impairments are very closely related (attenuation/power-

[20] Constant emitted power per area unit and solid angle.
[21] This bandwidth should not be mistaken for the optical bandwidth.

nonlinearities, chromatic dispersion-Four Wave Mixing (FWM), Self Phase Modulation (SPM)-laser chirp) and its individual treatment is not always simple, implying trade-offs and pragmatic choices.

This section describes the main impairments of our channel that affect the bandwidth, how they do it and their best cancelation approach if any.

Attenuation

Attenuation itself does not limit the bandwidth of the fiber, however, it does affect the total amount of power that reaches the end of the fiber. Since receivers need a minimum amount of power to perform accurately or even work, the losses per meter really represent a factor to consider.

Measured in decibels per kilometer (dB/km), the attenuation coefficient depends mainly on the material used for the fabrication of the fiber. Because electromagnetic waves at different frequencies behave differently when they impinge or propagate over certain and given the huge spectrum used for optic communication, it is sensible to measure the attenuation subjected by the light on silica with respect to the wavelength (see Figure A-7).

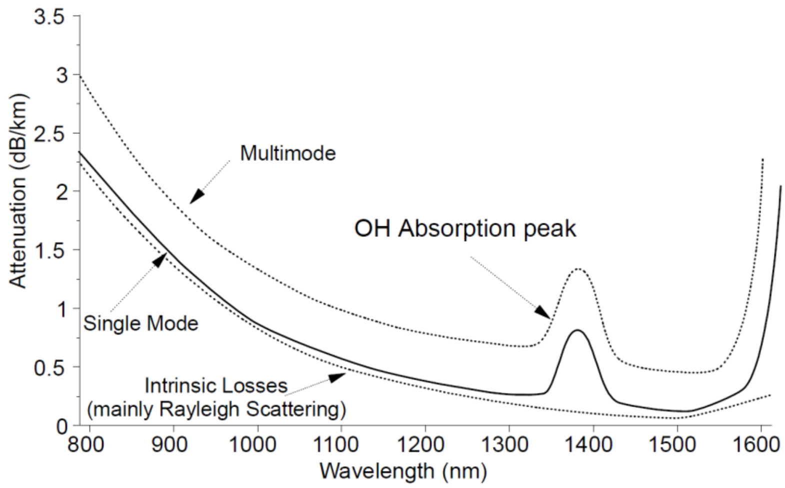

Figure A-7 Loss spectrum of typical singlemode and multimode fibers.

Attenuation in fiber is caused by absorption, scattering and radiation ([40], [48]). The improvement of the manufacturing techniques has permitted to lower the attenuation in general, and to create some interesting types of fiber that offer a solution for some individual aspects (“dry fibers” or “bend-insensitive fibers”). Notice in Figure A-7 that MMFs have greater losses than SMFs. This is because the amount of dopants used to make the profiles is lower for SMFs (see section A.2.1.3).

Intermodal Dispersion

It has been explained that certain types of fibers support more than one mode depending on physical and operational parameters (see section A.2.1.4). It is also known that every single mode is uniquely characterized by its propagation constant (A.9), whose effective index can be expressed as:

$$n_{effective} = n \cdot \cos\theta \quad \text{(A.11)}$$

with θ being the angle formed by the mode trajectory with respect to the rotational symmetry axis of the fiber. For step fibers the refractive index remains constant throughout the core and therefore, all the modes propagate at the same speed (see section A.2.1.2) but following different paths. Such modes will reach the end of the fiber at different moments (with different delays) generating a multipath situation that causes “pulse spreading”. Simply sticking to Fourier Transform rules, if a signal spreads in time shrinks in frequency; said in other words, our bandwidth decays.

In order to address this distortion:

- Grade/Graded index fibers:
  This profile was specifically devised to solve this impairment. Since multimode fibers will unavoidably support more than one mode, this solution gradually changes the refractive index of the core to equalize the channel and force outer modes (longer paths) to propagate faster than the inner ones. This profile is described by a power-law equation whose key parameter is the power coefficient α which, if correctly designed, can totally compensate the delays of meridional rays ([22]). Such optimum value depends on the index variation with the wavelength (P, profile dispersion parameter), the frequency itself (λ) and the index difference (Δ). Several proposals have been found for the specific formula ([51], [52]) and two situations are distinguished:

  - No wavelength dependence

$$\alpha_{optimum} = 2(1 - \Delta) \quad \text{(A.12)}$$

  - Wavelength dependence

$$\alpha_{optimum} = 2(1 - \mathrm{P}) + F(\Delta, \mathrm{P}) \quad \text{(A.13)}$$

  The profile dispersion parameter is defined as:

$$P = \frac{n_{core}}{n_{gcore}} \frac{\lambda}{\Delta} \frac{d\Delta}{d\lambda} \quad \text{(A.14)}$$

  with n_g or core group index:

$$n_{gcore} = n_{core} - \lambda \frac{dn_{core}}{d\lambda} \quad \text{(A.15)}$$

[22] Meridional rays are those that propagate within the plane that that contains the fiber’s rotational symmetry axis. On contrary, skew rays are those which propagate describing a spiral as they bounce on the core-cladding interface. Most of the skew rays end up being radiated thus they hardly contribute to the pulse spreading.

Although the ideal α exists in theory, in practice it is complicated to build. Within the most common deviations we find axial dips/peaks, inner profile coefficient variation, outer profile coefficient variation and core-cladding interface problems [53]. Notice that some skew rays will not be radiated and although at least one specific profile make the delays independent from such rays [52], they will also have some impact on the pulse spreading.

- Singlemode fiber
  Another more intuitive solution is to force the normalized frequency to be lower than 2.405 by tuning the fiber's size, wavelength and refractive index. This way, the fiber becomes singlemode and the intermodal dispersion is completely eliminated at the price small tolerances during the fabrication that increase the overall cost of any singlemode-based system. Conventional fibers are usually 8µm to 10µm in diameter for the core and are operated down to ~1100nm.

- Restricted Mode Launch (RML) and Offset Launch (OL)
  As the multipath problem that intermodal dispersion is, reducing the number of paths will result in a better performance. If only those that exhibit lowest relative delay are excited, the improvement would be even greater. This is exactly what RML+OL technique does. While RML helps couple light into a restricted number of modes, the radial displacement of the VCSEL's spotsize allows selecting those that give better response. If fine enough adjustments are done, it is possible to excite the LP_{01} mode exclusively having then, virtual singlemode propagation ([23]). However, that would require precise alignments that would increase the price and make it comparable to the one of a true singlemode set which offers better performance.

  The real benefit of the RML+OL technique is that, together with grade indices, it provides up to 4-fold bandwidth gain with respect to OFL with much more relaxed alignment constraints than for center launch situations (±5µm of radial offset and 6 degrees in angle) and great stability against environmental influences such as temperature, connector misalignments and mechanical vibrations [8]. The OL technique became feasible in late 90s and its benefits have been widely proved and tested.

Group Velocity Dispersion (GVD)

This type of distortion is usually negligible compared to intermodal. Notwithstanding, as the fabrication precision of the graded profiles improves and so does the light injection processes, the chromatic or intramodal dispersion has more and more impact on the pulse spreading. Notice that because there is no intermodal dispersion in singlemode fibers, this type mostly becomes the dominant [54].

[23] In general, modal power coupling due to connector misalignment, local bends, scattering or nonlinearities will make the propagation not be purely singlemode.

Intramodal dispersion is caused by frequency-dependent variations in the refractive index of the medium. The variations in frequency are due to the unavoidable linewidth that any optical source has ([24]). Two main subtypes are observed [40]:

- Material
  The physical properties of silica, namely the refractive index, change as it is illuminated with diverse frequencies. This contribution cannot be disregarded either for multimode or singlemode fibers.

- Waveguide
  It has been shown that the propagation constant is a function of the wavelength amongst other parameters. Given the spectral width of the source, every mode may have not only a characteristic refractive index but also a particular wavenumber.

The total coefficient is calculated by summing both contributions. The Figure A-8 shows an example of chromatic parameter calculation and representation for standard singlemode fiber. The blue trace corresponds to the material dispersion. The green curve represents the waveguide dispersion and it can be locally changed by varying the fiber's core radius. The red curve represents the total chromatic dispersion.

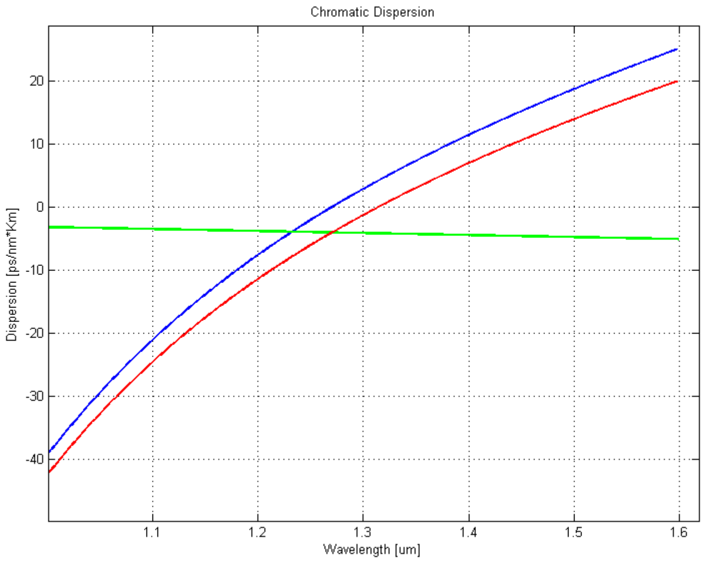

Figure A-8 Total chromatic dispersion (red) and relative contribution of material dispersion (blue) and waveguide dispersion (green) for a conventional singlemode fiber.

It can be observed that there is a wavelength for which the dispersion equals zero. It is usual to work as close to this point as possible though its usage has some drawbacks that need to be evaluated (FWM). Another interesting point is the fact that the waveguide dispersion can be tuned. It allows the creation of the so called "dispersion-shifted fibers" which move the zero dispersion point (around 1.32μm in Figure A-8) up to the third window.

[24] Atoms' energy levels become energy bands when they constitute molecules. Direct modulation causes chirp that in turn enlarges the linewidth. Finally, when the modulation bandwidth becomes proportional to the laser's linewidth, the latter may expand.

Polarization Mode Dispersion (PMD)

Although it is the least dominant factor, it cannot be fully compensated. It should only be consider when there is neither intermodal distortion nor GVD and working with high bit rates [40]. It is caused by symmetry variations along the core that make both polarizations be affected differently generating a completely random polarization at the final end of the fiber. The consequence is also a pulse widening that limits the system performance.

A.3 Receiver

A.3.1 Photodetector

Photodetectors or photodiodes (PD) convert light into electric current by exploiting the photoelectric effect. The most conventional semiconductor PDs for data-communication links are PIN and Avalanche (ADPs) however, there are several types that constitute a present alternative for specific applications or a future general-purpose replacement. Some of these are: Schottky-Barrier, Hetero-Interface, Travelling-Wave and Resonant-Cavity [48]. Schottky-Barrier and Hetero-Interface PDs are not often installed but they are being subject of deep research due to the promising properties they have shown so far, Resonant-Cavity show very high quantum efficiency at high bit rates at the price of being wavelength specific and difficult to build and Travelling-Wave exhibit high quantum efficiency at extremely high bit rates compared to PINs (double or triple).

A.3.1.1 PIN

The p-n junction, generally used as a light emitter, can be used as a light absorber if it is inversely polarized. On contrary to what is done when used as emitter, the already existing electric field in the depletion layer is made thicker by applying an inverse current. This has three main advantages [52]:

- As the electric field increases, the carriers leave the depletion layer faster. Higher bit rates supported.
- Because the depletion layer gets thicker, the number of absorbed photons is higher. Increased efficiency
- The widening of the active region with respect to the material extension reduces the parasitics. Improved electric bandwidth.

Nonetheless, p-n PDs have a great disadvantage that makes them unsuitable for >1Gbps datacom systems [55]. Some electron-hole pairs that are created outside the active region end up entering because of their intrinsic mobility. This generates current that drastically limits the systems bandwidth. PINs come to solve that problem.

By adding a slightly n-doped intrinsic layer between the p-doped and n-doped silicon (P-I-N), the depletion layer is made much thicker in comparison with the p/n zones. This solution, which is adjustable, keeps or augments the advantages of the p-n junction and reduces noticeably the diffusion current given that p/n zones can be much thinner.

To characterize a PIN diode, there are two important parameters: Quantum Efficiency (QE) and responsivity. They are very closely related and they give information about the number of electrons per photon generated (ideally 1). These parameters are usually accompanied with the wavelength since they directly depend on it. Responsivity can be seen as a QE that besides, accounts for the energy variation at different wavelengths.

A.3.1.2 Avalanche PhotoDiode (APD)

Avalanche PDs are PINs subjected to a very high reverse polarization. The aim is to create strong enough electric field so that the electrons generated by the photoelectric effect collide with other electrons transmitting the necessary energy to push them up to the conductive level thereby creating an electron-hole pair [55]. This is called “impact ionization” which results in “avalanche breakdowns”, hence their name. This gain of this type of photodiodes ranges between 10 and 100 what means that a single electron can produce from 10 to 100 electron hole pairs [55].

The structural difference with respect to PIN is the addition of a lightly p-doped segment between the n-doped and the intrinsic layer. This is where the gain generation takes place. Exactly as for PINs, the alloys and materials used for their fabrication restrict their wavelength range.

This type of laser is more complex to use and more expensive than PIN but it offers a very high sensitivity. The first window is conventionally used for SR communications whose attenuation is not big enough to need of such high sensitivity. However, they are commonly used for long-haul or link length measurements [48].

A.3.2 TransImpedance Amplifier (TIA)

TransImpedance Amplifiers are devices installed right after the PDs. They convert current into voltage and avoid the two principal problems that arise when dumping all the output current into a simple resistor. Because the PDs usually have non-negligible capacitance, if the load resistor is very high, the RC transient will increase and the electrical bandwidth will drop accordingly. On contrary, if the resistance is very low, there will be low gain and the Signal-to-Noise Ratio (SNR) will be insufficient. TIAs provide considerably faster RC transient and very high gain (tunable if necessary) [56]. Schematic shown in Figure A-9.

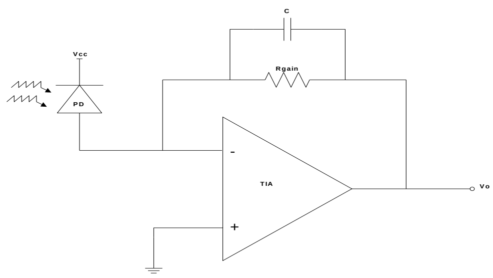

Figure A-9 Transimpedance amplifier schematic.

The ideally infinite input impedance of the operational amplifier guarantees that its negative pin's voltage equals ground. The capacitance "C" is used to reduce the oscillations produced by the amplifiers circuitry when working on negative feedback [56]. The resistor in parallel with the capacitor resistance constitutes the gain of the circuit ($V_0 = -I_{diode} \cdot (R_{gain} // C)$).

A.3.3 Filter

The last element of the front end is the low pass filter. It removes the harmonics created at the photodiode and the Out-Of-Band (OOB) noise. The accurate and correct election of the type, the order and the cut-off frequency is crucial to improve the SNR. The analogue filters may have non-linear ranges of operation, they are made up of electronic components that have a certain tolerance which moreover changes with temperature and high filter orders require more electronics with the subsequent increase of complexity and price.

If the insertion loss method is used for the design, the filter type is determined by the function used to define the power loss ratio. Depending on such function, the properties of the filter response will vary and they have to be assessed in order to choose the ones that adapt the best to the concrete system specifications [57].

Table A-2 Common eletrical filters and their representative characteristics.

Filter type	Cheracteristics
Butterworth	Flattest possible passband response.
Chebyshev I	Steeper roll-off than Butterworth but constant ripple in the passband.
Chebyshev II	Steeper roll-off than Butterworth but constant ripple in the stopband.
Elliptical or Cauer	Constant but independent ripples in the passband and stopband. Sharper roll-off than Chebyshev.
Bessel or linear phase	Flat passband. Linear phase response. Long roll-off.

For instance, if an amplitude modulation is being used, it is very important that the filter does not have ripple in the passband. Besides, the linear phase would not be a key requirement in that case. The proper choice would be a Butterworth filter. In the particular case of OFDM, constant phase variations rotate the received constellation proportionally to the relative phase shit. This distortion is easily corrected in the equalizer, thereby allowing us to discard the usage of Bessel filter. Albeit random amplitude variations could ruin the reconstruction, constant ripple do not represent a real problem because the narrowness of the subcarriers make them suffer flat fading that, again, is easily correctable with the 1-tap equalizer. All these means that the proper choice for OFDM would be a brickwall filter such as Cauer or high order Butterworth. The same type of analysis should be done for every system in order to find the cheapest and most suitable option.

A.4 OFDM

Orthogonal frequency division multiplexing can be seen either as a parallel transmission scheme or as a modulation technique itself. The concept behind OFDM is to divide a serial bit stream into a set of parallel streams each of which is transmitted on a separate frequency. As a result, the data rate of each individual channel is reduced proportionally to the number of subcarriers used for the transmission [58]. This bandwidth reduction makes ISI affect at most one symbol [59] since the symbol period is made long compared to the delay spread undergone in time-dispersive channels. This makes OFDM especially suitable for multipath scenarios such as wireless, MMFs or Plastic Optical Fibers (POF). Another advantage of having narrowband subcarriers is that they subject flat fading; this allows using simple 1-tap frequency domain equalizers instead of time domain ones, whose complexity scales-up quickly with the data rate and the channel dispersion [59].

Similarly to FDM, OFDM symbols can be regarded as ideally windowed sine functions. In the frequency domain this is represented as a sinc function centered at the sine's frequency. This is illustrated by Figure A-10, where a 1 Hz tone is windowed in the time domain with a 10 sec ideal rectangular filter. Nonetheless, unlike FDM or WDM, in OFDM the adjacent subcarriers are positioned at their respective "first zeros" of the sinc function. It is a well-known result that for a sinc function, these zeros are $1/T$ displaced from the center frequency and with respect to each other; with T being the window time.

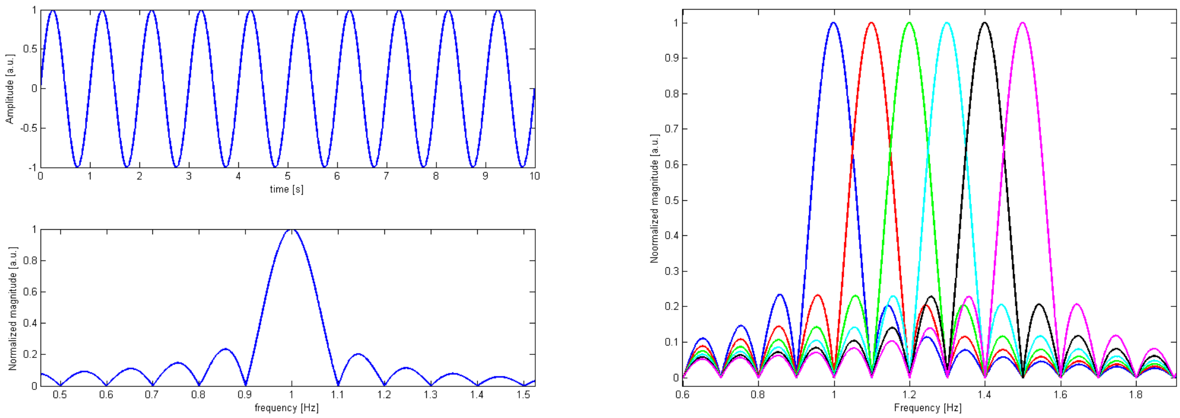

Figure A-10 Graphical demonstration of OFDM principle. Windowed sinusoid and and its spectrum (left). OFDM spectrum with six subcarriers (right).

Under these conditions the subcarriers are said to be orthogonal to each other, hence OrthogonalFDM. As observed in Figure A-10, this distribution of the channels allows overlapping thereby reaching a very high spectral efficiency. Besides, as long as the channel remains linear, each subcarrier can be demodulated without either interference or analogue filtering (typical in FDM) [59]. This simplifies the system and reduces its price. The drawback is that extremely high frequency accuracy is necessary, making OFDM very vulnerable to Doppler shift, frequency offset and random phase noise.

One crucial aspect is the robustness of OFDM against frequency and time-selective interferences and fadings [58], [60]. These distortions can be countered through the interleaving performed by the Serial-to-Parallel (S2P) conversion (it spreads the coded bits over a simultaneously transmitted set of frequencies) together with Forward Error Correcting (FEC) codes. Concerning FEC, the type of code needs to be carefully chosen so that it can handle worst case error lengths (chosen depending on the SNR and the data rate or the maximum estimated time interference). For its part, interleaving protects the link from frequency selective interferences or fadings. That way, although a carrier is removed, those bits which were supposed to be transmitted over that channel do not correspond to consecutive bits on the original sequence; therefore, the FEC processing can recover the data after undoing the process. The SP is usually reinforced with a pre-interleaving of the main stream itself [60]. Finally, adaptive modulation of every subcarrier based on previously chosen criteria can improve considerably the error probabilities and channel reliability.

Another important remark that must be discussed is the high Peak-to-Average Power Ratio (PAPR) of OFDM. Because the symbols are a summation of multiple sinusoids with different amplitudes and phases, they may interfere constructively at some random point in time, generating high power peaks. This forces key components such as output amplifiers or Digital-to-Analogue Converter (DACs) to have a wide dynamic range which is not always reachable or affordable. There are several techniques to face this problem [58].

Last but not least, OFDM moves the whole complexity of transmitter and receivers to the digital domain [59]. The demanding requirements and accurate designs for the analogue filtering are just substituted by DSPs and intelligent signal processing that, for instance, can correct for phase variations, frequency offsets and signal delays at almost no cost as well as recover the signal and demodulate it.

A.4.1 OFDM for optic communication (OOFDM)

Owing its good behavior in time dispersive channels, OFDM was firstly applied to wireless systems as soon as it became practical (mid-80s). Radio broadcasting and mobile communication were the first published applications [61]. Furthermore, the narrowband subcarriers and its good handling of frequency selective fadings promoted the application of OFDM on wired Digital Subscriber Line (DSL) in 90s. Nowadays, OFDM has been standardized for most WLANs (IEEE 802.11 a/g/n), broadband wireless and DVB as well as most of DSL applications [59].

In spite of being a very well investigated technique, OFDM has had a very little presence into the optical world owed to some structural and important working differences [59]. However, the emergence of 40Gbps and 100Gbps standards (IEEE 802.3ba) as a response to the increased bit rate demand and the improvements in digital signal processing have motivated the investigation of OOFDM. Moreover, its benefits are many: spectral efficiency, robustness against InterSymbol Interference (ISI) and InterCarrier Interference (ICI) cause by dispersive channels like MMF, simple equalization, efficient and cheap implementation through IFFT/FFT, robustness against selective frequency fading (interleaving plus FEC plus frequency spreading) and parallel structure that substantially decreases the processing load [61].

Today, OOFDM applications are still being investigated and tested for different types of fiber, lasers, configurations and parameters [62] and [63].

A.4.1.1 Considerations

In an IM-DD optical link, there are some important considerations that must be addressed before installing an OFDM modem. Firstly, in an optical link, the information is carried in the light intensity rather than the magnitude and the phase of the electromagnetic field. In the latter, the modulating signal can be bipolar because negative numbers are just phase shifted versions of their positive counterparts. Nonetheless, since the optical power cannot be negative, the modulating signal must be unipolar in an optical system. In order to achieve non-negative signals two main solutions are proposed: either DC-biased Optical OFDM (DCO-OFDM) or Assymmetrically Clipped Optical OFDM (ACO-OFDM) [64].

In DC-biased Optical OFDM a bias is injected so that the level of the signal is raised and all of it moved above zero. The problem of this technique is that it requires an increased dynamic range in the amplifiers and DACs to fully contain the signal in the positive side [64]. Seen differently, if such dynamic range is not sufficiently wide, there is going to be a large clipping distortion. Furthermore, if the bias is not well calculated, we may incur in extra clipping noise from the lowest negative peaks (too low bias); on the contrary, we may experience an unnecessary waste of power (too high bias). Its performance directly depends on the bias which in turn varies according to the constellation type [64].

Asymmetrically Clipped Optical OFDM clips the signal at the zero level. It has been proved [65] that if only the odd subcarriers are non-zero, all the clipping noise falls in the even subcarriers and hence the information can be perfectly recovered at the receiver. ACO-OFDM always requires double power than a bipolar system version and the same design is optimum for all constellations [64] and [65].

DCO-OFDM compared to ACO-OFDM is less power efficient for not too big constellations but on the other hand, its implementation simplicity is absolutely higher. Whereas DC-biased needs no modification on the conventional OFDM if a bias-t is used for the laser driving, ACO version requires a limiter, an external modulator and special digital signal processing in order to excite only odd frequency subcarriers. It has also being demonstrated that for low link attenuations, DCO gives the best signal quality [60]. The fact that its bias/design changes depending on the constellation, make it somewhat unsuitable for adaptive systems; something that does not happen in asymmetrically clipped OOFDM systems.

Another aspect to be aware of when using OFDM for an optical link is that the system must be linear between the IFFT/FFT pair to work properly [59]. This is because the equalization exclusively accounts for linear transformations such as delay and scaling thus, non-linear distortions will not be correctly compensated and the performance will drop. Square-law photodetectors used for direct detection create beatings that degrade the signal by generating interferences between subcarriers.

A.4.2 Discrete MultiTone modulation (DMT)

The Discrete MultiTone modulation is a variation of OFDM that takes advantage of the mathematical properties of the IFFT in order to generate at its output a real-valued signal [56]. This option allows removing the whole IQ modulator and operating at BB. The price is lowered and the complexity reduced since there is no need to install high-frequency, broadband analogue RF components [66].

It is known from complex conjugate relations of the Fourier transform that the IFFT of a spectrum with Hermmitian symmetry generate a real-valued signal. Based on this, the input coefficients must be rearranged to force such symmetry so that the first N remain as for conventional OFDM and the next N are flipped complex conjugate of the first half. Care must be taken to hold the “power of two” condition in the number of channels. In can be inferred from all this that double number of channels is necessary in the IFFT/FFT pair both in the transmitter and the receiver. This will slightly increase the computation however, the price and complexity are drastically reduced and the analogue processing in the modulator is practically removed (DAC/ADC are necessary). Another condition is that the DC component must be zero for DMT to work as expected. This is not a problem since most of the times the DC component is removed before any biasing or clipping procedure (for instance, a bias-T can be used in DCO-OFDM) [60]. Furthermore, the zero frequency subcarrier might be distorted by offsets in DAC or ADC or carrier feedthrough hence is removal is more of an advantage than a problem [60].

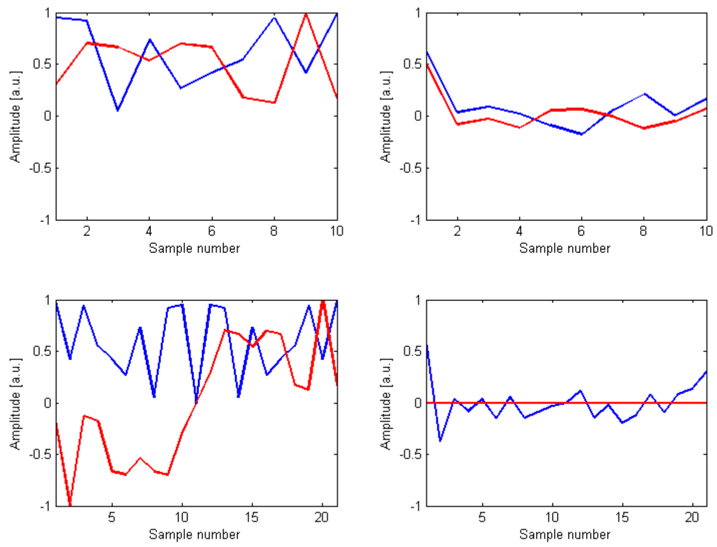

Figure A-11 DMT modulation example. The top pair of subplots represent a 10-samples long random signal in frequency (left) and time domain (right). The bottom pair show the DMT version of the same signal in time (right) and frequency domain (left). Read traces are the imaginary component and the blue traces are the real component.

It is observed in Figure A-11 that the imaginary part after IFFT is not zero owed to the lack of symmetry. If the Hermitical condition is applied (bottom left plot) the IFFT generates a purely real signal (the red curve remains constant and equal to zero).

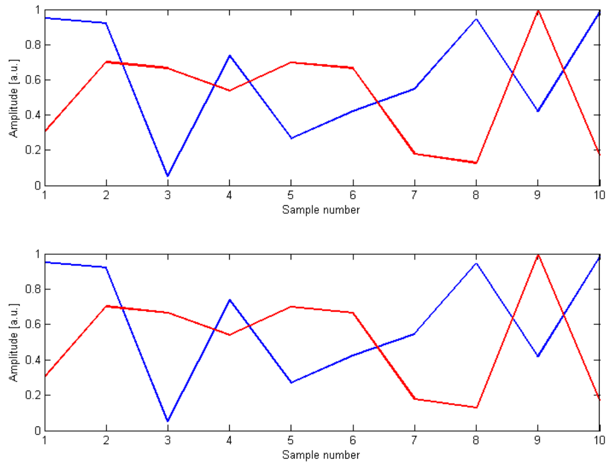

Figure A-12 On top, the FFT of a signal without DMT. On the bottom part, the FFT of the same signal with DMT.

As expected, both plots in Figure A-12 are exactly the same (duplication and zero padding have been undone). This shows the good working of DMT and also verifies its good implementation for later use in the final simulation.

A.5 Analysis and Design Tools

One of the most important phases in the preparation of a simulation is to make sure that your model working remains within reality. Analysis refers to the evaluation of the system's precision and how well it reproduces results from experimental exercises or alternative and verified simulations. For its part, design comprises the implementation of existing devices, procedures or subsystems into our specific simulation environment.

Both analysis and design are closely related however, little nuances make them differ from each other. First of all, the analysis validation is an upstream process unlike design, which is downstream or both. The system assessment implies a deep study of some low level physical aspects of specific modules and their comparison with real data (upstream). In the design, real data is collected, properly formatted and introduced in the software (downstream) for later evaluation (downstream and upstream). The analysis requires the user to stick to some standard measuring techniques and preset procedures so as to obtain valid comparative results. Those standards are often accompanied with some representative results or operative margins that are highly reliable and constitute a perfect reference point for the evaluation of the simulator. Another possibility is to compare your results with other simulations or experiments. This is often complicated to do because either the key parameters are not provided by the author/manufacturer or the results describe very specific characteristics that are not regulated by any standard. This forces the user to recreate (most often blindly) the specific scenario with extreme precision and use alternative evaluation procedures. Designing nonetheless, consists of interpreting the parameters correctly and give them the format that the simulator requires (which is not always trivial in "black-box" Computer-Aided Design (CAD) tools).

One of the things that makes a good software is the proper use of assumptions and approximations to skip unnecessary calculations and save time but still being accurate. This handling must be checked and it is basically the major source of errors. The concrete application and affordable margins will also play a significative part in determining how acceptable certain results are; for instance, assuming that there is not Polarization Mode Dispersion (PMD) in a short-reach 1Gbps transmission does not induce so much deviation as when it is assumed for a high-speed long-haul link.

This section summarizes the used tools for the evaluation/design of MMF and VCSEL in our specific optical link.

A.5.1 MultiMode Fiber (MMF)

A.5.1.1 Indirect bandwidth measurements (physical characterization)

These tools are used to make a deep and selective study of the causes of the distortion in the MMF. They are used to estimate the precision of the simulator and find out where the possible deviations are owed to.

Mode Dependent Attenuation (MDA)

Mode Dependent Attenuation is one of the three mode-depending distortion effects in a MMF and it has a strong influence in its characteristics [67]. It is caused by Rayleigh scattering, absorption and loss on reflection at the core cladding interface [20]. These loss mechanisms act differently on each mode, changing their individual attenuation coefficients. This effect does not have to be necessarily symmetrical or sensible given the random nature of the causes of such dispersions.

Strictly, the response of each of the loss mechanisms should be calculated to find out the exact influence on the MDA and build up a combined function. Nevertheless, this is complicated given the varied number of generated parameters that would not be easy to give correct numerical values [20]. Instead, separate and usual measurements of the fiber’s attenuation in the three transmission windows are done. The extrapolated function can be easily introduced in the simulation tool. In [20] the following formula is proposed:

$$\gamma(x,\lambda) = \gamma_0(\lambda) + \gamma_0(\lambda) I_p [\eta \left(x - \frac{1}{M(\lambda)}\right)^{\frac{2\alpha}{\alpha+2}}] \quad \text{(A.16)}$$

with $\gamma_0(\lambda)$ being the intrinsic fiber attenuation, I_p is the pth order modified Bessel function of the first kind, η is a weight constant, α is the profile exponent and $M(\lambda)$ is the number of modes, which for graded-index fibers is:

$$M(\lambda) = \left(\frac{\alpha}{\alpha+2}\right)\frac{V^2}{2} \quad \text{(A.17)}$$

Usually, MDA is also referred as Differential Mode Attenuation (DMA) to emphasize the fact that it is the difference in the attenuation of the modes what causes the impact. DMA affect the bandwidth by attenuating some modes so strongly that they do not contribute to the modal delay anymore. It can be inferred that if those modes with highest differential delay are filtered off, the attainable transmission rate can increase.

Mode Group Delay (MGD)

As it has been explained in section A.2.1, multimode fibers support many modes uniquely characterized by its propagation constant. All these guided modes with different velocities reach the end of the fiber at different time instants generating a multipath situation that reduces the attainable bandwidth. These group delays are a crucial property to describe the dispersion of signal transmitted over a MMF and its mitigation requires a detailed understanding of the results [68]. They are collected in the Modal Group Delay (MGD) measurement.

Under the assumption of weakly-guided modes, modes can be grouped in LPs, which are modes whose field components in the direction of propagation are negligible compared to the transversal ones. Besides, under those conditions, some LPs hold very similar group velocities thus they affect equally to the pulse spreading. This allows grouping them into numbered Degenerate Mode Groups (DMGs) [69]. The modes within a certain DMG will fulfill the following requirement [51]:

$$DMG_{NUMBER} = 2 * n + m - 1 \quad \text{(A.18)}$$

From the formula above, one can infer that the higher the DMG number, the more LPs contains. A consequence of this is that a radial light injection with a fixed spot size will excite a larger amount of modes the farther it is from the core center. This provides good modal noise immunity and stability despite the reduced dispersion [14].

One important advantage of the MGD study is that the injection condition dependence is, to some extent, eliminated from the intermodal distortion effect. It yields delay times for every DMG, which are selectively excited. MGD is also important to account for possible modal power coupling, since power transfer between modes is seen as a superposition of pulses with various group delays. This influence is clearly demonstrated in [70] where strong coupling in mode-division-multiplexed systems using coherent detection has been beneficial due to the modal dispersion reduction.,

MGD is often represented in a graph. In the Y axis the relative propagation delays with respect to the mode LP_{01} (DMG1). In the X axis the DMGs (see Figure A-13). The total amount of DMGs depends on the number of propagating modes.

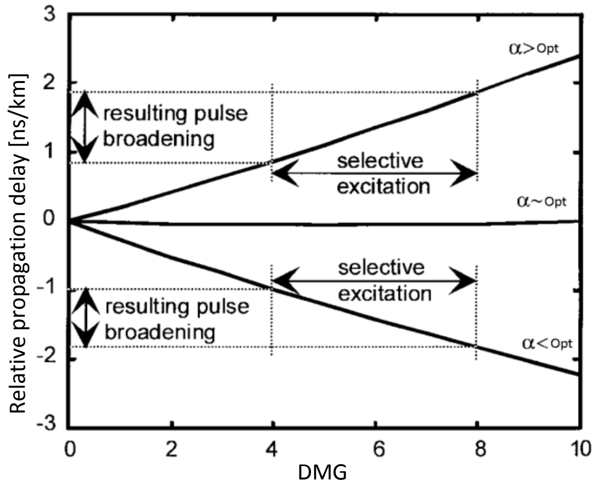

Figure A-13 MGD plot. It shows the dependence of relative propagation delay on mode group numbers for different cases of profile exponent values. [71].

As it can be seen in Figure A-13, there some expected tendencies depending on the profile exponent. If it is larger than the optimum, high order modes reach the opposite end later than the LP_{01} and vice versa. The three lines on the picture represent ideal alpha profiles. In practice it is impossible to obtain such straight lines but they exhibit curvatures and diverse oscillations owed to fabrication imperfections. For instance, a collapse during the production may generate an on-axis dip. Since the profile deviation is located in the center region, low order modes will propagate much faster that they should; this produces an oscillating MGD (like a sawtooth wave). Another example is when the profile exponent does not keep constant throughout the radius. If so, the relative propagation delay turns into a curved line rather than a straight one.

Mode Power Distribution (MPD)

It has been explained that RML limits the number of modes that are actually excited. If some of them do not contribute to the distortion, there could be a huge improvement of the bandwidth. It can also happen that imperfections in the fiber's cabling or fabrication cause that two neighboring modes yield very different delay times, resulting in a bandwidth close to the one obtained under OFL conditions. It is crucial to assure that an accurate mode excitation is calculated and that it corresponds to real parameters. Mode Power Distribution (MPD) determines whether only modes with similar velocities or the worst-case combination of modes will propagate along the fiber [51]. It is represented in a 2-D plot with Y axis being the percentage of the total power coupled for every DMG on the X axis. Figure A-14 shows a concrete example of MPD graph.

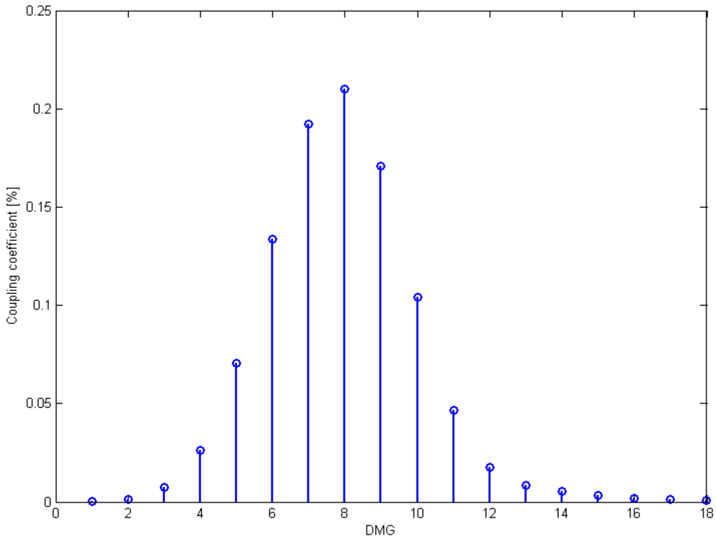

Figure A-14 MPD for a 62.5µm multimode illuminated with the output of a SMF that produces a 7µm Gaussian spot size at 1300 nm. The radial offset is 17µm.

MPD might be also called "mode coupling". It should not be mistaken for power cross-coupling between guided modes in optical fibers.

A.5.1.2 Direct bandwidth measurements (standards)

The next procedures represent regulated techniques for the determination of the MMF bandwidth. They are used to assure the fiber's compliance according to a certain transmission standard, which is often the relevant value in the development of a certain data-communication link.

The obtaining of satisfactory results based on any standard guarantees the good working within very well defined operational limits. When simulating, it is crucial to make sure that your system's behavior is sensible by comparing the results with these reliable and official references.

Differential Mode Delay (DMD)

The OFL and RML techniques are used for the bandwidth characterization of LED-based and VCSEL-based systems at less than 1Gbps respectively [72]. However, the appearance of VCSEL-based 10Gbps standard (IEEE 802.3ae) motivated the development of a more precise and complex standard for 50µm laser-optimized MMFs at 850nm called Differential Mode Delay. It characterizes the modal structure of a graded-index MMF without taking into account the type of laser source to predict the bandwidth [72] [73].

The measurement is conducted in accordance to IEC 60793-1-49 (2006) that replaces TIA-455-220-A (2003) and it consists of measuring pulse/impulse responses of the fiber for a SMF launch which radially scans the end-face of the fiber in increments of certain amount. The output graphs are called DMD plots and they provide dispersion cartographies that show where the fastest and slowest DMGs are located across the fiber core. The picture is then compared with “DMD masks” defined by ANSI/TIA or ISO/IEC, which establish minimum requirements for the DMD in order for the fiber to have certain transmission capabilities.

For the measurements, the mode field diameter is specified to be 5±0.5µm and the special resolution of the lateral scan is 1µm. With regard to the pulse duration, it depends on the estimated fiber class which is to be analyzed. For instance low resolution DMD for OM1 and OM2 use semiconductor lasers that generate 80ps to 100ps pulse, however, high quality fibers (OM3+/OM4) require very short duration pulses (around 10ps) which are achieved with Titanium Sapphire lasers [51]. The DMD is defined in Fiber Optic Test Procedure 220 (FOTP 220) as the maximum difference between the 25% (quarter maximum) threshold of the leading and trailing edges.

The standard divides the radius into three reference intervals for the DMD (see Figure A-15): inner section (5-18µm), outer section (0-23µm) and sliding sections (5µm width at 7, 9, 11 and 13µm offset launch) [51].

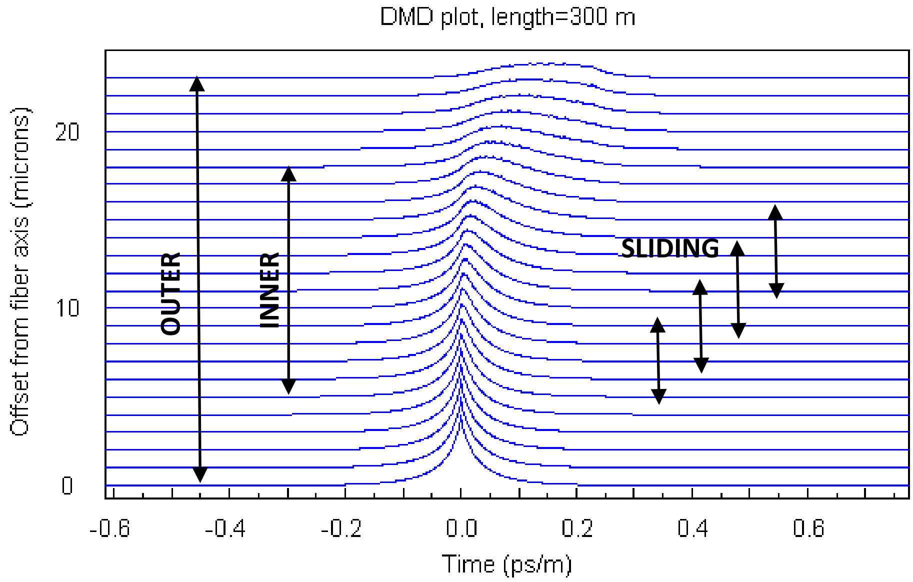

Figure A-15 Illustration of a DMD plot with the reference measurement regions superimposed. It was measured after 300m of parabolic alpha profile at 1300nm.

The standard definition contains the balanced combinations of the sections that need to be met for a fiber to belong to a certain fiber class which in turn, has associated a minimum bandwidth. These specifications are calculated for 300m-long reels. As an example, the DMD specifications for OM3 fiber type are shown in Table A-3.

Table A-3 DMD specifications for OM3 fiber.

Specifications	Inner DMD (ps/m)	Outer DMD (ps/m)	Sliding DMD (ps/m)
1	≤0.33	≤0.33	≤0.25
2	≤0.27	≤0.35	≤0.25
3	≤0.26	≤0.40	≤0.25
4	≤0.25	≤0.50	≤0.25
5	≤0.24	≤0.60	≤0.25
6	≤0.23	≤0.70	≤0.25

Encircled Flux (EF)

Covered in the IEC 61280-4-1 Ed2 (June 2009) standard, Encircled Flux measures the amount of optical power that emanates from a source and that penetrates a specific region of a fiber end-face as defined by prescribed radius limits [73]. It defines the launch specifications for diverse wavelengths and core diameters in order to standardize the illumination conditions.

It was firstly devised to provide an ideal general model of the output of an 850 nm VCSEL to allow mathematical modeling of laser-optimized fibers for the emerging high-speed Gigabit Ethernet networks (10Gbps, 40Gbps and 100Gbps). Later on, it was used as a method to define mode fill and increase the consistency in the bandwidth and loss measurements [74] not only for 850nm but also 1300nm and 62.5µm fibers to account also for "legacy" setups. It can be used as an independent reference or in conjunction with DMD to extrapolate the so-called effective modal bandwidth (EMB) that takes into consideration both delays and optical source field distribution for >10Gbps links [73].

EF is represented in a 2-D plot where the Y axis expresses the percentage of the total power transmitted within a circle of certain radius (X axis). Mathematically expressed as:

$$EF(r) = \int_0^{2\pi} \int_0^r i(r,\theta) r dr d\theta \quad \text{(A.19)}$$

with $i(r,\theta)$ being the normalized light intensity of the source.

Effective Modal Bandwidth Computed (EMBc)

Effective Modal Bandwidth Computed or Calculated EMB is a technique that reckons the worst case bandwidth that the fiber may exhibit when coupled to a VCSEL [51]. Therefore, it takes into consideration the type of source utilized. It consists of weighting each of the radial traces of the DMD plot by unit-less fractions specified for ten lasers that are representative of more than 10000 standard-compliant and commercially available VCSELs. These weights, generated from regulated EF calculations, are compiled in ANSI/TIA-492.AAAC-B (2009) which also reports the EMBc measuring procedure and a full description of DMD.

The standardized procedure follows the next steps [22]:

1. DMD calculation
2. Weighting the DMD radial traces with the corresponding ten factors (ten for each position)
3. The scaled pulses are summed up for each laser option. This generates ten scaled DMD plots.
4. The worst-case plot is multiplied time 1.13. The result is the EMBc

This system is mostly used by MMF manufacturers to assure 10Gbps (or more) compliance of the fiber for any existing type of VCSEL. Notice that, if the source is fixed and known, EMBc calculation is not necessary given that the field produced is very specific.

A.5.2 VCSEL

It is now known that this LDs exhibit some little desirable features that, although are present in many other sources, are noticeably more marked in VCSELs. Some of the possible factors are multimode operation, carrier diffusion, secondary pulsations in the turn-off transient and, above all, the thermal behavior [17]. Given their special impact, all these influencing factors require of a model that account for them (at least thermal dependence). Its development need of a very a deep physical insight that ends up in complicated and very computational demanding simulators. From the data transmission point of view, there are a group of key parameters which can be extracted from the three VCSEL's representative curves that allow the engineer to evaluate if the LD meets the pursued requirements or not. Nonetheless, the design of a VCSEL that satisfies those concrete specifications (downstream) is something completely different. In such case, a complete understanding of the model parameters and their specific impact on the communication-relevant figures of merit is required in order to tune the laser's properties within sensible/realistic intervals.

Here, the three main characterizing curves of a VCSEL are introduced.

A.5.2.1 Light-to-current-to-voltage (L-I-V)

The name comes from Light-Intensity-Voltage and it shows the output optical power and the device voltage with respect to the input current. It gives information about the maximum optical output power, threshold current, input impedance, safe current ranges, rollover region and some other thermal-dependent effects [17] [18] [16] .

Figure A-16, shows a VCSEL's LIV curve for a particular bottom emitting AlGaAs laser [17]. The blue, red and green traces represent the output power at 25^{o}C, 50^{o}C and 75^{o}C respectively. Their slope is given by the thermal resistance and the maximum power is achieved at the so-called "rollover current". From that point on, the laser's self-heating changes the physical properties and the power drops. Notice that it is a progressive process. The linear range for the output power is comprised between 5mA and 15mA. It can be also observed the threshold current increases with the temperature from 2.5mA to 3mA. The voltage function is represented in black and it exhibits non-linear behavior at low currents. The electrical input impedance can be estimated from its slope ([25]).

The LIV curves can vary considerably from laser to laser depending on the layout and materials used. In order to illustrate this, two more LIV curves are shown in Figure A-16 and Figure A-17 for index-guided InGaAs and a thin oxide AlGaAs 65.

[25] The laser behaves as a diode and, in theory, the resistance should me infinity in the other polarization

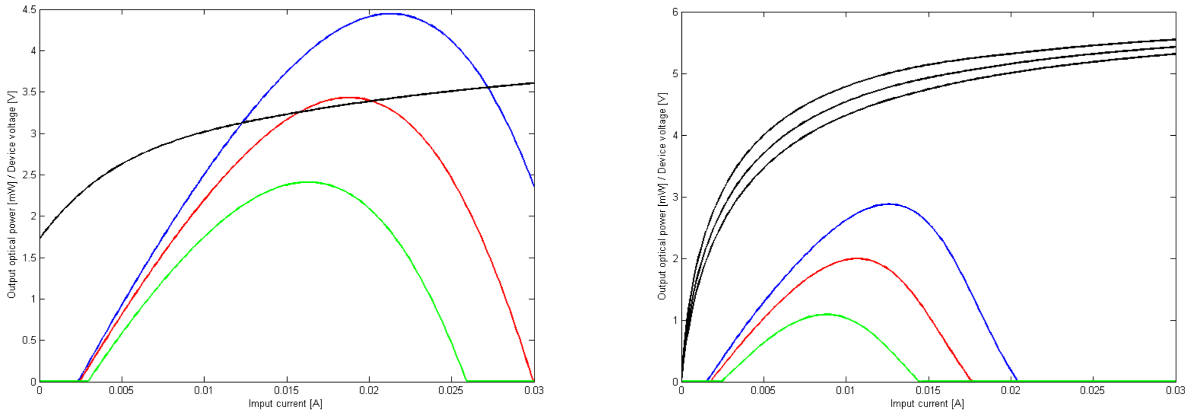

Figure A-16 LIV curves for AlGaAs VCSEL in (left) and index-guided InGaAs VCSEL(right).

The most remarkable difference between AlGaAs and InGaAs plot is the variation of the voltage with the temperature. From top to bottom, they correspond to voltages at 25°C, 50°C and 75°C.

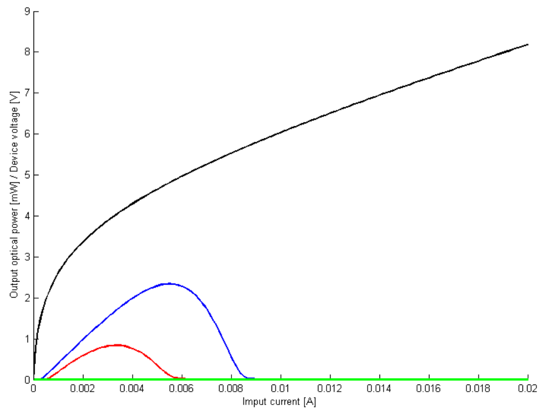

Figure A-17 LIV of thin oxide AlGaAs VCSEL.

The special property of the thin oxide AlGaAs is that it shows no output power that at 75°C. This is due to the excessive increase of the threshold current and the degradation of the slope efficiency [75].

A.5.2.2 S21 / transfer function

The next tool to characterize a VCSEL is the response of the system at different wavelengths or "dynamic response". This can be expressed either with the s_{21} parameter to account only for the device input impedance or with the transfer function, that considers the "source" impedance to account for possible mismatch at the input.

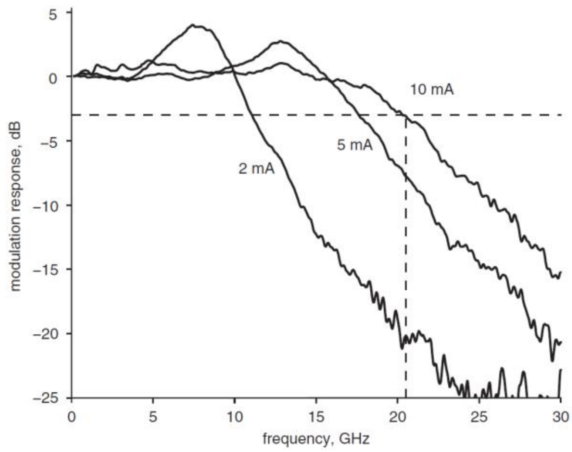

Figure A-18 Small-signal modulation response (s_{21}) for 3 different drive currents [76].

The measurement of the modulation bandwidth of a laser is strictly relevant when direct modulation is used. The transfer function provides information about the maximum reachable bandwidth (3dB bandwidth (BW)) for a given bias current. Figure A-18 shows an example of s_{21} for a particular 850nm VCSEL with an active region comprising multiple $In_{0.072}Ga_{0.928}As$ quantum wells to improve differential gain and reliability. It exhibits an especially high bandwidth at 10mA (>20GHz) and the key parameters and physical composition are described in [76].

Owed to the carrier density variations (see section A.1.2.1), LDs present resonances in their frequency responses which are proportional to the bias current and inversely proportional to the carrier and photon lifetime in the cavity. This can be clearly seen in Figure A-18, where two peaks at around 7.5GHz and 13Ghz are generated with 2mA and 5mA respectively. On the other hand, the damping factor is proportional to the bias, causing a fading of the peak as the injected current increases.

A.5.2.3 Spectrum

The linewidth, center wavelength and general spectral properties are also relevant in any LD characterization. Typically, the optical spectrum of a VCSEL is narrower than that of a Fabry Perot (FP) laser and broader than that of a Distributed Feedback Laser (DFB) which is designed for single wavelength operation [34]. In general, the linewidth has a direct impact on the optical link performance through chromatic dispersion hence it is convenient that the light spectrum is as confined as possible at the center frequency. For its part, undesired offset of the center frequency or instabilities may cause unexpected attenuation, pulse-spreading and a great performance worsening in case of coherent detection.

B Software evaluation: references and procedures

B.1 VPItransmissionmaker™

Because High-Speed Optical Communications Group already had licenses at their disposal, this CAD tool was the first one to be evaluated. This award-wining ([26]) program has been designed for modeling all types of photonic systems and networks and it has been reference for more than 650 publications up to 2010 [77]. It offers an intuitive modular graphical interface, a robust simulation scheduler and satisfactory signal representation. Nevertheless, it was not until the version 8.6 was released (March, 2011) that several enhancements on the MMF module and power coupling capabilities were included. This fact casted doubt about the precision of the multimode transmission and spatial field distributions. No information was found concerning the VCSEL.

B.1.1 MMF module

B.1.1.1 Differential Mode Attenuation (DMA)

REFERENCE

The test was carried out based on the results found in [14]. In the experiments, two different types of fiber were tested; labeled fiber A and fiber B (see Table B-1). The MMF was illuminated through a SMF lens launch technique, which produced a 3 µm spot size. The laser in the end facet of the SMF was a FP at 1300nm. The method utilized to measure the DMA is the following:

1. Perform a radial sweep of the laser's core. Measure the overall fiber loss over a short length of fiber (2m for fiber A, 0.3m for fiber B) for every position. The losses observed are only owed to light injection. The curve is normalized to set the maximum power at 0 dB.
2. Perform a radial sweep of the laser's core. Measure the loss over a long link length (1Km for fiber A, 0.8Km for fiber B) for every position. This measurement accounts for the losses due to light injection, propagation and DMA. The curve is normalized to set the maximum power at 0dB (propagation loss removed).
3. Normalize the latter with respect to the first one in order to remove the light injection dependent attenuation. The resulting graph represents the DMA.

In [14], this third step is skipped and a combined plot of step one and two is shown instead. In such case, it is the difference between the traces what determines the DAM effect at a given radial offset. Simulations are also performed to support the results obtained in practice. One of the assumptions is a Gaussian shaped near-field distribution out of the SMF-lens launch. The results are shown in Figure B-1.

[26] Optical Society of America Technical Excellence Award 1999

Table B-1 Parameters of fiber A and fiber B [14].

Fiber	Core diameter	Length	Maximum profile height	Index approximation	Real profile
A	50µm	2km (2 connectors)	1.45%	2.1	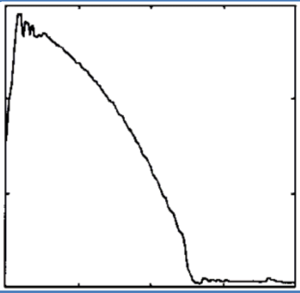
B	62.5µm	2.2km	2.54%	1.9	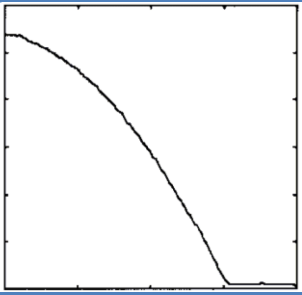

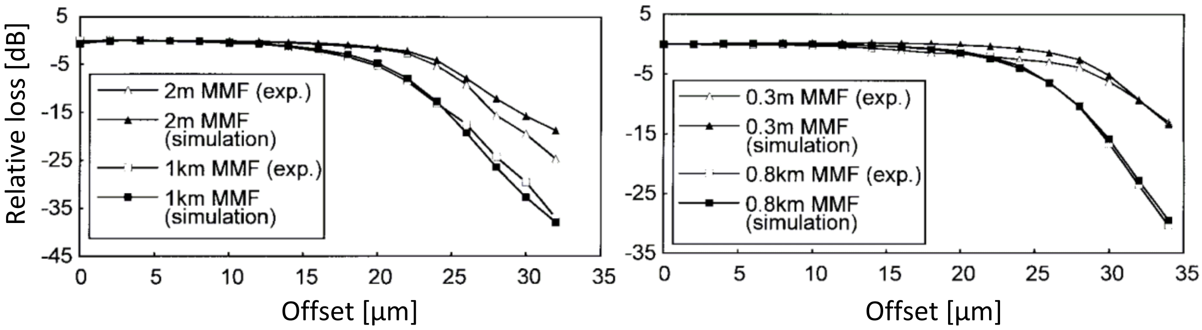

Figure B-1 Normalized loss versus lunch spot position for fiber A (left) and fiber B (right).

SIMULATION PREPARATION

The objective of the simulation was to verify the implementation of a selective mode attenuation algorithm and in positive case, evaluate its precision. The first step was to achieve digital descriptions of the index profiles. For that, the software puts at our disposal two different ways of introducing graded-index profiles: alpha coefficient or user-defined. The first one yields an ideal index profile for a specific alpha, core diameter, profile height and maximum refractive index. The second allows the user to introduce a custom refractive index described point by point in a text file with a concrete format. Given the relatively smooth profile of fiber B, the index approximation for the alpha mode was considered sufficiently accurate for the initial approach. In the case of fiber A, an alpha-fitting was discarded owed to the distinct central index depression that it exhibited. Instead, a full digitalization was performed with Engauge Digitalizer. The data was interpolated to generate equidistant data values and reformatted to use it in the user-defined mode. Figure B-2 shows the resulting profiles.

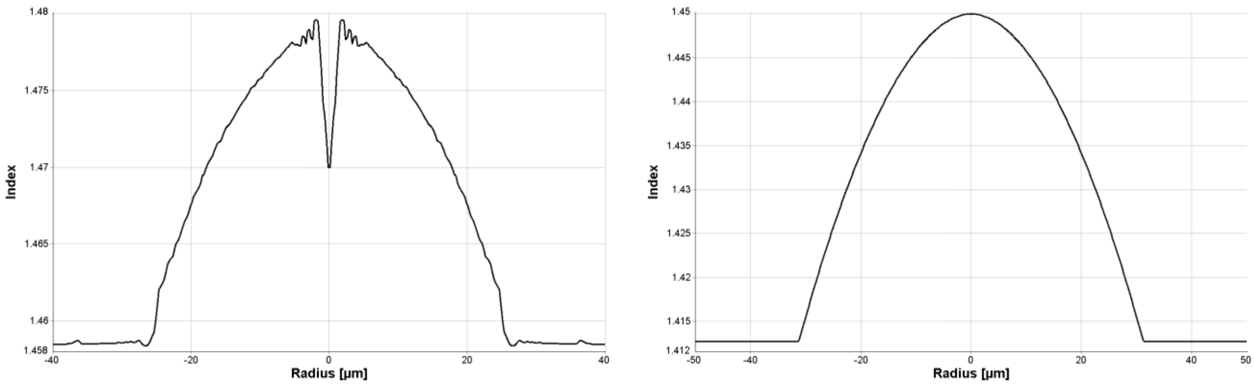

Figure B-2 Digitalized profile of fiber A (left) and fiber B (right).

One of the main problems was that the maximum refractive index was not reported. This is a necessary data for the definition of the maximum number of propagating modes and consequently, for DMA (2.16). Therefore the indices had to be sensibly approximated. Several datasheets from different manufacturers were consulted (see anexo F for examples), concluding that the average index for an OM1 fiber (B) is 1.5 and for an OM2 fiber (A) is 1.48.

Once the profile was set, the fiber attenuation per kilometer had to be determined. The calculation was based on information gathered about Corning© InfiniCor® fiber type.

One of the useful features in the MMF module is that it can model the incoming light to a Gaussian shaped field distribution independently of the actual optical source utilized. This permitted us to introduce the assumption in [14] into the system instantaneously so as to compare not only with the real data but also with the simulations. Besides, the "offset" field allows radial shifting of the impinging field which along with some TCL scripting can be used to represent any variable (attenuation in this case) as a function of the radial position.

SCHEMATIC

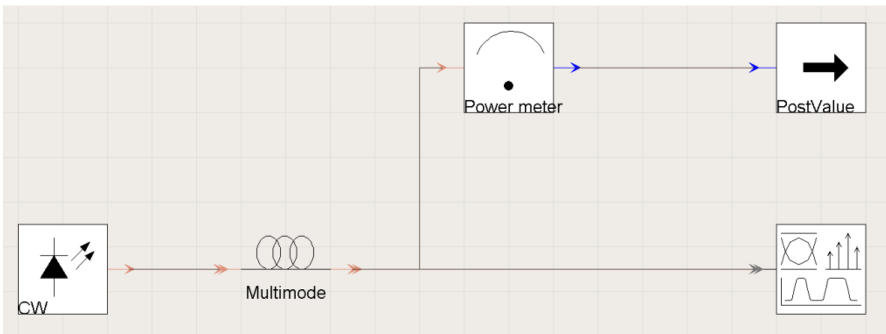

Figure B-3 DMA test schematic.

The laser source chosen was a Continuous Wave laser at 1300nm with an output power of 0dBm. The corresponding attenuation file, the fiber type and the link length are changed in the MMF block depending on the test. The spot size is set to 3µm. After the MMF, one signal analyzer and an optical power meter have been connected. The "PostValue" block makes its input value available for simulation scripts.

The script sweeps the core radius in steps of 2µm from 0 to 32µm. The output of the power meter (in dBm) is stored and represented as a function of the offset

RESULTS

For 50µm fiber, Figure B-4 shows 2m-link attenuation and 1000m-link attenuation.

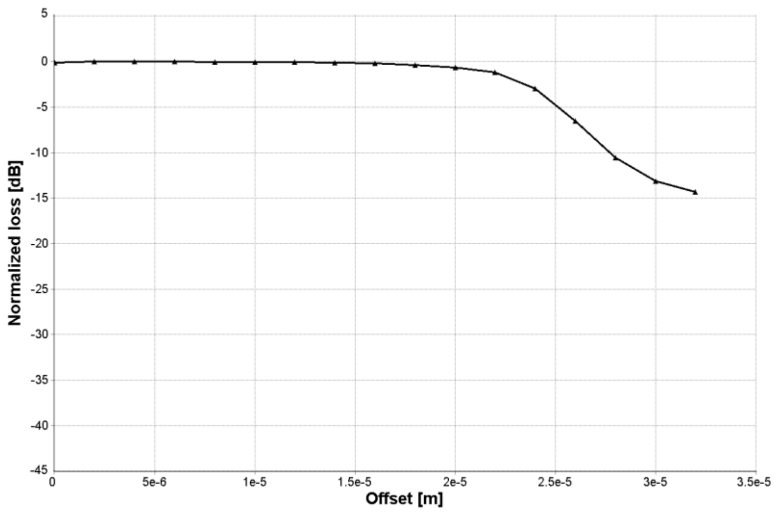

Figure B-4 Normalized loss versus launch offset for after 2m and 1km of fiber A.

The lack of numerical results to contrast, limits the evaluation to a simple and to some extent inaccurate graphical comparison; however, it is easy to realize that the previous curves are exactly the same. This means that the modal attenuation has not been considered by VPIPhotonics™ engineers. This gets confirmed after the test for fiber B (see Figure B-5).

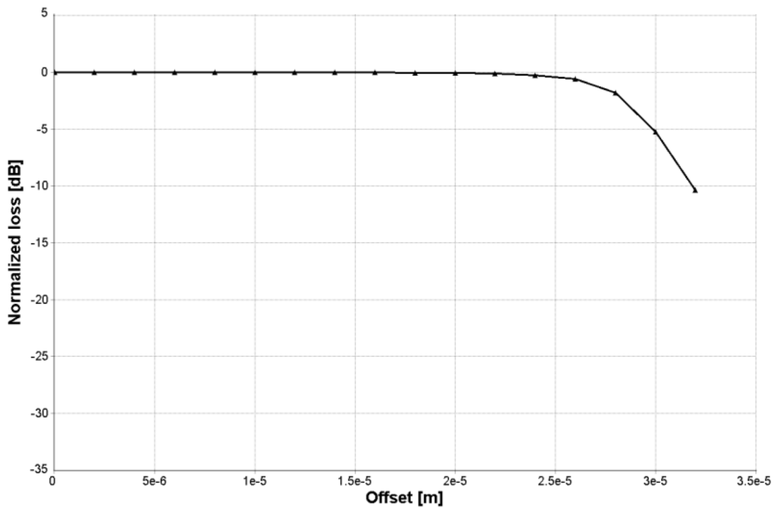

Figure B-5 Normalized loss versus launch offset for after 2m and 1km of fiber B.

Another conclusion is that the simulation results fit considerably well the curves for short link lengths (see Figure B-1, Figure B-4 and Figure B-5). This means that the spot size, wavelength and index profiles have been correctly adjusted. The last two points for 50µm (at 32µm and 30µm offset) represent the only considerable deviations with respect to the reference, presenting 2 dB and 6 dB less attenuation. The reason is that these offsets are 5um and 7 um away from the core-cladding interface, which is 20% and 28% of the core radius. At these distances, with a 3µm spot size, the light does not illuminate the core and the behavior is unpredictable.

B.1.1.2 Mode Group Delay (MGD)

REFERENCE

The Modal Group Delay test was based on the dataset from the 108-fiber model created by the University of Cambridge [78]. This statistical analysis provides scaled refractive index, frequency response, scaled MGD, and coupling coefficients for each radial position for 108 combinations of pre-defined fiber imperfections.

Table B-2 Profile defects considered in the 108-fiber model by the University of Cambridge

Defect	Description
Profile exponent (inner region)	1.89, 1.97 and 2.05
Profile exponent (outer region)	1.89, 1.97 and 2.05
Core-Cladding interface	No perturbation (0) or exponential decay (1)
On axis perturbation	Dip (-1), no perturbation (0) or peak (1)
Kink ([27])	No perturbation (0) or radius associated in µm

All the fibers are 62.5µm in core diameter, the maximum refractive index is 1.5 and the cladding's is 1.474 (NA=0.28).

The analysis done by the University of Cambridge can be divided into four steps

1. Generate the set of perturbed refractive index profiles.
2. For each of them, calculate the electric-field distribution and propagation delay of the guided modes.
3. For each of them, calculate the DMD and OFL bandwidth.
4. For each of them, perform a scaling process to adjust the DMD to a target 2ns/km[28].

The last step consists of exploiting the inverse relation between bandwidth and modal delay to adjust each fiber's response for it to provide a DMD of 2ns/km. Therefore if a certain DMD is worse than the limit, it is scaled down and its bandwidth is scaled up proportionally. The resulting bandwidths should be regarded as

[27] It represents a misfit between two perfect alpha profiles. The inner has a slightly higher delta and smaller core radius and the outer has a slightly lower delta and larger core radius. The two profiles agree at a single radius (further infomartion can be downloaded from [78]).

[28] This value was believed to be the 5 percentile limit of fiber performance.

the needed performance specifications for the given number to yield 2ns/km DMD. Typically, the factor is calculated by:

$$F = \frac{DMD}{2ns/Km}$$

After the calculation of the constants for every fiber, the MGD needs to be corrected. The usual means of achieving the scaling to a worst-case DMD of 2 ns/km is to adjust the calculated modal delays for each of the 108 fibers in accordance with the reckoned constant. An alternative is to use the DMD scale factor to adjust the perturbations in the original refractive-index profile. This process, which is described in [79], tunes the physical descriptors of the profiles so that the result after conventional MGD calculation is already scaled. This procedure is an approximation and the information on the success for each fiber is provided in anexo G.

The tests were conducted with the parameters in Table B-3.

Table B-3 Parameters adopted by the University of Cambridge to develop the 108-fiber model.

Parameter	Value	Unit
Wavelength	1300nm	nm
Launch type	SMF	-
Field distribution	Gaussian	-
Spot Size (FWHM)	7	µm
Link length	300m	m
DMD Sweep	From 0 to 30 in steps of 1	µm
DMA	0 for DMG<18 and ∞ for DMG>18	dB
GVD	0	ps/nm·km

The results for the corrected MGD, the spectra and the modified profiles are collected in 756 text files. The 108 scaling factors are provided in another text file. The refractive index files are made up of 1499 equispaced points (Δr = 0.0328333µm).

SIMULATION PREPARATION

The MGD calculation was made for a subset of 13 fibers. Such fibers were chosen so that all the possible combinations of core-cladding interface and on-axis defect were evaluated at least once. Furthermore, some of those combinations were also assessed for multiple inner-outer exponent pairs. The “kink” perturbation was not included because most of the complementary references ([53], [80], [81]) were based on the previous release of the Cambridge model (81-fiber model) in which such defect was not present. Table B-4 shows the characteristics and numbers of the fibers used.

Table B-4 Fibers tested and their corresponding perturbations.

#	Inner profile exponent	Outer profile exponent	Core-Cladding interface	On-axis perturbation	Kink
7	1.89	1.89	1	-1	0
17	1.89	1.97	0	1	0
31	1.89	2.05	1	-1	0

37	1.97	1.89	0	-1	0
51	1.97	1.97	0	0	0
59	1.97	1.97	1	1	0
61	1.97	2.05	0	-1	0
65	1.97	2.05	0	1	0
81	2.05	1.89	1	0	0
95	2.05	1.97	1	1	0
101	2.05	2.05	0	1	0
103	2.05	2.05	1	-1	0
105	2.05	2.05	1	0	0

The index files were introduced in the software with the user-defined profile mode after giving them the proper format. The attenuation parameter was again extracted from Corning© InfiniCor® database for 62.5µm. The fiber length, spot size, wavelength, field distribution, GVD and sweeping mode were set accordingly to Table B-3.

SCHEMATIC

No specific schematic was used for the simulation. Instead, the program provides as an extra feature the possibility of saving the calculated MGD into a text file. This facilitates its importation to MATLAB® in order to perform quantitative and more accurate comparison with the 108-fiber model files. This process was repeated for each of the 13 profiles under test.

RESULTS

The files from the model and from VPItransmissionmaker™ calculations were imported to MATLAB®, properly scaled and represented jointly. The results are plotted in order according to the fiber number.

Concerning the data evaluation, anexo G constitutes the base of our validity reference. Nevertheless, it depicts the DMD differences instead of the raw MGD. Despite the close relation between DMD and MGD it is not possible to extract the exact DMD (or undo the calculation) without accounting for the amount of excited modes and the percentage of power coupled in each of them [53]:

$$IntermediateDMD = \sum_{m=0}^{MAX\ OFFSET} \frac{\sum_{n=1}^{DMG} N_{n,\tau}^{m} P_{n,\tau}^{m} \tau_n}{\sum_{n=1}^{DMG} N_{n,\tau}^{m} P_{n,\tau}^{m}} = \sum_{m=0}^{MAX\ OFFSET} \frac{\sum_{n=1}^{DMG} K_{n,\tau}^{m} \tau_n}{C_{\tau}^{m}} \quad \text{(B.1)}$$

with $N_{n,\tau}$ being the number of modes in the group n, $P_{n,\tau}$ the coupling coefficient for the group n and τ_n the MGD. This is done for each of the 31 offsets. The subscript τ indicates that the coupling-dependent parameters are specific for each index profile. After the calculation of the intermediate DMD, the minimum value is subtracted and the maximum absolute value is extracted. That is the final DMD number, also called “mean DMD”.

With the intention of illustrating the impact of a variation of the MGD in the DMD, the following mathematical development of (B.1) is presented:

$$IntermediateDMD = \sum_{m=0}^{MAX\ OFFSET} \frac{1}{C_{\tau}^{m}}\left(K_{1,\tau}^{m}\tau_1 + K_{2,\tau}^{m}\tau_2 + \cdots\right)$$
$$= \frac{1}{C_{\tau}^{1}}\left(K_{1,\tau}^{1}\tau_1 + K_{2,\tau}^{1}\tau_2 + \cdots\right) + \frac{1}{C_{\tau}^{2}}\left(K_{1,\tau}^{2}\tau_1 + K_{2,\tau}^{2}\tau_2 + \cdots\right) + \cdots = \quad \text{(B.2)}$$
$$= \tau_1\left(\frac{K_{1,\tau}^{1}}{C_{\tau}^{1}} + \frac{K_{1,\tau}^{2}}{C_{\tau}^{2}} + \cdots\right) + \tau_2\left(\frac{K_{2,\tau}^{1}}{C_{\tau}^{1}} + \frac{K_{2,\tau}^{2}}{C_{\tau}^{2}} + \cdots\right) + \cdots$$

The mean DMD is obtained as described above. The normalization with respect to the minimum allows ascribing the whole DMD to a single DMG. Therefore:

$$meanDMD = \tau_{\tau MAX}\left(\frac{K_{\tau MAX,\tau}^{1}}{C_{\tau}^{1}} + \frac{K_{\tau MAX,\tau}^{2}}{C_{\tau}^{2}} + \cdots\right) \quad \text{(B.3)}$$

Associating τ_{MAX} to the maximum delay for the scaled MGD, the same procedure can be done to calculate the mean DMD generated by the scaled index profiles (T_{MAX}) :

$$meanDMD = T_{TMAX}\left(\frac{K_{TMAX,T}^{1}}{C_{T}^{1}} + \frac{K_{TMAX,T}^{2}}{C_{T}^{2}} + \cdots\right) \quad \text{(B.4)}$$

The information provided in the model comprises τ_n and $P_{n,\tau}^{m}$ for every offset. For its part, T_n is obtained through simulation. The number of excited modes ($N_{n,\tau}^{m}$) can be calculated based on $P_{n,\tau}^{m}$ and applying (2.18). However, there is not explicit or implicit information about the light coupling for the test performed by the University of Cambridge on the scaled profiles. This prevented us from transforming the simulated T_n into DMD plots with (B.4).

The next most accurate option to assess the accuracy of VPItransmissionmaker™ implied the assumption that the factor accounting for light coupling in (B.3) and (B.4) was very similar. This is not a bad approximation given that the launch conditions are very clearly stated (see Table B-3) and that the profile scaling sticks to little modifications of the perturbations rather than a complete remake of the index contour [79]. In such case, the ratio between the mean DMDs can be expressed as:

$$\Delta DMD(\%) = \frac{\tau_{\tau MAX}\left(\frac{K_{\tau MAX,\tau}^{1}}{C_{\tau}^{1}} + \frac{K_{\tau MAX,\tau}^{2}}{C_{\tau}^{2}} + \cdots\right)}{T_{TMAX}\left(\frac{K_{TMAX,T}^{1}}{C_{T}^{1}} + \frac{K_{TMAX,T}^{2}}{C_{T}^{2}} + \cdots\right)} \approx \frac{\tau_{\tau MAX}}{T_{TMAX}} \quad \text{(B.5)}$$

Because the idea behind scaling the profiles is to make the DMD difference equal to zero, it is not a bad approximation to assume that at least the tendency of the MGD curves is maintained. This means that the

DMG that causes the maximum delay is likely to be the same for both scaled profile and scale MGD. This would permit to rewrite (B.5) as:

$$\Delta DMD(\%) \approx \frac{\tau_{\tau MAX}}{T_{TMAX}} \approx \frac{\tau_{MAX}}{T_{MAX}} \quad \text{(B.6)}$$

With this method, the ratio of the DMDs is calculated and compared with the ratio of the maximum absolute delays in the MGDs. The more similar the more accurate the simulator is. Given the little usage and the poor future perspective of OM1 fibers, it was not possible to find information about the DMD ranges for this type of fiber. Nevertheless, it was observed that the ratio between the minimum "outer" DMD and the maximum one for OM3 and OM4 was around 50%. Since the DMD calculated by the University of Cambridge could be considered "outer" type (see Table B-3) this factor of proportion was also assumed for our 62.5µm fibers. Based on that and accounting for the error caused by the approximation, it was decided to establish the fifth part of it as the validation percentile (10%) for the ratio deviations. That is, it will be considered that there is good agreement when the difference keeps below 10%.

The evaluation procedure is structured as follows

1. Estimate the difference between the red circle and the black circle for the fiber under test in APPANDIX. Calculate the ratio.
2. "A" case: Pick the maximum absolute value of the blue and red traces. Calculate the ratio. (B.6)
3. "B" case: Pick the absolute value of the red trace at the position of the maximum value of the blue trace. Calculate the ratio. (B.5)
4. Ratio comparison

As a general consideration, it must be said that the delays at the highest DMGs (18, 17 and even 16) should not be taken into so much consideration as the rest. The modes within these groups propagate very close to the core-cladding boundary and at those radial positions the propagation is unpredictable. Those modes end up being radiated most of the times; therefore, associating a "propagation" delay to them is meaningless.

The results are summarized in Table B.5.

Table B-5 Individual delay ratios and similarity result. Green shaded cell are hits, red cells are misses.

	$\Delta DMD(\%)$	$\Delta MGD(\%)$	$\frac{min\{\Delta DMD(\%), \Delta MGD(\%)\}}{max\{\Delta DMD(\%), \Delta MGD(\%)\}}$
FIBER #7	0.9482	0.9702	97.73%
FIBER #17	1.00755	1.2103	83.24%
FIBER #31	0.809523	0.8008	98.92%
FIBER #37	1	0.8441	84.81%
FIBER #51	8.9	-	-
FIBER #59	1	1.1379	87.88%
FIBER #61	0.9756	0.8488	87%
FIBER #65	0.9389	1.0294	91.20%
FIBER #81	0.6043	0.8946	67.54%

FIBER #95	0.7407	0.8691	85.22%
FIBER #101	0.9350	0.9609	97.30%
FIBER #103	1	0.9526	95.26%
FIBER #105	0.985	0.7858	79.77%

Five of the fibers are above the threshold, what means that more than 61% are in disagreement. The results correspond to the ratio calculated with (B.5). FIBER #51 and #81 are discarded according to Cambridge recommendation.

B.1.1.3 Mode Power Distribution (MPD)

REFERENCE

The reference used for measuring the power-coupling accuracy of VPItransmissionmaker™ is Cambridge 108-fiber model [78]. Together with MGDs and spectra for each of the fiber, a spreadsheet with 18 power coefficients (18 DMGs considered) for each of the 31 radial positions is included. Expressed as the percentage of power coupled, anything below 0.5% is neglected and rounded down to zero. Notice that we are working with DMGs and not modes hence considerable less power that 0.5% of the total is actually coupled into the modes contained in the corresponding DMG.

The measurements are done with the launch conditions summarized in Table B-3.

SCHEMATIC

Similarly to the MGD case, the CAD tool generates a text file with the coupling coefficients for a given radial offset and spot size whose values are introduced in the MMF module itself. MATLAB® was used for post-processing the data and to perform the evaluation.

RESULTS

Two things are important regarding power coupling: the power percentage and the concrete DMGs into which it is being injected. Both aspects are accounted in the analysis.

Firstly, the power coefficients have been plotted with respect to the DMGs and compared qualitatively. The spot size in the simulator is set to 7µm FWHM with Gaussian field distribution. For the ease of representation, only 8 of the 31 curves are presented in Figure B-6. They correspond to radial offsets of 0µm, 4µm, 8µm, 12µm, 16µm, 20µm, 24µm and 28µm. Besides, the coefficients have been joined with a continuous trace. It should be clarified that any value within DMGs (non-integer) may not be exact and should not be considered.

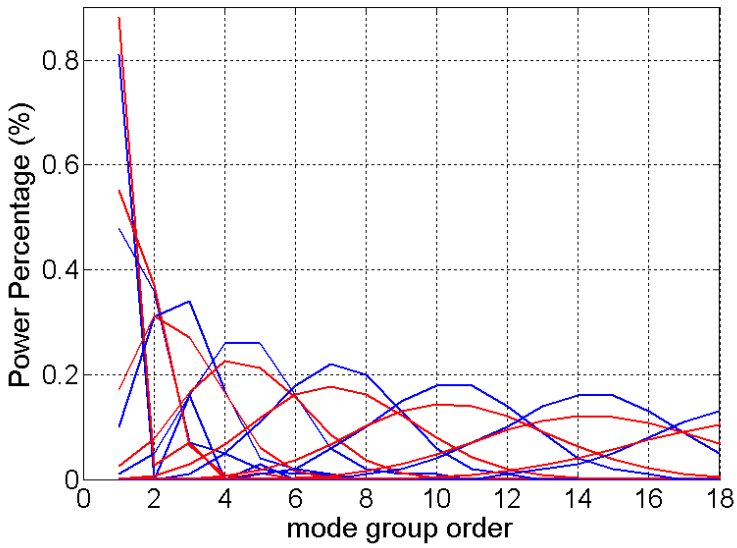

Figure B-6 Percentage of power coupled into each DMG for different radial positions.

The blue curve represents the coupling coefficients provided by the University of Cambridge and the red trace the coefficients calculated with the simulator. It can be seen that the amount of power coupled into the main DMGs (for offsets higher than 4µm) according to Cambridge model is noticeable greater than the one calculated with the simulator. The difference is in average 4% that represents approximately between 13% to 22% of the maximum percentage coupled to one mode (expect for offsets from 0µm to 4µm). Furthermore, and despite Figure B-6 is not the best representation, is can be foreseen a wrong excitation based on the excessive width of the individual red curves. Note that as the offset increases, the power spreads over a larger number of DMGs. This is because the degeneracy of the modes is approximately twice the group number [14] and hence, a selective excitation of a high order DMG will divide the power into a larger number of modes than for instance DMG 1 (only LP_{01}).

In order to check if the excited modes are the correct ones, Figure B-7 is presented

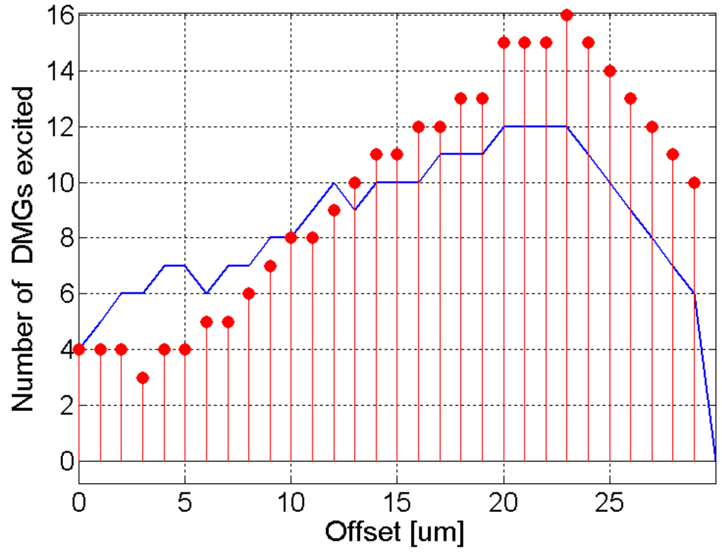

Figure B-7 Number of excited modal groups as a function of the radial offset. The FWHM spot size of the source is 7µm with Gaussian field distribution.

It is observed that there is hardly agreement between both references. Albeit some discrepancy is expected for high order modes, in any case a difference of 4 DMGs could be reached (33% of the target maximum). The differences for low order modes are also high, with a maximum of 3 missing DMGs at 3µm, 4µm, 5µm offset. The average number of mistakes is 2.

B.1.2 VCSEL module

The analysis of the VCSEL module performance in VPItransmissionmaker™ was as short as decisive: the range of nominal emission frequency goes from 50THz up to 300THz. This means that it cannot be used for simulations with wavelengths higher than 1000nm. Given the special interest in using the first window, the only option would have been to create our VCSEL model.

B.2 OptSim™ (ModeSYS™)

Due to the limitations found in the previous software, it was decided to test this well-known simulator. ModeSYS™ supports the design and simulation of multimode optical communication systems. With a primary focus on data communication applications, it allows both temporal and spatial analysis of optical signal and their propagation. Similarly to its counterpart, it provides together with OptSim™ an intuitive graphical interface and lab-like measuring instruments.

B.2.1 MMF module

B.2.1.1 Differential Mode Attenuation (DMA)

REFERENCE

Same reference as for VPItransmissionmaker™

SCHEMATIC

Replicating the setup in [14]:

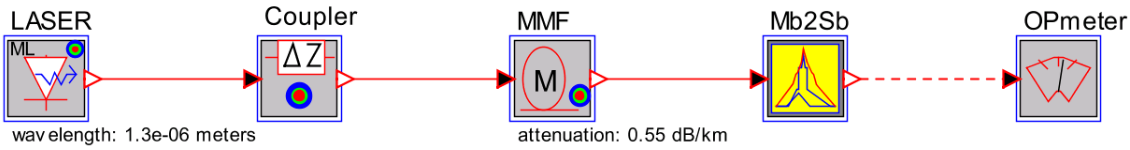

Figure B-8 Schematic for DMA test in ModeSYS™-

From left to right: LASER, spatial coupler, MMF, multiband to singleband converter and optical power meter. The "Mb2Sb" is used to collapse every mode into one unique optical signal. Given that the only intention is to measure the power, it is convenient to treat them as an aggregate group rather than as individual entities. The multimode fiber and LASER are adjusted according to the description in section B.1.1.1. The coupler is ideal (neither insertion loss nor misalignments) and it is necessary to couple spatially distributed fields into MMF.

The “scan” button is used to sweep the offsets and represent the power variation in correspondingly. The power values were saved in a text file and imported into MATLAB®.

RESULTS

DMA is explicitly implemented in this simulator. It requires the user to fill out two fields: order of the modified Bessel function of the first kind and scaling factor (see (2.16)). Based on the attenuation tendency observed in Figure B-1 (constant attenuation and decay for high offsets), the order of the Bessel function was set to one. In order to find the correct or most approximate value for the scaling factor, a range within 1 and 30 was scanned (finally set to 21). It is important to realize that the formula for the DMA does not depend on the distance although the physical effect does. This is somehow confusing but it facilitates a lot the determination of the scale factor. The result for fiber B is shown in Figure B-9.

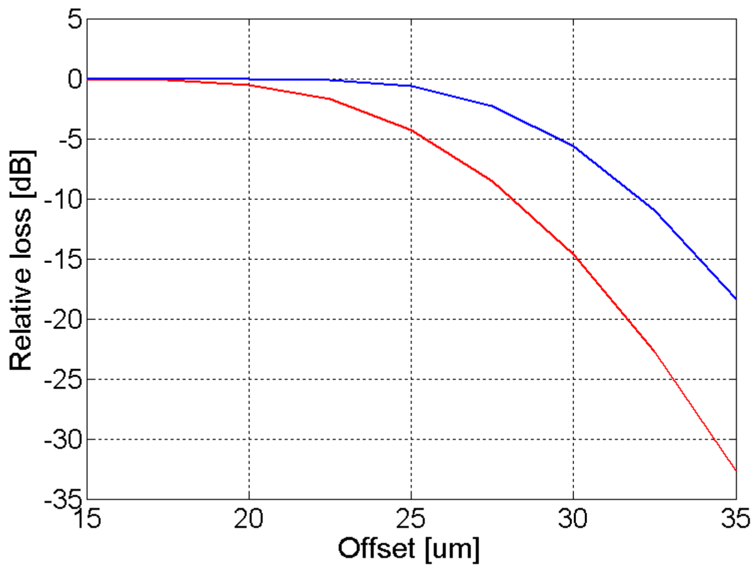

Figure B-9 Normalized loss vs. launch offset after 2m and 1km of fiber B.

The blue trace corresponds to the attenuation for 0.3mtransmission link and the red line represents 800m transmission. The offset was ranged between 15µm and 35µm to avoid unnecessary computational load and increase the precision of the representation. High level of agreement is exhibited by using 20µm, 25µm and 30µm as reference points. According to Figure B-1, their values should roughly be -1dB, -4dB and -15dB. This is exactly what is observed in Figure B-9.

Similar results were obtained for fiber A, whose profile had to be readapted to the new format supported by ModeSYS™.

B.2.1.2 Mode Group Delay (MGD)

Unlike VPItransmissionmaker™, ModeSYS™ do not generate the MGD plot. Instead, it creates a file that contains the modal delays influenced by the launch conditions in a way which is not described. This means that the result is completely dependent on, at least, the spot size and radial offset. This complicates enormously the calculation of the relative MGD even assuming that the impact of the launch conditions is known and reversible. It requires undoing the DMG groups, invert the effect mode by mode, group them back in DMGs and perform the comparison described in section B.1.1.2. Notice that the first 18 DMGs contain 190 modes in total and that this process should be repeated for each of the 13 fibers at least for two different offset positions. This possibility was discarded as a result of the excessive workload and time needed.

Owed to the possibility of calculating the DMD in ModeSYS™, the next option was to calculate the simulated DMDs and compare with the corresponding results obtained by the University of Cambridge. This was a straight-forward and more reliable method since no assumption is taken and it is not necessary to calculate ratios for indirect comparison. However, as explained in section B.1.1.2, the DMD definition in the 108-fiber model differs from the one in the software. The first one is called “mean DMD” and the second corresponds to the standardized method described in TIA-455-220. This fact prevented us from making a reliable validation as it was impossible to modify the DMD module in ModeSYS™ and transform it to calculate a mean DMD. Furthermore, the results from both definitions could not be compared since the relation of proportion between them was not known with sufficient precision.

Consequently, the publications presented by the RSoft Design Group regarding the simulation of communication links based on the 81-fiber model (previous version to 108-fiber model) ([80] and [81]) together with the application notes called “CambridgeModel_case1” and “CambridgeModel_case2” in [82] were evaluated. [80] was a mere exposition of results without any direct comparison or conclusion. However, in [81] it was proved that an error of less than 5% in the scaling factors is achieved for three different fibers of the 81-fiber model. The tests are done based on the mean DMD and impulse response instead of MGD, which constitutes a much more reliable and decisive validation method for the modal delay algorithm. The application notes investigate the effect of index distortions in the 81-fiber model on fiber performance and, subsequently, on eye diagrams in data-modulated multimode link. The calculation of the resulting MGDs is included as well as bandwidths. No reason was found so as not to trust the good results obtained by the design group.

B.2.1.3 Mode Power Distribution (MPD)

REFERENCE

Same reference as for VPItransmissionmaker™

SCHEMATIC

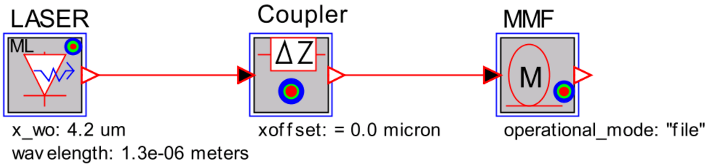

Figure B-10 Schematic for MPD test in ModeSYS™.

The LASER spot size is set to 7µm which corresponds to 4.2µm of beam width for Laguerre-Gaussian mode profile. The wavelength used is 1300nm. The offset is increased by one every iteration (31 iterations). Notice that it was not necessary to terminate the link.

The text file is formatted and imported into MATLAB®

RESULTS

Figure B-11 shows the MPDs for 0µm, 4µm, 8µm, 12µm, 16µm, 20µm, 24µm and 28µm of radial offset.

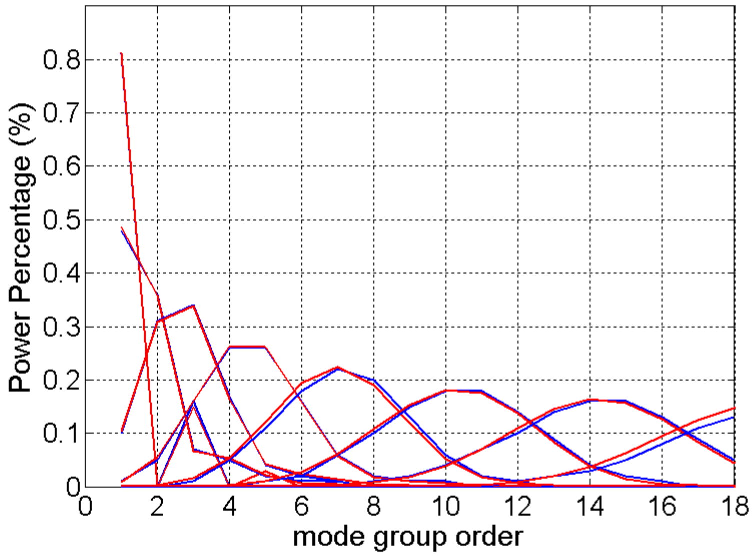

Figure B-11 Percentage of power copled into each DMG for different radial positions.

The blue curve represents the coupling coefficients provided by the University of Cambridge and the red trace the coefficients calculated with the simulator. It can be observed a considerable increment of the accuracy in the power percentage compared with Figure B-6. The average difference of the power coupled into the two most excited DMGs for each offset is reduced from 4% to 0.78% (more than 5-fold accuracy increment). In the worst case, that percentage constitutes 5% of the maximum power coupled into one mode (offsets of 28µm and higher).

For its part, Figure B-12 shows the excited DMGs for every offset.

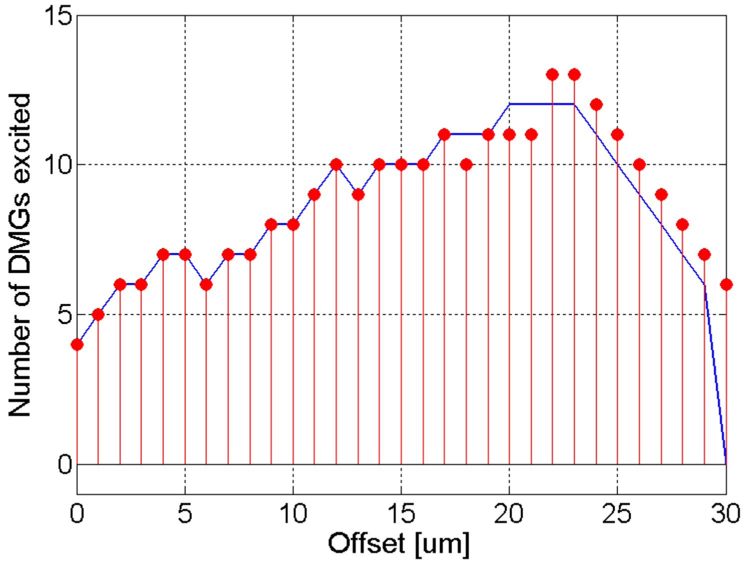

Figure B-12 Number of excited modal groups as a function of the radial offset. The FWHM spot size of the source is 7µm with Gaussian field distribution.

It can be seen that it does not exist deviance at all for the first 17µm. From that point on we approach the core-cladding interface (7µm FWHM spot size) and some oscillation is comprehensive. Besides, the maximum deviation never exceeds 1 DMG fault (8% of the target maximum) and the tendency is followed perfectly.

B.2.2 VCSEL module

ModeSYS™ provides a VCSEL model that takes into consideration the spatial distribution of the output field so that it can be combined with the MMF through a spatial connector. Besides, the module not only sticks to general behaviors but other important ones such as spatial hole burning, lateral carrier diffusion, thermally dependent gain and thermal carrier leakage are all accounted for.

The study of the physical model was beyond the reach of this investigation however, it was necessary to assure that it behaved properly when introduced into a communication system. Given the confidentiality and in some cases uncertainty about the exact values of the physical parameters that characterize a VCSEL, it resulted impossible to provide any more accurate test than a graphical comparison of the LIV, s_{21} and Back-to-Back (B2B) eye diagrams.

REFERENCES

The references used are [76], [83] and [84]. They provide complementary information about a very similar VCSEL model developed in the Department of Microtechnology and Nanoscience in Chalmers University of Technology. It generates 9mW of maximum output power and has 20GHz bandwidth at 10mA (very high speed). The series resistance is around 80Ω, the slope efficiency 0.7-0.8W/A and the current threshold is 0.6mA. Figure B-13 shows the LIV at 25°C and s_{21} for three diverse bias currents.

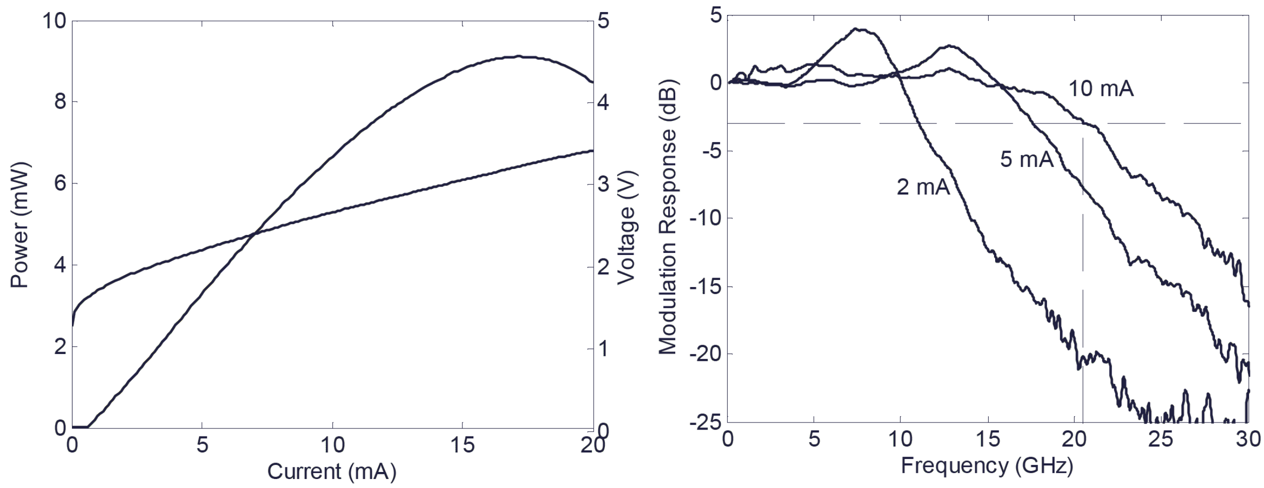

Figure B-13 Targeted LIV curve and small-signal modulation response [76].

Another parameter that can be estimated from the LIV is the turn-on voltage, which is around 1.7V. The capacitance is mostly canceled in order to reach such high modulation frequencies. The s_{21} shows the progressive increment of the damping factor with the bias current for a fixed photon lifetime inside the resonance cavity.

Once the response of this concrete laser was estimated, [85] was used to include it into a full transmission simulation. The authors used the VCSEL in [85] to launch a 4-PAM signal into an OM4 at 12.5GBd and 15GBd, which is equivalent to 25Gbps and 30Gbps. The 4-PAM modulation was achieved by decorrelating two binary signals of 2^7-1 length and 900mV and 450mV amplitude. The experiment is done over 200m and 300m fiber spans and the propagated signal is received with an amplified photodiode of 12GHz BW. The error counting is done through an adapted On-Off Keying (OOK) BER tester under the assumption of high enough SNR to consider that errors are exclusively caused by neighboring symbols. The formula utilized to calculate the total bit error rate is:

$$BER = \frac{1}{8}(P_{01} + P_{10} + 2P_{12} + 2P_{21} + P_{23} + P_{32}) \quad \text{(B.7)}$$

with P_{xy} being the conditional probability of receiving y when x was sent.

SCHEMATIC

LIV & s_{21}

The VCSEL module in ModelSYS™ has its own test feature. The user selects the plot or report wanted and the result is presented in an autogenerated graph or a text file respectively. It is not necessary to select any PRBS length, bit rate or voltage/current modulation input levels to check the LIV and s_{21}. The temperature point and the bias current are provided within the same test tool hence it is not necessary to change them in the final VCSEL parameters. This separation allows for a more comfortable design process and faster detection of the problematic parameters.

4-PAM

The reproduction of the experiment described in [85] required the inclusion of the previously design VCSEL into the experimental setup.

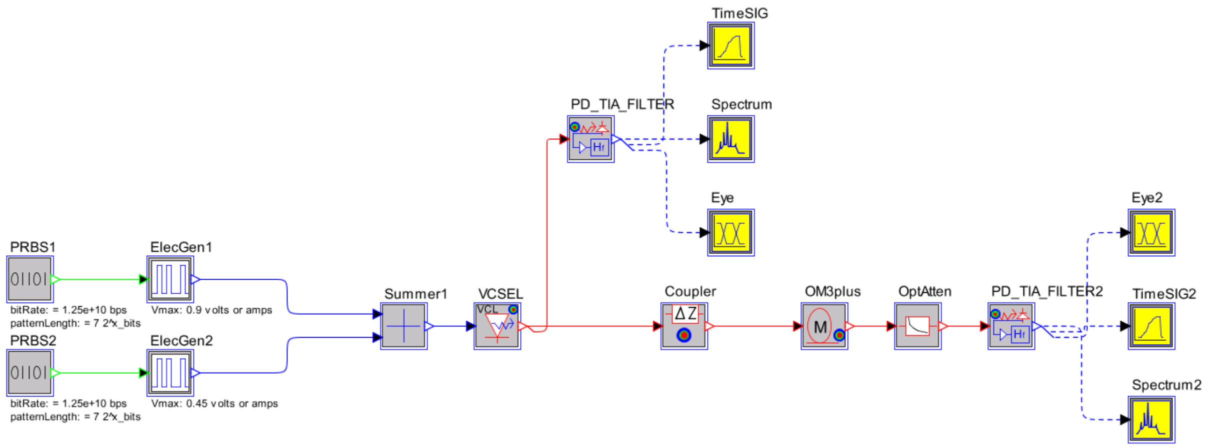

Figure B-14 4-PAM simulation setup.

Two binary streams with appropriate amplitudes and decorrelation are combined and injected into the spatial VCSEL model through an ideal bias-T. The light goes through an ideal coupler up to the OM3+ fiber whose parameters were based on the predefined model of a Corning© InfiniCor® SX+ at 850nm. After the propagation, the attenuator is used to vary the optical input power when needed. The noise in the receiver was adjusted to achieve a sensitivity around -5dBm for 25Gbps and -3.8dBm for 30Gbps according to the reference. “PD_TIA_FILTER” is used for B2B measurements.

RESULTS

LIV & s_{21}

The quantum wells of the lasers in the references were made of InGaAs in different proportions. Consequently, the predefined index guided InGaAs model provided by the software was used as a starting point. The next step was to fill out the well-known parameters such as wavelength (850nm) and temperature (25°C). Later, based on the targeted LIV and explicit stated parameters, the voltage to intensity curve was defined by introducing the series resistance (80Ω) and turn-on voltage (1.7V). The variables were modified by visual comparison with Figure B-13 after evaluating their impact on the LIV and s_{21}. Amongst the most relevant we find: power-coupling coefficient, injection efficient and parasitics. It should be mentioned that all the adjustments remained within reasonable values according to [76], [83], [84] and [17]. The result is shown in Figure B-15.

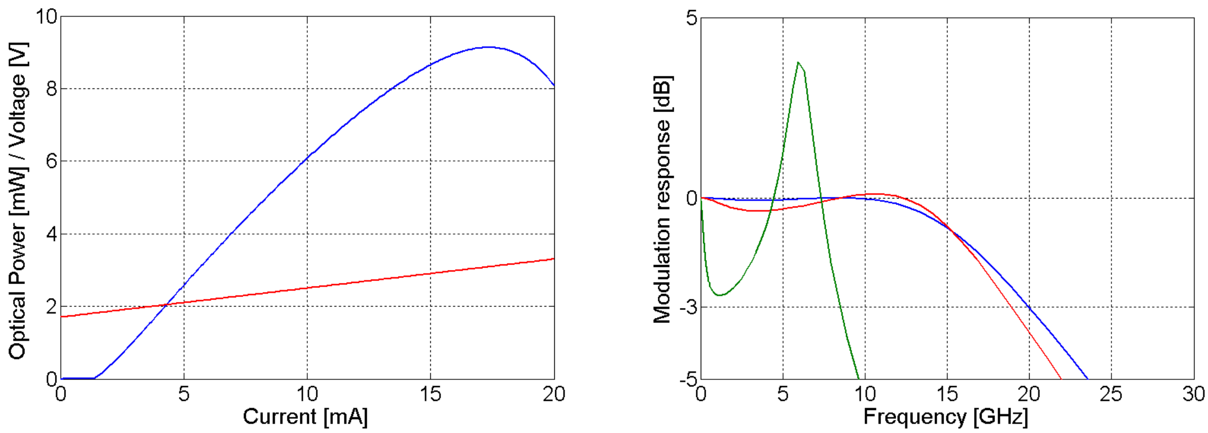

Figure B-15 LIV curve and small-signal modulation response after design.

The red line in the LIV is the device voltage and the blue line represents the output optical power. The voltage function approximation is calculated as follows:

$$V = 80\Omega \cdot \text{Current} + \text{V}_{\text{TURN}-\text{ON}}$$

As it can be seen the agreement is perfect except for the lowest current values due to the linear approximation (Notice scale). This can be disregarded since the VCSEL is never operated below threshold. The optical power also fits very well the aimed curve. Using 5mA, 10mA and 15mA as reference points, the average deviation is 0.333mW which represents 6% of the average output power and 3.7% of the maximum output power.

The discrepancy in s_{21} is a little higher. It shows the modulation response for 2mA (green), 5mA (red) and 10mA (blue). Whereas at 10mA the frequency at -3dB is exactly 20GHz, the bandwidth for 2mA and 5mA is around 2.5GHz less for the first one and 1Ghz more for the latter. The deviation at 2mA is owed to the shift in the resultant threshold current, which is around 0.7mA higher (1.3mA). Thereby, 2mA approaches the minimum current and the bandwidth decreases. Concerning the extra bandwidth obtained at 5mA, it can be caused by little inaccuracies in the values of the physical model parameters. It should be stated that, for instance, a variation of 0.1pF in the equivalent parasitic capacitance caused a drop of 1GHz in bandwidth. The level of required exactitude for correcting 1GHz would be $0.01 \cdot 10^{-12}$ (assuming linear relation) only for the capacitance (one out of thirty six variables).

The conclusion is that ModeSYS™ can model with very high precision a real InGaAs VCSEL starting from the default set of parameters and changing the meaningful ones within reasonable intervals. To assure a general compliance, several compositions should be checked; however, similar precision will be assumed for all of them.

4-PAM

The parameters were loaded in the “VCSEL” module in Figure B-14. The 4-PAM signal described in section B.2.2 was ideally generated and injected into the laser through a bias-T. The bias current was set to 7mA according to [85]. Given that the TIA gain was not provided, it was set to one and the power of the thermal noise was adjusted to meet the requirement of BER=10^{-12} at -5dBm input optical power at 25Gbps or 12.5GBd. This specification was extracted from the experimental BER curves obtained by the authors (see Figure B-16). The bandwidth of the Low-Pass Filter (LPF) was established at 12.5GHz and no other noise source but thermal was accounted for.

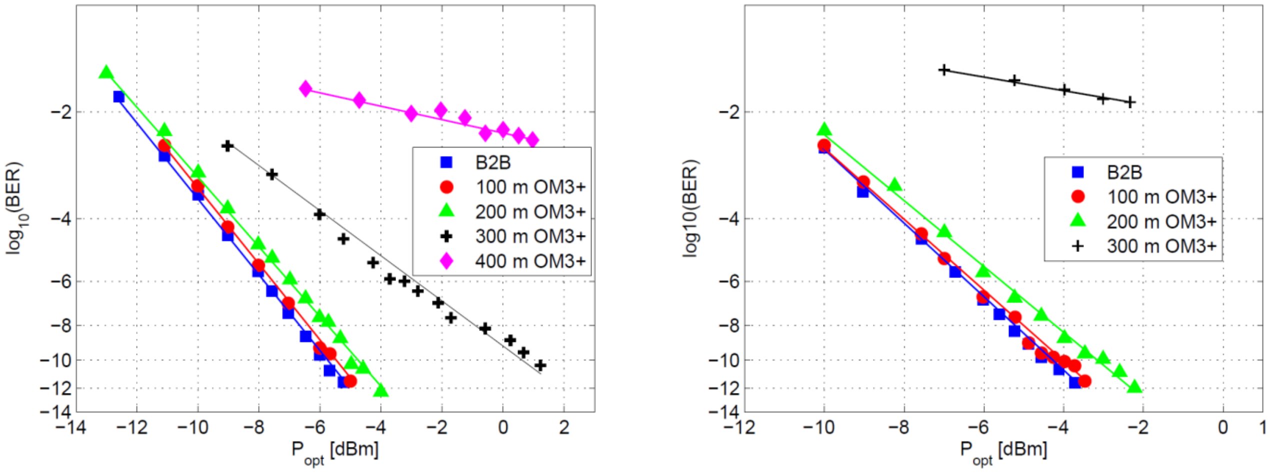

Figure B-16 4-PAM experimental results [85]. BER curves are shown for 25Gbps (left) and 30Gbs (right).

Provided that the objective was to validate the VCSEL model, B2B measurements were found as the easiest and most reliable ones given that the OM3+ performance was not checked in advance. The output power of the laser was regulated with an ideal variable optical attenuator and the signal was received by “PD_TIA_FILTER”. The electrical output data was stored in a text file and imported into MATLAB® in order to process it with a 4-PAM demodulator. The demodulator performed an optimum sampling point detection based on signal variance, determination of the optimum thresholds and BER calculation. Owed to the necessity of detecting BERs lower than 10^{-6}, a Gaussian fitting and subsequent overlap integral calculation was implemented and the BER estimated based on (B.7). The results for B2B are shown in Figure B-16.

(CONTINUE IN THE NEXT PAGE)

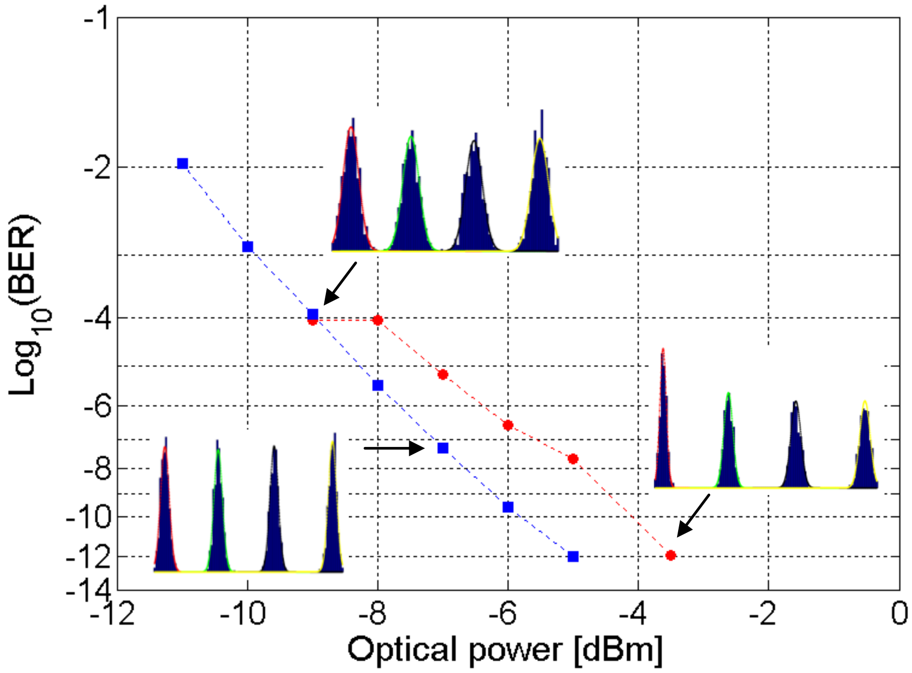

Figure B-17 4-PAM simulation results. BER curves are shown for 25Gbps (blue) and 30Gbs (red).

.

Despite the inherent inexactitude of the Gaussian approximation, both curves exhibit a high agreement with the experimental results. In none of the cases the error represents more than half an order of magnitude except for the outliers observed for -9dBm and -5dBm power at 30Gbps. It should be taken into consideration that no explicit information about the receiver was presented and that the method used in [4PAM] for BER calculation was error counting rather than Gaussian-based estimation. The LPF bandwidth had to be slightly adjusted to obtain the best fitting as well as little corrections on the bias current (±0.5mA)

Due to the lack of information about the receiver, the spot size and the bad performance exhibited by the OM3+ implementation, the transmission results were discarded. Besides, the distance utilized (200m and 300m) was sufficiently short to neglect chromatic dispersion; hence the outcomes were meaningless for our purpose of testing the VCSEL model.

Concerning the contribution of this specific test, it has been proved the high accuracy of the spatial VCSEL model implemented in ModeSYS™ not only as a pure optical source but also as a part of a real data communication link utilizing a concrete modulation format which is not even supported by the program itself. This shows the generality and precision of the physical model and the feasibility to use it for any type of transmission.

From the personal point of view, an enhanced version of the 4-PAM demodulator developed alongside the thesis was adapted and used for an experimental exercise that reported single VCSEL 100Gbps transmission with adaptive FEC for the LSB and MSB separately. It was submitted and accepted as postdeadline paper at 2012 OFC conference [2].

B.3 MATLAB® mode solver

Despite the satisfactory results obtained with a 30-day evaluation copy of OptSim™, the large investment required to purchase a ModeSYS™ license had to be considered. Due to the uncertainty about the acquisition of the software, a MATLAB®-based implementation of the link was started. As soon as the software was deemed affordable, this option was discarded; however, a step fiber mode solver was developed. Figure A-6 was generated with the model.

C Design: schematics, specifications and procedure

C.1 VCSEL

C.1.1 Schematic and specifications

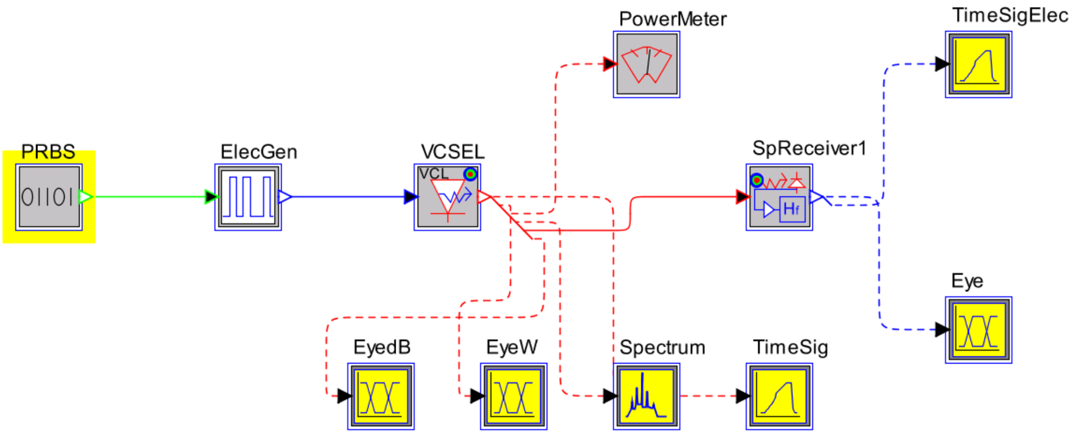

Figure C-1 Modular setup utilized for the VCSEL design.

The block “PRBS” accounts for the generation of the pseudorandom sequence and its nominal bit rate and “ElecGen” transform ideal square binary sequences into electric streams with defined flank progression. “EyedB” and “EyeW” are the eye diagrams in decibels and watts respectively. “PowerMeter” calculates the average optical power over infinite of specified bandwidth. The receiver was necessary to terminate the link and create a data flow through the VCSEL module however, its function is irrelevant.

The specifications for the main blocks based on D-lightsys’ datasheet are summarized in Table C-1 ([29]):

Table C-1 Summary of the specifications for the main blocks in the transmitter.

Block	Parameter	Min	Typ	Max	Unit
PRBS	Length	-	2^{11}-1	-	-
	Bit rate	0.5	-	10	Gbps
ElecGen	Flank type	-	On/off ramp	-	-
	Differential voltage	100	**600**	950	mV
	Raise/fall time ([30])	-	**30**	45	UI[31]
	Timing Jitter	**0**	**-**	0.6	UI
VCSEL	Wavelength	840	850	860	nm

[29] Bold numbers represent estimations.
[30] Rise/Fall time and timing jitter are specified as optical characteristics. Owed to the impossibility of performing their tuning in the optical domain, these two parameters are adjusted from the electrical generator.
[31] Unit Interval. Normalized time to the bit rate period.

	Max. Linewidth	-	-	0.85	nm
	Min. OMA	-4.3	-	-	dBm
	Typ. ER	3	5	-	dB
	Avg. Output power	-4	-2	-0.7	dBm
	Temperature	-40	**25**	90	^{o}C
	Max. Output power variation over the specified temperature range	-	0.5	1	dB
	Bias current	-	**8**	**9**	mA
	Mod. Response[32]	-	**11±1**	-	GHz

No information about the spot size or field distribution was provided hence absolute flexibility was assumed. Consequently, the encircled flux analysis was not required.

C.1.2 Procedure

Firstly, the PRBS block and the binary to electrical converter are adjusted with the parameters from the table. With regard to the bit rate, it was set to 10Gbps given that a compliance with 10GBASE-SR standard was intended. Because of that, we had to assure the best agreement possible between simulation and requirements at that specific bit rate. The rise/fall time was set to 30ps (66% of the maximum) and the differential input voltage to the laser was fixed at 600mV.

Concerning the VCSEL, its modeling consisted of tens of iterative sweeps of parameters. Starting from the AlGaAs predefined model, the variables were progressively tuned from the most stable and clear (wavelength, driving system or room temperature) to the most uncertain ones (thermal gain, parasitics, turn-on voltage or current injection efficiency). The LIV and s_{21} were constantly checked to assure reasonable behavior and thereby restrict at maximum the sensible intervals for the parameters based on the operational ranges provided. Special care was put in the stability of the laser with respect to the temperature (check “Max. Output power variation over the specified temperature range” in Table C-1) since it turns crucial in avionic networks; where the ranges are drastically larger than in ground level. The extinction ratio was checked with “EyedB” and the OMA with “EyeW”. The linewidth was measured with “Spectrum” at 3dB.

C.2 Receiver

C.2.1 Schematic and specifications

[32] Bandwith at bias currents within the predefined interval [8mA,9mA].

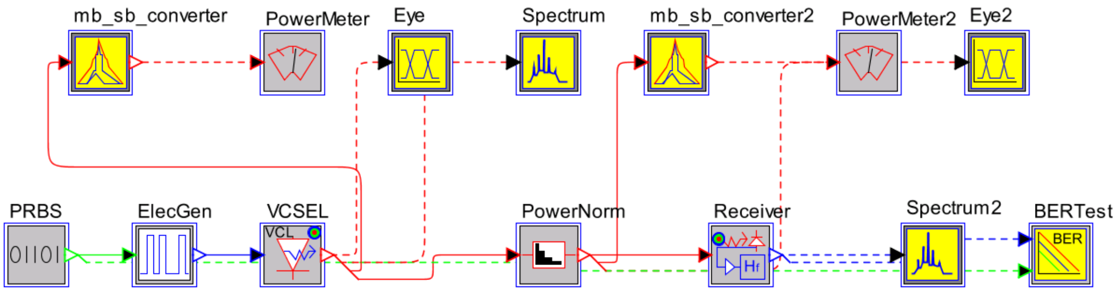

Figure C-2 Schematic utilized for the receiver design.

The "PRBS", "ElecGen" and "VCSEL" are responsible for the signal generation. The outgoing data stream passes through "PowerNorm" that regulates the average optical power to set it at a certain level pre-established by the user. Finally, the signal is converted to electrical in the PD, amplified in the TIA and filtered in the LPF. All these stages are embedded in the "receiver" block. The rest of the blocks are measuring tools like power meters, eye mode in scopes, OSAs and BERtester.

The electrical and optical specifications are collected in Table C-2 ([33]).

Table C-2 Specifications for the receiver.

Parameter	Min	Typ	Max	Unit
Wavelength	760	850	860	nm
Max. Linewidth	-	-	1	nm
Max. Average optical power	**-5**	**-3**	0	dBm
Optical sensitivity at 10Gbps	-	-15	-12	dB
Differential output voltage	200	400	700	dBm

C.2.2 Procedure

Following the natural route of the ligh/current, the PD was the first device faced. As the type (PIN) and the composition (GaAs) were given, the only parameter to be set was the quantum efficiency (QE). It is defined as the degree of effectiveness of the incident radiant flux for producing current [21] and it is a different way of expressing the PD responsivity.

The output of the adjusted photodiode was analyzed in order to calculate the necessary gain in the TIA to generate values within the range of the differential output voltage (see Table C-2). This is done modifying the feedback impedance of the transimpedance amplifier.

When reasonable values were obtained, the noise power was adjusted to achieve the target sensitivity. For this, the LPF's cut-off frequency was set to 10GHz and "PowerNorm" was set to -15dBm. The tuning was done accordingly to the BER result.

[33] Bold numbers represent estimations.

C.3 MMF

C.3.1 Schematic and specifications

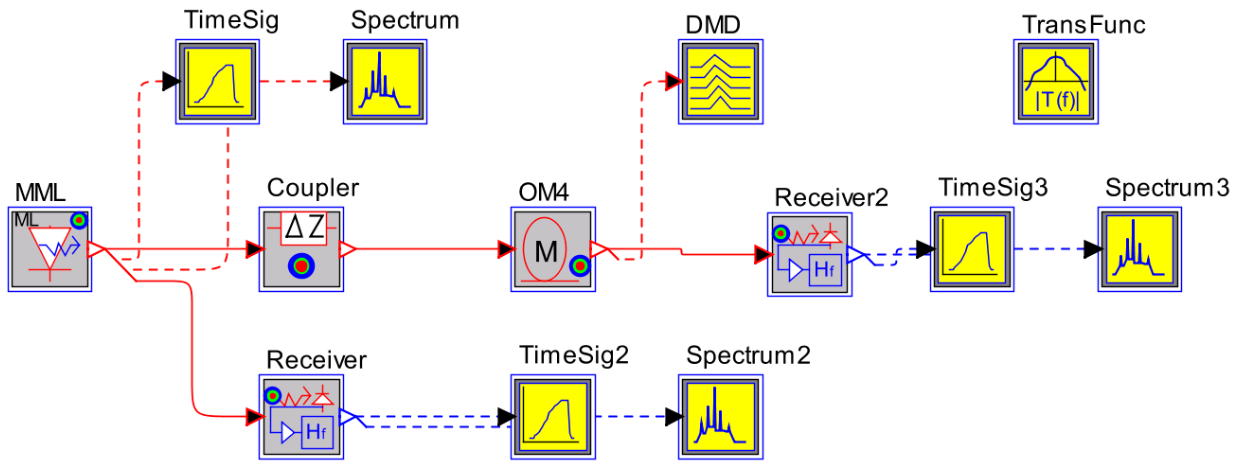

Figure C-3 Schematic used for the MMF design.

The “MML” block is a mode-locked laser. It simulates the response of a 5µm mode field diameter Titanium Sapphire laser to generate the necessary 10ps FWQM pulses for the DMD test on OM3+ and OM4 fibers. The spatial coupler is responsible for the radial scan of the OM4’s end face every 1µm. After propagation, the pulses are collected and processed into the DMD module, which builds the DMD plot and calculates the accumulated time spread. The receivers and “TransFunc” are used to follow the evolution of the bandwidth with every change.

Recalling what was discussed, the DMD specifications provide maximum delays for each of the three intervals. One fiber that remains below those particular values, guaranties certain transmission capabilities certified by the committee. For OM4, the particular delays are still under discussion but a first draft has been released (see Table C-3).

Table C-3 DMD specifications for OM4 fiber [51].

Specifications	Inner DMD	Outer DMD	Sliding DMD
1	≤0.10	≤0.30	≤0.11
2	≤0.11	≤0.17	≤0.11
3	≤0.14	≤0.14	≤0.11

C.3.2 Procedure

The general parameters from the datasheet were loaded into the OM4 module. The most relevant ones and their values are summarized in Table C-4.

Table C-4 List of specifications reported in Darka's datasheets for their OM4 fiber.

Parameter	Value	Unit
Attenuation (850nm)	<2.2	dB/km
Zero dispersion wavelength	$1295 \leq \lambda_0 \leq 1340$	nm
Zero dispersion slope	≤0.105	$ps/nm^2 \cdot km$
Group refractive index (Typ.)	1.482	-
Refractive index difference	1	%

The core refractive index was approximated through the group refractive index as first approach. The Sellmeier's equation (FORMULA) for fused silica was used as an approximation for the refractive index variation with respect to the wavelength. The dispersion wavelength was initially set to 1315nm, the zero dispersion slope was established at 0.102 $ps/nm^2 \cdot km$ and 2.1dB/km for the attenuation.

The effects of material dispersion on group velocity were taken into consideration. The group refractive index was introduced and the profile dispersion parameter was set to zero at the beginning. This allowed us to set an initial value of 2.07 to the profile exponent based on the estimation in [51] of the optimum coefficient for 50µm silica fibers at 850nm.

The DMA feature was deactivated at first. This was done in order to see the actual delay of high order DMGs on the DMD plot and thereby understand the impact of each parameter.

Once the starting values were established the corresponding adjustment was performed. The process can be simplified in the next four steps:

1. Variation of the profile exponent and core refractive index
2. Check MGD
3. Adjustment of the profile dispersion parameter
4. Check DMD

The MGD was used because its generation was almost instantaneous and it can be associated indirectly to the DMD behavior hence saving a lot of time. The impact of the chromatic dispersion parameters was also tested however, the DMD hardly showed any variation for values within the ranges in Table C-4. Consequently, those parameters together with the refractive index difference remained the same as initially.

C.4 10GBASE-SR

C.4.1 Specifications

All the specifications were obtained from the 10GBASE-S definition (Short Wavelength Serial PMD) in the IEEE 802.3ae standard.

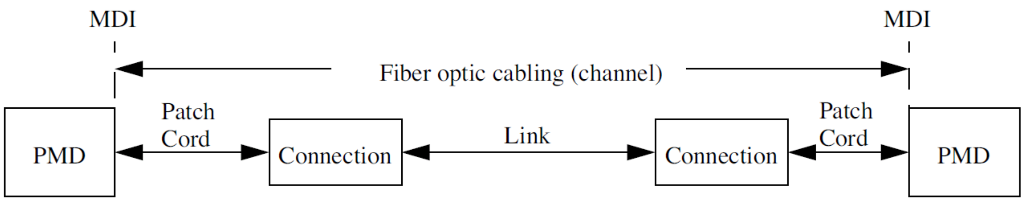

Figure C-4 Fiber optic cabling model

It is important to remark that the IEEE 802.3 group assumes a link operation over a reasonable range of environmental conditions related to temperature, humidity, and physical handling (such as shock and vibration). The final implementation of the network will need the usage of specific aerospace connectors such as Diamond AVIM connector family and the Deutsch MC3 MkII and MC5. Up to date, there is no OM4 equivalent for airborne systems. Its re-design or protection will be necessary as well as for the rest of conventional components which will be exposed to those strict conditions and whose official adaptation has not been stipulated yet. Another important consideration is the ease of splicing and maintenance which should be as simple and reliable as possible. In this regard, there are some mechanical splicers that have been proved to pass most stringent aerospace qualifications (see [86])

C.4.2 Transmitter

A direct comparison between the PMD requirements and D-lightsys' emitter is presented in Table C-5.

Table C-5 Comparison between 10GBASE-SR transmitter requirements and D-lightsys's transmitter.

Description	10GBASE-SR	D-lightsys transceiver	Units
Signaling speed (nominal)	10.3125	10 ([34])	GBd
Wavelength	840 to 860	840 to 860	nm
Max. RMS spectral width	0.45	0.85	nm
Max. Average launch power	-1	-0.7 ([35])	dBm
Min. Average launch power	-7.3	-4	dBm
Min. OMA	-4.3	-4.3	dBm
Extinction ratio	3	3	dB
Max. RIN	-128	-117	dB/Hz
Encircled flux	See footnote[36].	**See Figure C-6**	-
Eye mask definition {X1, X2, X3, Y1, Y2, Y3}	{0.25, 0.40, 0.45, 0.25, 0.28, 0.40}	**See Figure C-5**	-

[34] The maximum bit rate is determined by the modulation response at a certain temperature and bias. No information is provided about signaling speed variation but it is plausible to assume that 10.3125Gbps is attainable with a correct control and adjustment of both parameters.
[35] The transceiver is Class 1M according to IEC 60825-1 but the output power can be adjusted through a 2-wire serial interface to keep it below -1dBm.
[36] The encircled flux at 19 µm shall be greater than or equal to 86% and the encircled flux at 4.5 µm shall be less than or
equal to 30% when measured into Type A1a (50/125 µm multimode) fiber per ANSI/TIA/EIA-455-203-2001.

For the sake of simplicity, it is assumed that the RMS spectral width and Relative Intensity Noise remain below 0.45nm and -128dB/Hz respectivelty. It should be noticed that these parameters, as well as the signaling speed, are readily tunable in the simulator to keep them below maximum ratings. Encircled flux and eye mask tests are done with ModeSYS™.

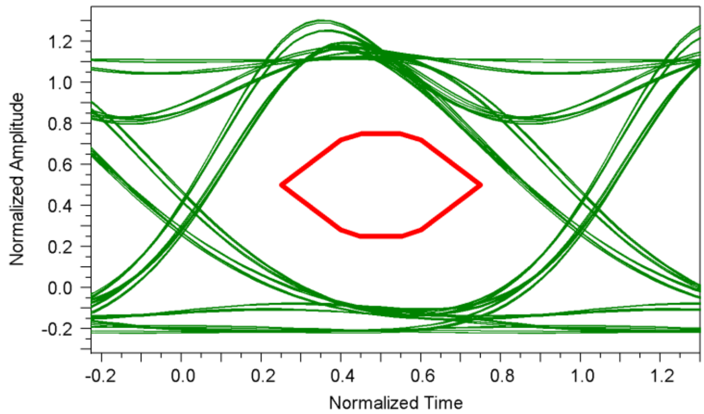

Figure C-5 Optical eye diagram and the 10GBASE-SR eye mask specification.

Figure C-5 illustrates a combined plot of the optical eye and the corresponding eye mask. For the eye to fulfill the 10GBASE-S specifications, it has to contain the calculated eye mask inside the aperture. Such mask is built according to the format described in the standard. Notice the normalization.

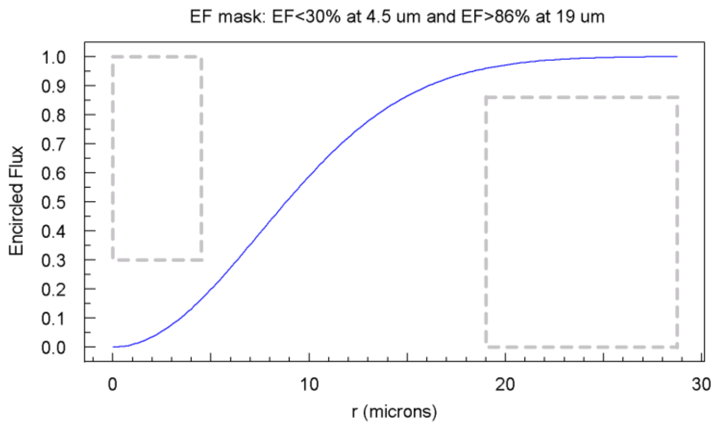

Figure C-6 Encircled flux of the VCSEL model and reference masks.

As described above, the modal field distribution of the VCSEL must have less than 30% of the total radiated power within the first 4.5µm and more than 86% between 0µm and 19µm to be deemed compliant with the 10GBASE-S PMD. Figure C-6 shows the VCSEL's EF for a center launch (0µm offset) with 15µm diameter Laguerre-Gaussian spot size. It is widely contained in the acceptable operational region.

The conclusion is that all the parameters fully comply with the specifications with the exception of the uncertainty about the RIN and linewidth assumptions.

C.4.3 Receiver

A direct comparison between the PMD requirements and D-lightsys transceiver is presented in Table C-6 ([37]).

Table C-6 Comparison between 10GBASE-SR receiver requirements and D-lightsys's receiver.

Description	10GBASE-SR	D-lightsys transceiver	Units
Signaling speed (nominal)	10.3125	**10.3125**	GBd
Wavelength	840 to 860	840 to 860	nm
Max. Average receive power	-1	0	dBm
Min. Average receive power	-9.9	-15	dBm
Max. SRS in OMA	-7.5	**-15.5**	dBm
Max. Receive electrical 3 dB upper cutoff frequency	12.3	**12.3**	GHz
Max. Return loss	-12	-12	dB

The receiver shall be able to tolerate, without damage, continuous exposure to an optical input signal having a power level equal to the Max. Average receive power plus at least 1 dB. Besides, a received power below Min. Average receive power cannot be compliant; however, the lower limit is said to be purely informative thereby it will not be regarded as long as we stay below it [25]. In any case, the requirements are met.

The Stressed Receive Sensitivity is the way how sensitivity is specified in 1GbE standards. It establishes the maximum OMA of the incoming signal at which the receiver is required to attain BER equal or lower than 10^{-12}. Compliance is achieved when the receiver is equal or lower than the standard. In our case, it was measured with conformance test signal at TP3 [25] for BER = 10^{-12}.

Concerning the maximum 3dB bandwidth of the LPF, since the filter it is not part of the transceiver it is assumed to equal the standard.

C.4.4 Channel and power budget

The specifications for 50µm MMF at 850nm and their comparison with the simulation results are gathered in Table C-7.

[37] Bold numbers represent estimations.

Table C-7 Comparison between 10GBASE-SR channel requirements and OM4 model.

Description	10GBASE-SR	OM4 model	Unit
Min. OM4 operational distance	550	550	m
Max. OM4 operational distance	N/A	700 (see fotnote[38])	m
Max. Insertion loss	2.6 ([39])	2.6	dB
Max. Fiber cable attenuation	3.5	2.2	dB/km
Zero dispersion wavelngth	1320	1315	nm
Max. Zero dispersion slope	0.11	0.102	$ps/nm^2 \cdot km$

As indicated in the standard, the maximum operational distance is calculated based on an allocation of 1.1dB[40] total connection and splice loss, leaving 1.5dB for fiber attenuation. In the worst case of 2.1dB/km the maximum reachable distance is 714.28m (700m). The attenuation after 550m of OM4 fiber at 2.1dB/km is 1.155dB, what leaves 1.445dB margin for connectors and splices. In simple point-to-point links where two connectors are used, this corresponds to two connectors of 0.3dB[41] loss and six 0.15dB[42] splicings.

C.5 Optical Orthogonal Frequency-Division Multiplexing (OOFDM)

C.5.1 Modulator

C.5.1.1 Design parameters

The design parameters are chosen with respect to the previously stated constraints. Table C-8 presents the summary.

Table C-8 Design parameters for the OOFDM modulator.

Description	Value	Unit
Number of subcarriers	256	-
Modulation per channel	4/16/32-QAM	-
Training sequences	2	-
Cyclic prefix	1	%
Oversampling	2/4	-
IM mode	DCO-OFDM	-

[38] Maximum reachable distance assuming $BER \leq 10^{-12}$

[39] It includes losses due to connectors, splices and fiber attenuation (OM3 reference). It should be noted that when IEEE 802.3ae was released in 2002, the fiber with the best performance was OM3.

[40] This number results of the estimated adaptation of 10GBASE-S power budget requirement to the OM4 fiber type [87]. Connectors and splices are much more precise for OM4 and thereby the loss reduction.

[41] Maximum registered for OM4 being 0.2dB/0.25dB the typical value for aerospace connectors.

[42] Maximum splice losses of Draka's bend-insensitive 850 MMF.

PAPR handling	Clipping	-
Sampling rate	Variable	GS/s

The number of subcarriers is determined by a combined trade-off. Given a fixed bandwidth, increasing the number of channels assures almost completely flat fading hence facilitating the equalization and making it more accurate. Besides, the number symbols per OFDM symbol is greater and this increases the effective bit rate. On the other hand, it will worsen the maximum PAPR thereby raising the non-linear effect of clipping or the necessary dynamic range of the DAC. Furthermore, the subcarriers get closer and closer within the available bandwidth and this makes the whole system more sensitive to ICI. All in all, and based on different literature ([88] and [89]), the number of channels was set to 256.

The constellation per subcarrier is chosen to be M-QAM owed to the benefits that it offers respect to other modulation formats when applied on OFDM [59]. With regard to the number of bits per symbol, several possibilities were implemented (2, 4 and 5).

The determination of the channel response is done through the analysis of the distortion undergone by two training sequences. These sequences are built so that all subcarriers are excited with equal magnitude and phase. At the receiver, the transfer function is calculated seizing on the fact that FFT transformation is required. According to [58] two training symbols is a reasonable choice because it gives 3dB lower noise level by simple averaging both symbols.

The cyclic prefix was roughly calculated according to maximum expectable delay per meter and maximum tested distance. As it has been explained above, the maximum delay was set to the closest maximum affordable outer DMD (0.14ps/m). In the worst-case channel modulation (BPSK), 256 channels, 10.3125Gbps and 1km fiber reel, it does not exceed 1% of the symbol duration (~0.6%).

Another important aspect is the oversampling factor. Oversampling in OFDM is absolutely necessary to fulfill the Nyquist criterion before the DAC conversion. Some studies have shown that a factor of 1.5 is sufficient [59] however, it was fixed to 2 or 4. The latter for representation issues. Notice that an excessive oversampling for a steady sampling rate will increase the symbol duration and hence the effective bit rate. This highlights the importance of choosing the lowest factor possible.

Biasing the output stream was the technique used to guarantee unipolar driving signal. Despite the power-efficient advantages of other alternatives it was chosen to stick to the cost-effective network requirement and take advantage of the unavoidable biasing of the VCSEL (directly modulated) to solve two problems with only one solution: creation of a unipolar signal and population inversion with only one bias current.

The peak-to-average control was decided to be done through clipping. It is the simplest method and it gives the best error ratio for a certain SNRb according to [90] compared to other solutions. However, it generates an undesired noise called "clipping noise" due to the selective truncation of concrete peaks and also OOB noise. To solve the latter the signal is filtered with a Hamming window, taking advantage of the reconstruction filter after DAC. That is, one filter offer solution for both OOB noise generated after clipping and reconstruction of the oversampled signal.

Finally, the sampling rate is chosen depending on the rest of variables in order to attain the mandatory 10.3125Gbps (±100ppm).

C.5.1.2 Process description

The binary bit sequence could be taken either from ModeSYS™ when the module was integrated in the optical link or from a predefined set of pseudorandom sequences. After loading the binary vector and replicating it to create a longer stream, it was divided into 256 parallel channels (one for each subcarrier) and transformed into symbols according with the chosen constellation.

Once the data was formatted, the necessary replication and complex conjugation for DMT was performed. After that, the IFFT was calculated and the output matrix was transformed into a vector to create the digital OFDM symbol frame. Right after including the training sequences, the cyclic prefix was added and the signal was clipped.

The next block is the DAC conversion. Firstly, the normalized amplitude range is transformed into values within the differential input voltage limits of the transceiver. Once this was done, up-sampling and LPFing were applied to generate the final outgoing data stream.

C.5.2 Demodulator

C.5.2.1 Design parameters

No special parameters need to be reported. The ADC works at the same rate as DAC, the number of inputs in the FFT is the same as outputs in the IFFT, the length of the discarded window is exactly the same as the cyclic prefix duration and the demodulation is done according with the chosen constellation in the transmitter.

C.5.2.2 Process description

Before setting the receiver in the default mode, two things needed to be done: calculate the optimum sampling point and the channel's transfer function. The first one was done by setting the wanted parameters in the transmitter and launching a 2^7-1 PRBS sequence into the channel. The received signal was correlated with the ideal PRBS and the resulting deviation utilized to set the optimum sampling point in the first position of the vector. With regard to the channel's transfer function, it was calculated from the averaged transfer function obtained from the pair of training sequences. The coefficients were stored and applied at each of the FFT outputs (1-tap equalizer).

From this point on the regular working mode was established. The incoming electrical signal was sampled every 2 starting from the first position in the vector. The cyclic prefix was removed and the resulting stream was serial-to-parallel converted and FFTed. The outputs were equalized with the calculated coefficients and parallel-to-serial converted in order to perform the 1/0-mapping from the corresponding modulation format. Once the binary stream was ready, two forms of BER calculation were implemented: error counting and Gaussian fitting plus overlapping calculation. The second was used when the resulting BER was lower than 1/simulated bits.

D OOFDM: cases of study

D.1 25ºC

D.1.1 4-QAM

Figure D-1 shows the transmitted and received electrical DMT frame spectra (after IFFT and before FFT respectively) and the comparison between the spectrum of the transmitted and received signal (after DAC and after filtering respectively).

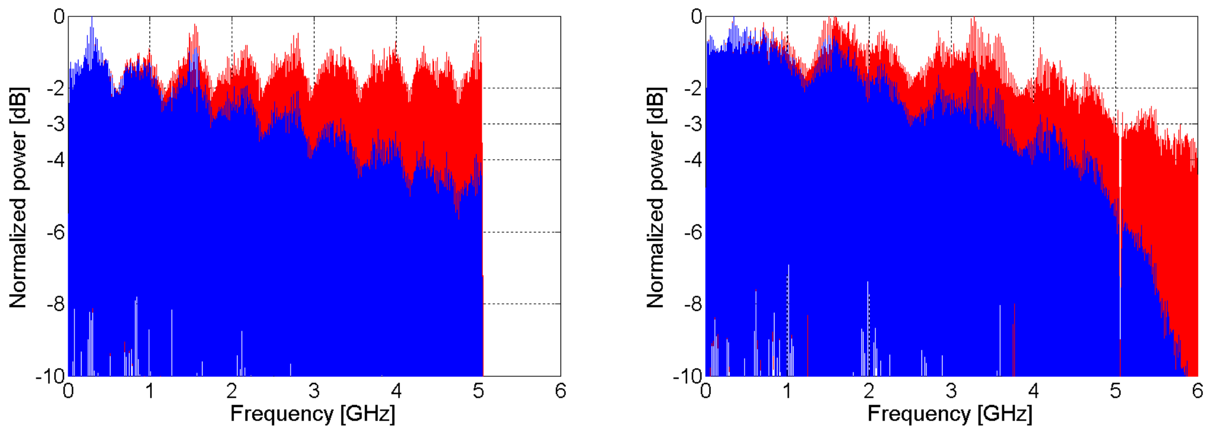

Figure D-1 Transmitted and received electrical DMT frame spectra (left) and the comparison between the spectra of the transmitted and received signals (right). 4-QAM.

In both plots, the red trace represents the sent signal and the blue line represents the received one. From both pictures, it can be seen that only 5GHz transmission bandwidth is necessary with 4-QAM to generate a nominal bit rate of 10.3125Gbps; something absolutely impossible if OOK is utilized. The ripple that can be observed is due to the cyclic prefix of 1% but has been proved not to have any impact on the result [59]. The system's transfer function can be inferred from the right graph where the steep roll-off of the Butterworth filter is noticed.

The constellation obtained after FFT and equalization for 1% cyclic prefix and without cyclic prefix are shown in Figure D-2.

(CONTINUE IN THE NEXT PAGE)

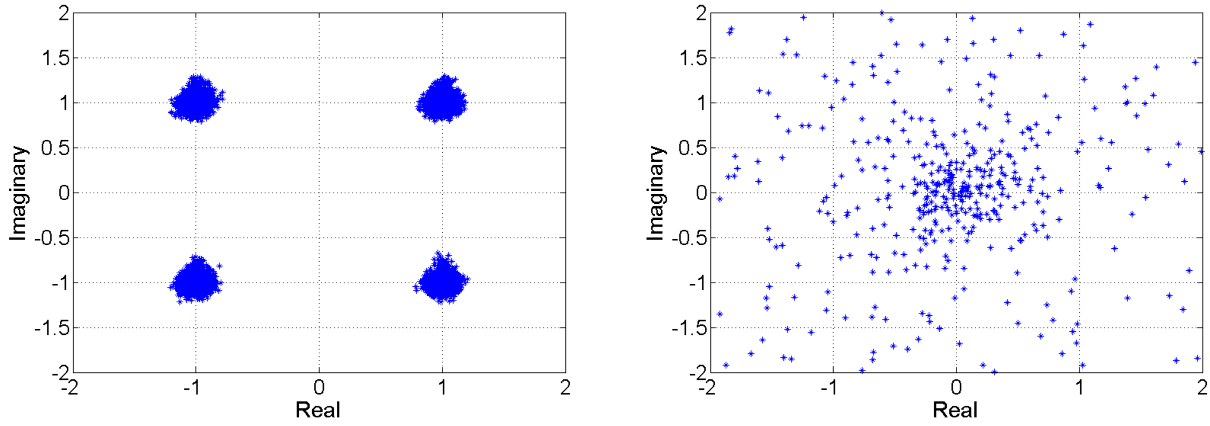

Figure D-2 Received 4-QAM constellation with 1% cyclic prefix (left) and without cyclic prefix (right).

The effect of the extra 6 samples (1% of 512 rounded upwards) is the difference between error free and 0.466 error rate. The cyclic prefix is equivalent to 287.63ps at 20.86GS/s, almost triple of the estimated maximum delay spread.

Because the number of error counted after 64770 bits was lower than 10^{-5}, the estimated BER was calculated. For that, the histograms for the real and imaginary dimension were calculated and along with a Gaussian fitting of the resulting levels. The result is shown in Figure D-3.

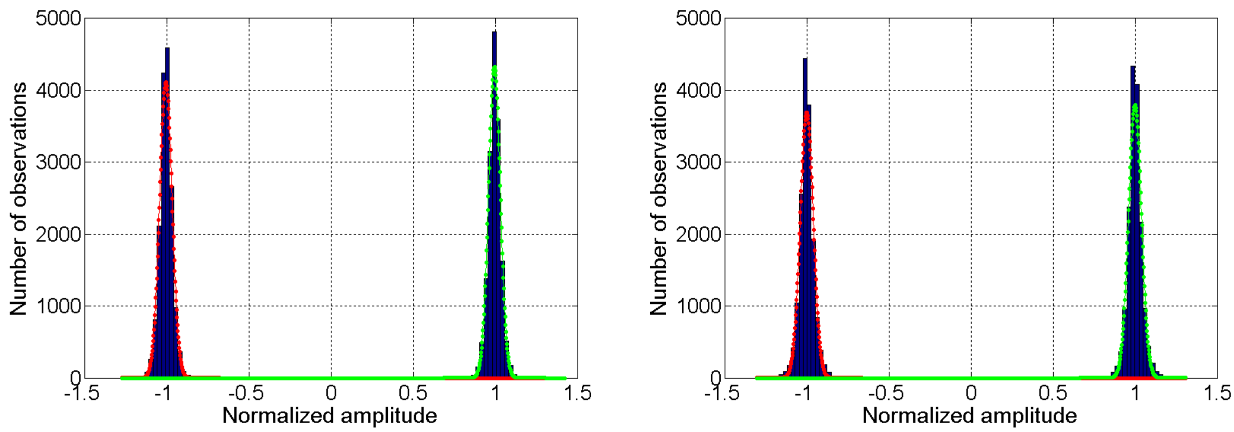

Figure D-3 Received histogram of the real dimension (left) and of the imaginary dimension (right).

For the BER calculation, it was considered that the SNR was sufficiently high in order to assume that only errors between nearest symbols occur. In such case, the BER can be calculated by simply taking the worst one, that is, $max\{BER_{IMAGINARY}, BER_{REAL}\}$. The result shows an error rate of 10^{-90} ([43]).

For 10.3125Gbps the sensitivity is -14dBm (see Figure D-4).

[43] Such low estimated BERs are a good indicators of satisfactory performance but in any case should be taken as accurate measurements.

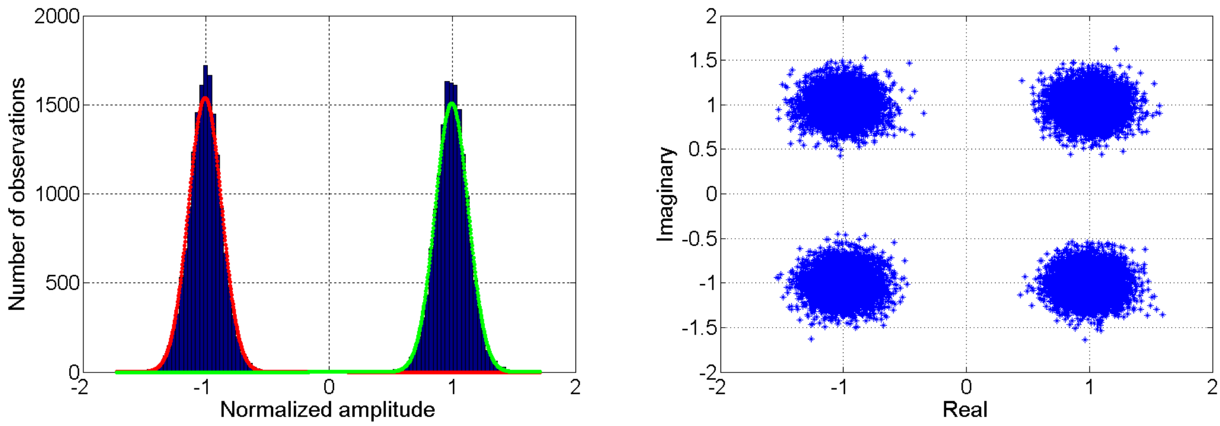

Figure D-4 Histogram and constellation of the received 4-QAM OOFDM signal for -14dBm input optical power (BERα10^{-12} at 10.3125Gbps)

As the power decreases, the influence of the thermal noise increases hence the Gaussian fitting hardly deviates. The minimum power margin (laser emitting at -4dBm) with respect to the transmission at 10.3125Gbps goes down to 7.9dB[44].

D.1.2 16-QAM

The spectra of the DMT frames and the output/input signals are shown in Figure D-5.

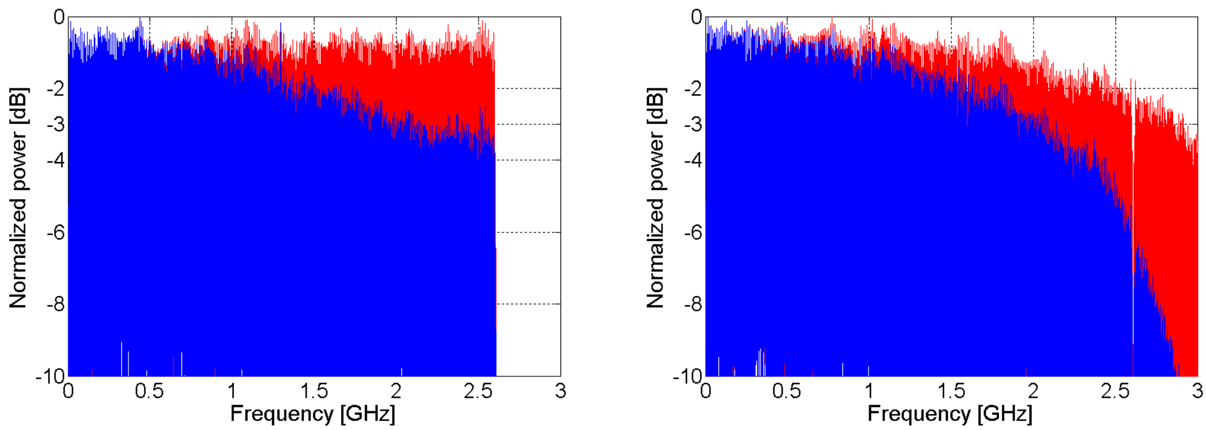

Figure D-5 Transmitted and received electrical DMT frame spectra (left) and comparison between the spectra of the transmitted and received signals (right). 16-QAM.

The red trace represents the outgoing frame/signal and the blue is the incoming one. It can be seen the extreme efficiency that 16-QAM and OOFDM offers. Not only the subcarriers can overlap without interfering with each other but they also do it at 4bit/s/Hz generating an overall efficiency very close to

[44] Connector loss of 0.6dB (2 times worst-case connector loss) and 1.5dB loss due to fiber.

optimum for 16-QAM. The attenuation visible in the DMT is mainly caused by the LPF, whose cut-off frequency has been adjusted to 2.6GHz.

After the FFT and the 1-tap equalizer, the following constellation is observed:

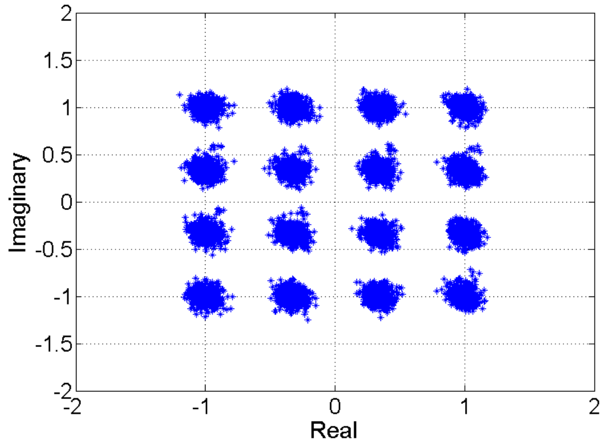

Figure D-6 Received 16-QAM constellation.

The error counting method for the BER calculates zero errors. The subsequent estimation yields the histograms presented in Figure D-7.

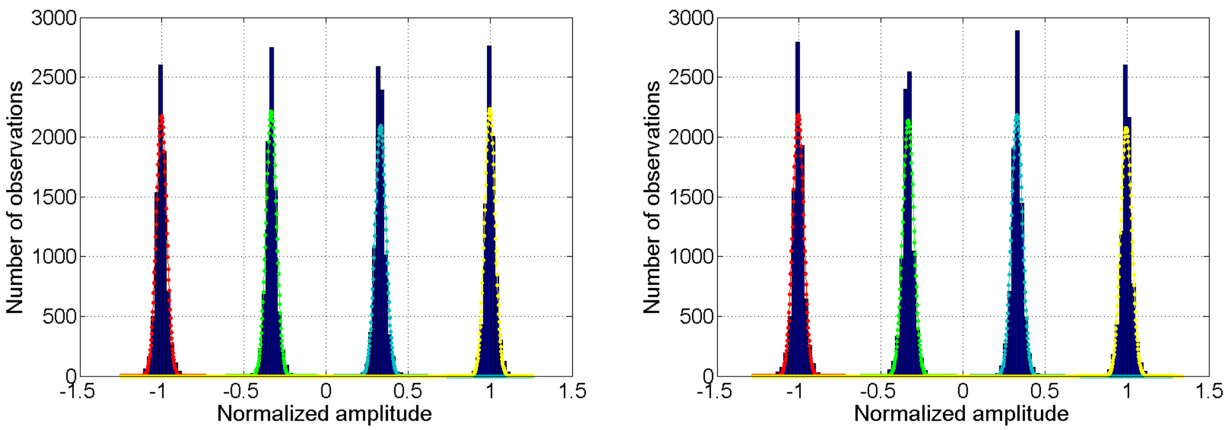

Figure D-7 Received histogram of the real dimension (left) and of the imaginary dimension (right).

It is observed that the fitting has been adjusted to follow the bottom part of the levels in the histogram rather than the peaks. This has been done to be more accurate in the overlap integral calculation. The deviations from the Gaussian distributions may be caused by the distortion introduced by clipping (not the OOB noise). The BER result is $5 \cdot 10^{-18}$.

The sensitivity changes to -7.5dBm, this gives around 1.5dB power margin. Notice that we are already working close to the error free limit with -4dBm of output power

D.2 -40ºC

D.2.1 4-QAM

The spectra for the DMT frames and the signal show high resemblance with Figure D-1. The histograms show that the highest peaks for both real and imaginary accumulate 1000 samples less than at 25°C (see Figure D-8 and Figure D-3) meaning that, since the same number of symbols is transmitted, they are not so concentrated in the optimum levels. The consequence is an estimated BER of 10^{-76}, 14 orders of magnitude worse than at 25°C

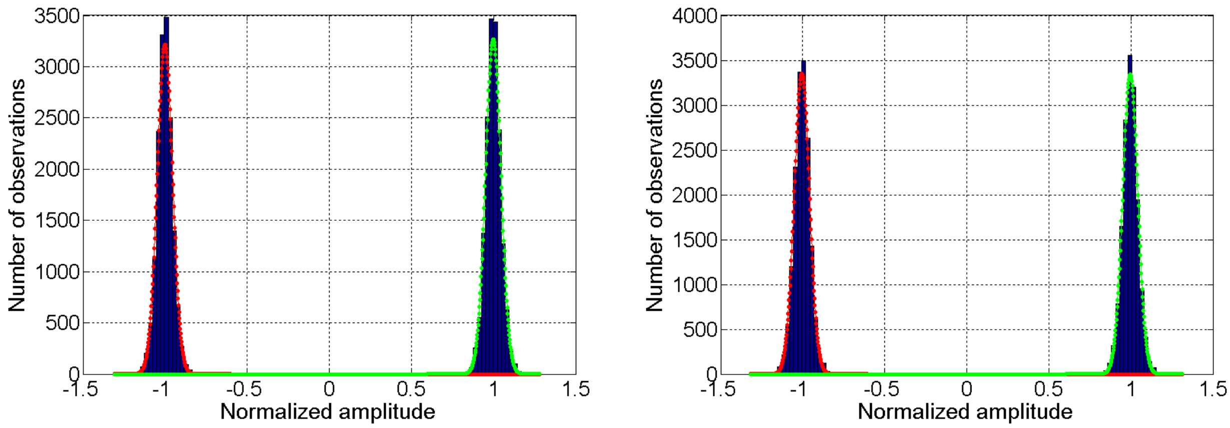

Figure D-8 Received histogram of the real dimension (left) and of the imaginary dimension (right).

The sensitivity is reduced to -12dBm and the corresponding minimum power margin equals 5.9dB.

D.2.2 16-QAM

The BER obtained was very similar to the one at 25°C. This is reasonable based on the tendency of the BER to input power curve at 9mA shown in Ilustración 4-6. The constellation is very clean and the Gaussian fitting almost exact.

(CONTINUE IN THE NEXT PAGE)

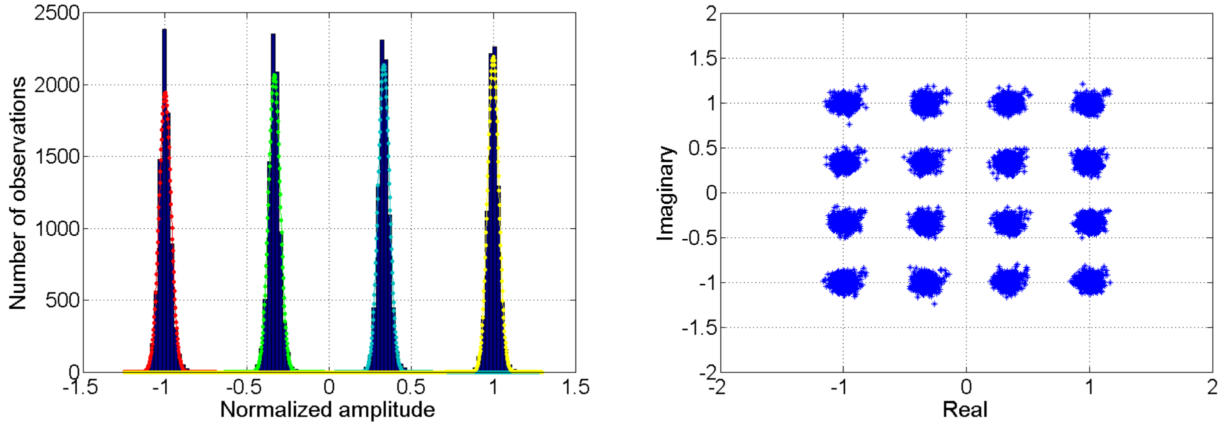

Figure D-9 Histogram of the real dimension (left) and received 16-QAM constellation (right).

The estimated BER is $8 \cdot 10^{-17}$. Despite the symbols in the constellation are more defined compared to 25°C, there is a lower concentration of samples in the optimum levels; it is reflected in the histogram. The consequence is that, as the Gaussian fitting algorithm disregards those bins with small concentration compared to the maximum, the result for 25°C are thinner bells that yield improved BER. This should be taken into consideration and use the estimated BERs as qualitative references exclusively.

The sensitivity is around -7.5dBm. Similarly to 25°C, the power margin is around 1.5dB.

D.3 90ºC

D.3.1 4-QAM

The BER is the worst of all cases for 4-QAM modulation per subcarrier. The histograms show a higher accumulation of samples in the optimum compared to -40°C however, the rest of observations are considerably more spread than for any other temperature. This can be inferred from the difficulties to make an exact Gaussian matching of the whole level (see Figure D-10).

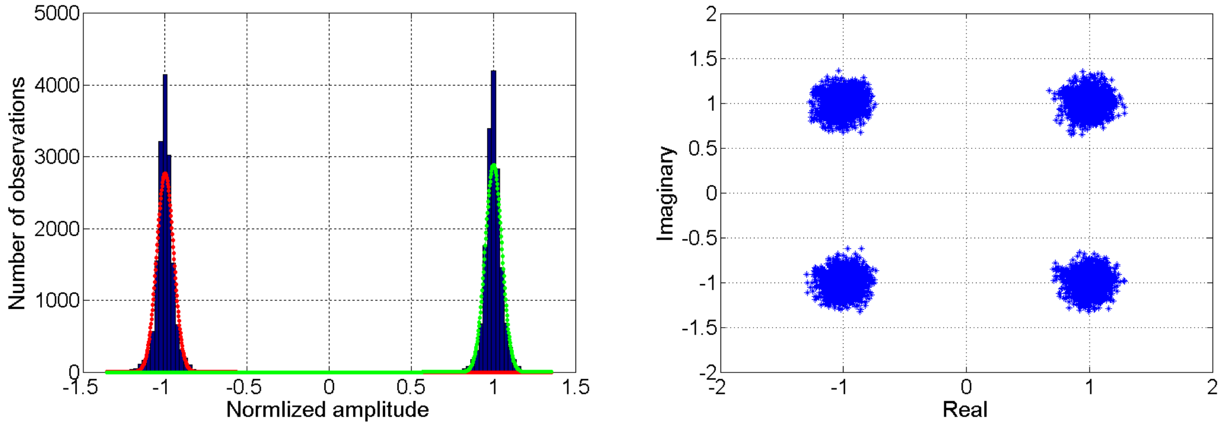

Figure D-10 Histogram of the real dimension (left) and received 4-QAM constellation (right).

The mentioned spreading is also visible in the constellation when compared with 25°C. Despite this effect, the BER is still widely below error free. The counted errors equal zero and the estimated error rate is $2{\cdot}10^{-67}$. The sensitivity equals -14dBm, leaving a minimum power margin of 7.9dB.

D.3.2 16-QAM

Against what was expected based on the worse performance for 4-QAM, the results obtained at 90°C on 16-QAM are better than for any other temperature. The estimated BER equals 10^{-25} and the symbols are perfectly defined in the histogram (see Figure D-11).

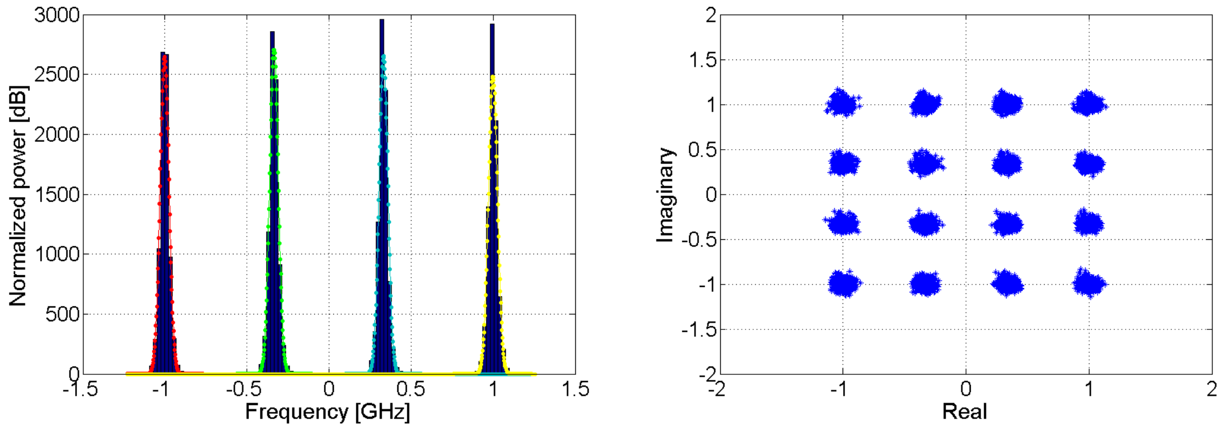

Figure D-11 Histogram of the real dimension (left) and received 16-QAM constellation (right).

The sensitivity experiences an improvement of 1.5dB (-9dBm) with respect to 25°C and -40°C, permitting a power margin of 3dB.

E Estándares de fibra multimodo en la industria y distancias típicas de transmisión soportadas

Regulating standards:

Industry Standards	Fiber Type		
ISO/IEC 11801	Type OM4 fiber	Type OM3 fiber	Type OM2 fiber
IEC 60793-2-10	Type A1a.3 fiber	Type A1a.2 fiber	Type A1a.1 fiber
TIA/EIA	492AAAD	492AAAC-B	492AAAB-A
ITU	G.651	G.651	G.651

Using ISO/IEC 11801 notation, the standardized (gray) and typically supported transmission distances for diverse standards [59]:

Fiber Class 11801 OFL BW 850/1300 nm	Fiber Type 850/1300 nm	1 Gb/s		10 Gb/s 850 nm serial	10 Gb/s 1300 nm CWDM	10 Gb/s 1300 nm serial
		850 nm	1300 nm			
		1000BASE		10GBASE	10GBASE	10GBASE
		SX	LX	SR	LX4	LRM
OM 1 62.5 µm 200/500 MHz·km	Standard OM 1+ 200/600 MHz·km	275 m 500 m	550 m 1000 m	33 m 65 m	300 m 450 m	220 m 220 m
OM 2 50 µm 500/500 MHz·km	Standard OM 2+ 600/1200 MHz·km	550 m 750 m	550 m 2000 m	82 m 110 m	300 m 900 m	220 m 300 m
OM 3 50 µm 1500/500 MHz·km	Standard EMBc = 2000/500MHz·km	1100 m	550 m	300 m 300 m	300 m 300 m	220 m 220 m
OM 4 50 µm 3500/500 MHz·km	EMBc = 4700/500MHz·km	1100 m	550 m	550 m	300 m	220 m

F Especificaciones para diversos tipos de fibras ópticas comercialmente disponibles

Draka: Bend-Insensitive OM4 fiber

Draka: Regular OM4 fiber

Draka: Regular OM2 fiber

Draka: Regular OM1 fiber

Corning: Bend-Insensitive OM4 fiber

Corning: Regular OM1 fiber

G Rendimiento del proceso de escalado de perfiles de índice de refracción en comparación con el método habitual de escalado de retraso modal [78]

DMD scaling results (blue dots: unscaled DMD; red circles: DMD after usual scaling process; black circles: DMD of the scaled refractive-index profile):

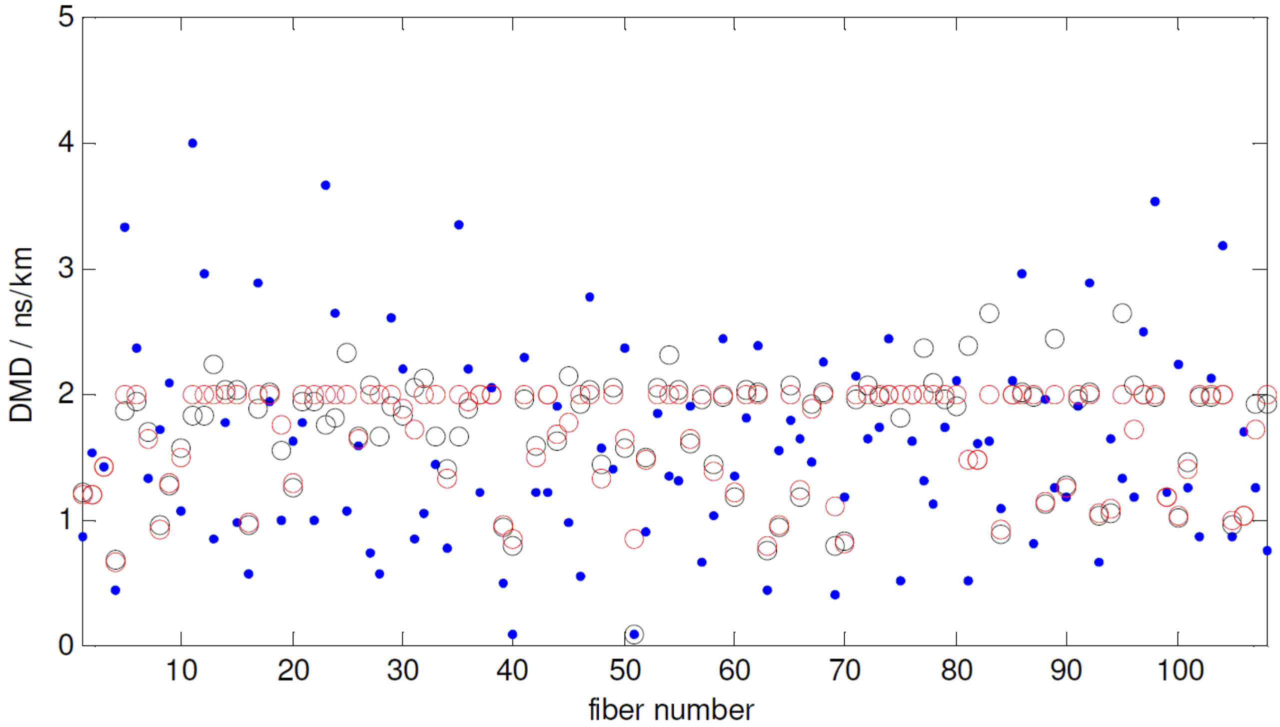

H Publicaciones

- R. Rodes, <u>**J. Estaran**</u>, B. Li, M. Mueller, J. B. Jensen, T. Gründl, M. Ortsiefer, C. Neumeyr, J. Rosskopf, K. J. Larsen, M. Amann, and I. Tafur Monroy, "100 Gb/s single VCSEL data transmission link," *in Optical Fiber Communication Conference and Exposition (OFC/NFOEC), 2012 and National Fiber Optic Engineers Conference* , PDP5D.10 March 2012.
- R. Rodes, <u>**J. Estaran**</u>, T.T. Pham, E. Hviid, I. Tafur Monroy, "Next Generation WDM-PON enabling Gigabit Per-User Data Bandwidth," *Conference Proceedings of 3nd Annual Workshop on Photonic Technologies for Access and Biophotonics*, 2012, University of California, Berkeley, California, Jan. 2012
- <u>**J. Estaran**</u>, R. Rodes, T. T. Pham, M. Ortsiefer, C. Neumeyr, J. Rosskopf, I. Tafur Monroy, "Quad 14Gbps L-Band VCSEL-based System for WDM Migration of 4-lanes 56Gbps Optical Data Links," accepted for oral presentation ECOC'12.
- R. Rodes, T. T. Pham, <u>**J. Estaran**</u>, M. Iglesias Olmedo, I. Tafur Monroy, "GigaWaM WDM-PON System Demonstrator: 10Gbps/2.5Gbps Bidirectional Link Performance."
- <u>**J. Estaran**</u>, J. J. Vegas Olmos, G. A. Rodes, I. Tafur Monroy, "Bidirectional uncompressed HD video distribution over fiber employing VCSELs," submitted IPC´12.